Institut für Theoretische Physik
TU Dresden

Modeling of QED Effects in Particle Decays on the Basis of the Yennie-Frautschi-Suura-Formalism

von

Marek Schönherr

2008

Institut für Theoretische Physik
Fakultät Mathematik und Naturwissenschaften
Technische Universität Dresden

Modeling of QED Effects in Particle Decays on the Basis of the Yennie-Frautschi-Suura-Formalism

Diplomarbeit
zur Erlangung des akademischen Grades
Diplom-Physiker

vorgelegt von
Marek Schönherr

Dresden 2008

Eingereicht am 27.09.2007

1. Gutachter: Prof. Dr. M. Kobel

2. Gutachter: Dr. F. Krauss

Abstract

In calculating the decay matrix elements of elementary particles, e.g. τ-leptons or massive gauge bosons, and composit objects, e.g. hadrons, higher order QED corrections, i.e. soft and collinear real photon emission and virtual corrections, are usually unaccounted for. This is especially true when effective theories are used, as is the case in many hadron decays. Yennie, Frautschi and Suura presented a method to include such corrections to all orders in α. In this diploma thesis the Yennie-Frautschi-Suura (YFS) Formalism will be described and reformulated using the language of dimensional regularisation to handle the occurring divergent integrals. The extraordinary power of this formalism is its universality, i.e. its independence of the underlying process.
Furthermore, its reformulation into a form suitable for Monte Carlo event generation is presented and the implementation as an indpendent module PHOTONS++ into the SHERPA event generator is explained in detail. The program works fully exclusive, meaning it generates all real photons (beyond a certain infrared threshold) separately with their full kinematics.

Zusammenfassung

Bei der Berechnung von Zerfallsmatrixlelementen elementarer Teilchen, wie z.B. τ-Leptonen oder massive Eichbosonen, und kompositer Objekte, wie z.B. Hadronen, und werden QED-Korrekturen höherer Ordnung, also softe und kollineare Photonenabstrahlung und virtuelle Korrekturen, normalerweise nicht berücksichtigt. Das gilt insbesondere bei der Verwendung effektiver Theorien, wie es vorallem bei Hadronenzerfällen der Fall ist. Yennie, Frautschi und Suura entwickelten eine Methode um diese Korrekturen aus allen Ordnungen der Störungstheorie miteinzubeziehen. In dieser Diplomarbeit wird nun der Yennie-Frautschi-Suura (YFS) Formalismus dargestellt und mit Hilfe der Sprache der dimensionalen Regularisierung zur Behandlung divergenter Integrale reformuliert. Die außergewöhnliche Stärke dieses Formalismus liegt in seiner Universalität, das heißt seiner Unabhängigkeit vom zugrundeliegenden Prozess.
Desweiteren wird dieser Formalismus in eine Form gebracht werden, die für Monte Carlo Ereignisgeneratoren genutzt werden kann und die Implementation als unabhngiges Modul PHOTONS++ innerhalb des Ereignisgenerators SHERPA wird detailliert beschrieben. Das Programm arbeitet völlig exklusiv, gleichbedeutend damit, dass alle Photonen jenseits einer gewissen Mindestenergie separat mit ihren vollen Kinematik generiert werden.

Contents

1 Introduction

Since the earliest days of quantum field theory it was known that the presence of massless stable particles, e.g. gauge bosons like the photon, leads to divergent results in perturbative calculations when their momentum vanishes. These infrared divergences, as opposed to ultraviolet divergences, are associated with the behaviour of the theory at small momentum transfers corresponding to long distance interactions (soft limit). Unlike their ultraviolet counterparts they cannot be removed by redefining the meaning of Lagrangian parameters of the theory, but have to somehow cancel exactly for the theory to be sensible.
Such a cancellation indeed occurs when divergent terms originating when a virtual photon's momentum vanishes are added to the corresponding terms involving the emission of a real photon of vanishing energy instead of the virtual photon. Now it can be argued that this cancellation might be valid in totally inclusive calculations and measurements not differentiating the final state, but exclusive cross sections or decay rates with a well defined final state are still divergent because they only contain the soft virtual photon. However, such an exclusive production or decay channel can never be measured in reality. Even the most sensitive physical detector allways has some minimal detectable energy threshold for direct measurements or a non-vanishing error on the momentum configuration of all other particles recorded for indirect ones. Thus, all measurements are insensitive to soft emissions of such massless particles. There cannot be a totally exclusive measurement and, consequently, for sensible observables the described cancellation between contributions of different final state configuration indeed occurs giving a finite result. This was proven for the case of electron scattering in an electromagnetic field by Bloch and Nordsieck [1] in 1937 and on general grounds by Kinoshita, Lee and Nauenberg [5,6] in 1962/64. Of course, the result will depend on how "inclusive" the measurement is. In case of soft photon radiation, as is considered in this work, large logarithms occur when e.g. the sensitivity for infrared photons is very high.
In 1961, Yennie, Frautschi and Suura (YFS) presented a formalism to systematically extract and cancel those singularities associated with soft virtual and real photon emissions in higher order corrections in Quantum Electro Dynamics (cf. [2]). Their work is based on a universal factorisation of the matrix element independent of the spin of the emitting charged particle, cf. Section 2 and Appendix A,C. Such a factorisation was first shown for elementary processes by Low [3] in 1958. Feynman's treatment of gauge invariance [4] plays a key role in relating emissions of photons off a virtual charged particle to emissions off exterior lines to carefully treat possibly overlapping divergences. While Yennie, Frautschi and Suura could only argue such a factorisation for processes with a more involved interior structure, this was shown by Gribov [7] in 1967. Finally, the work of Chaichian and Ermolaev [8] provided a factorisation at leading logarithmic level for emissions off the interior of multiple hard interactions.
The Yennie-Frautschi-Suura-Formalism sums and exponentiates all contributions arising in soft photon emissions, both real and virtual, and cancels their respective singular terms.

Furthermore, it allows the systematic inclusion of fixed order matrix elements to account for effects from emissions of photons away from the singular region. Thus, the YFS-Formalism allows to correct any leading order[1] process to any order within the scope of QED-effects. To be precise, the corrected process will contain contributions stemming from the soft limit of all orders in perturbation theory and contributions from outside this soft region of the phase space to the given order of included exact matrix elements. While, as already mentioned, the soft limit is universal, the latter contributions are not. They are process-specific. However, they can be approximated in certain limits, cf. Section 4. Nonetheless, for higher accuracy these matrix elements have to be calculated specificly, as is done for certain cases in Section 5.
Finally, Section 6 will show and discuss the results of an implementation of above formalism as the module PHOTONS++ within the SHERPA event generator.

[1] In fact, this basic process may not be at tree level at all but may already contain loops and multiple other more involved interactions, also outside the scope of QED.

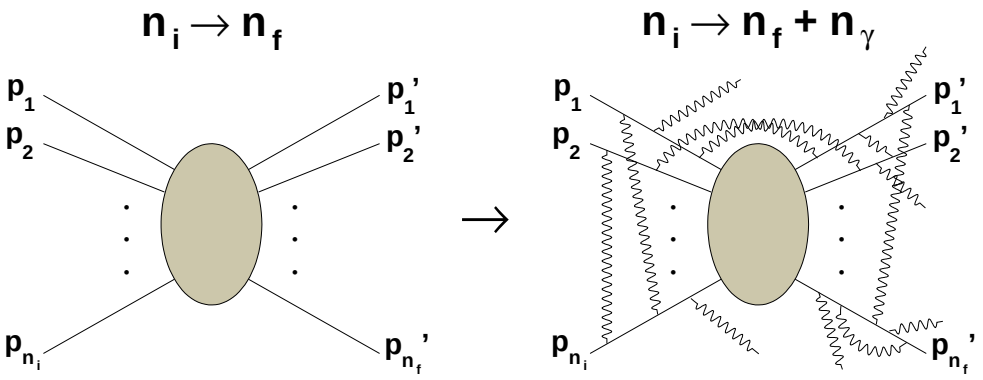

Figure 2.1: Sketch of the Yennie-Frautschi-Suura Formalism. Arbitrary matrix elements are dressed with QED corrections to all orders in α.

2 The Exponentiation of Soft Photon Emissions

Rephrasing the statements of the last section, this work aims at "dressing" (adding QED effects to all orders) all "undressed" (without any higher order QED effects) (decay) matrix elements. Fig.2.1 gives a pictorial representation of that statement. Thus, if

$$\sigma \sim \int \mathrm{d}\Phi_{p_f} (2\pi)^4 \delta^4 \left(\sum p_i - \sum p_f \right) \left| \mathcal{M}_0^0 \right|^2 \tag{2.1}$$

is the cross section (or decay rate) without any higher order QED corrections, then the cross section (decay rate) for the fully inclusive, dressed reaction reads

$$\sigma \sim \sum_{n_R=0}^{\infty} \frac{1}{n_R!} \int \mathrm{d}\Phi_{p_f} \mathrm{d}\Phi_k (2\pi)^4 \delta^4 \left(\sum p_i - \sum p_f - \sum k \right) \left| \sum_{n_V=0}^{\infty} \mathcal{M}_{n_R}^{n_V+\frac{1}{2}n_R} \right|^2 , \tag{2.2}$$

wherein the matrix elements $\mathcal{M}_{n_R}^{n_V+\frac{1}{2}n_R}$ contains (several) divergences due to soft real and virtual photons. p_i here is a generic label for all initial state momenta while p_f stands for the final state ones. Along the lines k stands for all bremsstrahlungs photons emitted as a consequence of higher order QED corrections. Consequently, $\mathrm{d}\Phi_f$ and $\mathrm{d}\Phi_k$ are the

final state phase space elements for the primary particle subspace and the bremsstrahlung photons subspace. The notation on the matrix element will be explained in Section 2.2.
The divergence associated with real photon emission can also be exemplified by considering the probability to emit one photon in a semi-classical argument:

$$P(k)\mathrm{d}^3k = \frac{\alpha}{4\pi^2}\left(\frac{p}{E-\vec{p}\frac{\vec{k}}{k}}-\frac{p'}{E'-\vec{p}'\frac{\vec{k}}{k}}\right)^2 \mathrm{d}\Omega\frac{\mathrm{d}k}{k}\,.$$

This differential probability diverges for $k \to 0$. Thus, the probability that only a finite number of photons with energies lower than the detector threshold is emitted and, hence, escapes detection is precisely zero [1].

2.1 Factorisation in the Soft Limit

Following the approach of Yennie, Frautschi and Suura [2] one can show explicitly that any matrix element containing up to one hard interaction factorises upon the insertion of a virtual ore real photon into an eikonal factor times the underlying matrix element plus an additional finite term for $k \to 0$.
To see this, consider all possible ways to insert an additional virtual photon into an existing diagram as depicted in Fig.2.3. For definiteness, the charged line is assumed to be a fermion. The argument may easily be generalised for a line of arbitrary spin (see App. A). Before the insertion of the photon the matrix element will contain a factor

$$\bar{u}_{p'}\Gamma(p,q_i)u_p \tag{2.3}$$

where the q_i are all momenta transferred to the charged fermion line in the basic matrix element, including other potentially soft photons. Thus, momentum conservation demands

$$p' = p + \sum q_i \tag{2.4}$$

If now one end of the photon is attached to the fermion line it removes the 4-momentum k, it is then necessary to adjust the q_i to $\bar{q}_i$ in order to hold p and p' fixed and fullfill momentum conservation.

$$p' = p + \sum \bar{q}_i - k \tag{2.5}$$

The $\bar{q}_i$ differ from the q_i by an amount of order k. If now the photon is inserted in the initial state line, i.e. before all other interactions, the matrix element factor reads

$$\begin{aligned}\bar{u}_{p'}\Gamma(p-k,\bar{q}_i)\frac{1}{\not{p}-\not{k}-m}\gamma^\mu u_p = \\ \bar{u}_{p'}\Gamma(p-k,\bar{q}_i)u_p\frac{2p^\mu-k^\mu}{k^2-2(k\cdot p)} - \bar{u}_{p'}\Gamma(p-k,\bar{q}_i)\frac{\frac{1}{2}f\left(\not{k},\gamma^\mu\right)}{k^2-2(k\cdot p)}u_p\end{aligned} \tag{2.6}$$

The singularity of order $\frac{1}{k}$ is contained in the first term while the second, upon closer examination, has no divergence in k. It has the form of a magnetic moment interaction

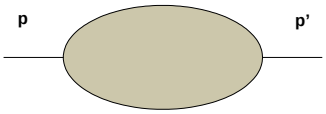

Figure 2.2: A representation of the set of basic diagrams containing all possible interactions and any set of real and virtual photons.

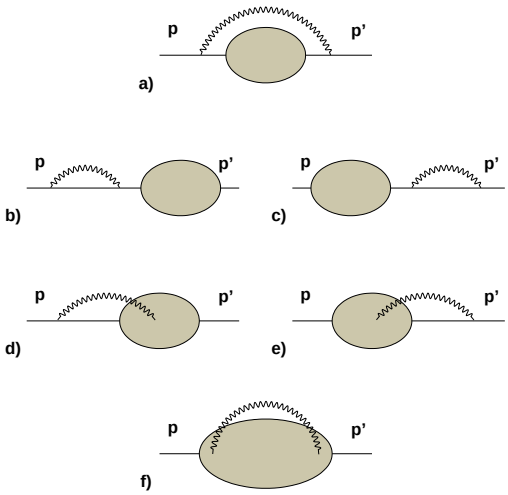

Figure 2.3: All possible insertions of one extra virtual photon into the basic diagram of Fig.2.2.

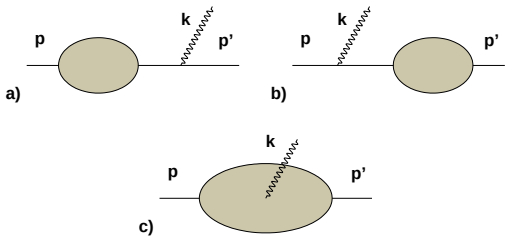

Figure 2.4: All possible insertions of one extra real photon into the basic diagram of Fig.2.2.

and is no stronger divergent than without this newly attached photon. This can be seen by examining it directly

$$\begin{aligned}
\frac{1}{\not p - \not k - m}\gamma^\mu &= \frac{\not p - \not k + m}{(p-k)^2 - m^2}\gamma^\mu \\
&= \frac{2p^\mu - 2k^\mu}{k^2 - 2(k\cdot p)} - \gamma^\mu \frac{\not p - \not k}{k^2 - 2(k\cdot p)} + \gamma^\mu \frac{m}{k^2 - 2(k\cdot p)} \\
&= \frac{2p^\mu - k^\mu}{k^2 - 2(k\cdot p)} - \gamma^\mu \frac{\not p - m}{k^2 - 2(k\cdot p)} - \frac{k^\mu - \gamma^\mu \not k}{k^2 - 2(k\cdot p)} \\
&= \frac{2p^\mu - k^\mu}{k^2 - 2(k\cdot p)} - \frac{k_\nu \left(g^{\mu\nu} - \gamma^\mu\gamma^\nu\right)}{k_\nu \left(k^\nu - 2p^\nu\right)} \\
&= \frac{2p^\mu - k^\mu}{k^2 - 2(k\cdot p)} - \frac{e_{k\,\nu} \left(g^{\mu\nu} - \gamma^\mu\gamma^\nu\right)}{e_{k\,\nu} \left(k^\nu - 2p^\nu\right)}
\end{aligned} \tag{2.7}$$

where $k_\nu = |k|\, e_{k\,\nu}$. Its convergence is evident in this form.

Now, if the photon is soft, i.e. its momentum tends to zero, then $\bar{q}_i \cong q_i$ and $p - k \cong p$ giving an approximation for the first term by

$$\frac{2p^\mu - k^\mu}{k^2 - 2(k\cdot p)} \bar{u}_{p'} \Gamma(p, q_i) u_p \tag{2.8}$$

The difference between the approximation and the complete first term is

$$\frac{2p^\mu - k^\mu}{k^2 - 2(k\cdot p)}\, \bar{u}_{p'} \left(\Gamma(p-k, \bar{q}_i) - \Gamma(p, q_i)\right) u_p \tag{2.9}$$

Allthough, this difference seems to tend to zero as $k \to 0$ a very careful treatment of overlapping divergences has to be performed because, as it turns out, this terms might just be as divergent as both terms individually. The reason for this is that one of the q_i might be a soft photon. The new divergences are now related to $\bar{q}_i \to 0$ due to this new photon despite the original q_i being finite. Following Feynman's treatment of gauge invariance in [4] one can interpret this term. If $\Lambda^\mu(p, \bar{q}_i; k)$ is the matrix element for the emission of an additional photon from the internal part of the fermion line as in Fig.2.4c, then

$$k_\mu \Lambda^\mu(p, \bar{q}_i; k) = \Gamma\left(p-k, \bar{q}_i\right) - \Gamma\left(p, q_i\right) \tag{2.10}$$

is a matrix identity. Thus the combination of the contributions of all photon emissions off the initial fermion line and from the interior are contained in

$$\bar{u}_{p'} \left(\Lambda^\mu + \frac{2p^\mu - k^\mu}{k^2 - 2(k\cdot p)} k_\nu \Lambda^\nu\right) u_p \tag{2.11}$$

This is identical to replacing

$$\gamma^\mu \;\to\; g^\mu = \gamma^\mu + \frac{2p^\mu - k^\mu}{k^2 - 2(k\cdot p)}\, \not k \tag{2.12}$$

Interestingly, this emission operator is gauge invariant

$$k_\mu g^\mu = 0$$

Further considering the emission from the internal section of the basic diagram and summing up all momenta $Q = \sum q_i$ interacting with the fermion line before the photon emission then the propagator will be modified as follows

$$\frac{1}{\not p + \not Q - m} \;\rightarrow\; \frac{1}{\not p + \not{\bar Q} - \not k - m}\, g^\mu \frac{1}{\not p + \not{\bar Q} - m} \tag{2.13}$$

Problems arise if both k and $\bar Q$ are small simultaneously, then the single divergent denominator in Γ is replaced by two divergent denominators. This would result in another singularity in one of the q_i-integrations. Fortunately, this additional singularity cancels when combining the two contributions by using (2.12), resulting in

$$\begin{aligned}\frac{1}{(\bar Q - k)^2 + 2(\bar Q - k)\cdot p}\Bigg\{ &-\left(\gamma^\mu + \frac{2p^\mu - k^\mu}{k^2 - 2(k\cdot p)}\not k\right)(\not p + \not{\bar Q} - m) \\ &+ 2\left(\bar Q^\mu + \frac{(2p^\mu - k^\mu)(\bar Q\cdot k)}{k^2 - 2(k\cdot p)}\right) - \frac{1}{2} f\,(\not k, \gamma^\mu)\Bigg\}\frac{1}{\not p + \not{\bar Q} - m}\,.\end{aligned} \tag{2.14}$$

Upon expanding the curly bracket all three terms are well behaved as $\bar Q \to 0$. The first terms cancels the last potentially divergent propagator. The second one vanishes as $\bar Q \to 0$. The third term can be seen to be regular by setting $\bar Q = 0$ in the first propagator. It then reverts to the same form as the finite second term in (2.6). The k integration then is completely convergent at $k = 0$ and the contribution from emission from the interior (2.14) is regular at $\bar Q = 0$. This is especially relevant if $\bar Q$ is comprised of other photons inserted earlier, meaning that the soft limit of different possibly overlapping virtual photons can be taken independently without consequences for the divergence structure.
Adding (2.8) to the contribution from an emission off the final state fermion line gives in the soft limit

$$\left(\frac{2p^\mu - k^\mu}{k^2 - 2(k\cdot p)} + \frac{2p'^\mu + k^\mu}{k^2 + 2(k\cdot p')}\right)\bar u_{p'}\Gamma(p, \bar q_i)u_p \tag{2.15}$$

Here, again, the same analysis of overlapping divergences has to be performed resulting, again, in finite terms only.
Special care has to be taken when the basic interaction contains self energy parts in the external lines. Then, some of the $\bar Q$ may be identically zero. It can be shown that these parts will result in the same wave function renormalisation as in the original matrix element.
If now one wants to lift the restraint to small momentum transfers one has to assume that at least one of the q_i's is large. If then the photon is inserted in the initial external charged line before the first hard interaction it will only appear in the propagators up to that point where the large momentum transfer can absorb the change in k without introducing any divergence. Thus, k can be set zero in those lines and a result like (2.8) will be obtained. The rest of the terms not factorising are infrared finite if all possibilities of insertions before the first hard interaction are summed. The insertions after the last hard interaction may be handled in the same way resulting again in (2.15).
Serious problems only arise if there are more than one hard interactions in the basic matrix element. Here a proof for a factorisation for photons in between both hard interactions cannot be accomplished, but it can be argued that these insertions do not give rise to divergences and, thus, are part of the finite residue. The argument proceeds as follows. When the part of the fermion line where the photon is supposed to be attached to is enclosed

in between two hard interactions, terms form (2.14) can no longer be neglected in the limit $k \to 0$. Especially when $\bar{Q}^2 + 2(\bar{Q} \cdot p)$ is small it gives rise to another singularity. However, such an internal momentum transfer is subject to integration in the matrix element. Thus, the term giving rise to the singularity is a pole in that integration and setting $k \to 0$ does not change its behaviour. It will still be part of the finite residue.
A more precise handling of the factorisation of photons in such multiple hard interactions is offered in [7] and [8].
This can be summarised in the following way. If one end of a virtual photon is inserted in an external fermion line in all possible ways, there are two types of contributions. The first is the original matrix element times a factor

$$R^\mu(p, p', k) = \left(\frac{2p^\mu - k^\mu}{k^2 - 2(k \cdot p)} + \frac{2p'^\mu + k^\mu}{k^2 + 2(k \cdot p')} \right) . \tag{2.16}$$

This factor is gauge invariant

$$k_\mu R^\mu = 0$$

and provides a natural high-energy cut-off for the photon momentum ($R^\mu \to 0$ as $k^\mu \to \infty$). The second contribution is a residue which is finite in the limit when the photon turns soft. This residue contains all subtleties of the exact matrix element, i.e. spin correlations, interference terms and the high energy behaviour, nonrelevant in the soft limit.
The results obtained in the preceding arguments can be generalised to photon emission off any charged line. Even double photon vertices in scalar QED and the electroweak coupling to charged vector boson lines give no rise to any extra divergent structure. This can be seen by considering inserting an additional photon to a single photon vertex of a charged scalar line. This insertion does not increase the number of possibly divergent denominators and, therefore, does not produce an additional infrared divergent structure. Its contribution is part of the infrared finite residue.
All preceding arguments did not assume any value for k^2, i.e. whether the end of the photon line inserted belonged to a virtual or a real photon. Therefore, the same analysis can be performed for real photons and the same results will be obtained, only with $k^2 = 0$. Therefore, in the soft limit the factor the basic matrix element is to be multiplied with reads

$$\tilde{R}_\mu(p, p', k) = \left(\frac{p^\mu}{k \cdot p} - \frac{p'^\mu}{k \cdot p'} \right) \tag{2.17}$$

The terms k^μ in the numerator are no longer needed for gauge invariance and can be moved to the infrared finite residue. The complete factorised matrix element for one additional real photon (emitted or absorbed) reads

$$\frac{e}{2(2\pi)^3 k^0} \sum_i \tilde{R}^\mu(p_i, p_i', k) M + \tilde{K}^\mu(k) , \tag{2.18}$$

where the sum runs over all external charged particles. Gauge invariance demands $k_\mu \tilde{K}^\mu = 0$. It is to note, however, that, if there are identical particles in the initial or final state, the single term $\tilde{R}^\mu(p_i, p_i', k)$ is not invariant under interchange of these particles, but their sum is. Thus, the original symmetry of the basic matrix element is preserved.
Comming back to the case of virtual photon emission. Still, the other end of the photon line has to be cared for. If this photon is emitted by an external charged line one has to

differentiate whether this virtual photon terminates on the same or another charged line. If it terminates on a different charged external line the outlined analysis can be carried out separately for both lines resulting in two factors R with the sign of k reversed in one factor. Thus, the original matrix element has to be multiplied by

$$-\frac{ie^2}{2(2\pi)^4 k^2}\sum_{i\neq j} R_\mu(p_i, p_i', k) R^\mu(p_j, p_j', -k)\,. \tag{2.19}$$

The factor $\frac{1}{2}$ comes from statistics to insert both ends to give the same virtual photon and the $\frac{1}{k^2}$ is the remnant of the photon propagator.

If on the other hand now the photon terminates on the same line which emitted it, it will result in an ultraviolet as well as infrared divergent diagram. The ultraviolet divergences either cancel as a consequence of Ward's identity or are handled by renormalisation.
First there is a class of diagrams where one end of the virtual photon line is held fixed and sum over all contributions where the other end terminates before that fixed point. They are illustrated by Fig.2.3a,b,e,f. When the fixed point is on the final state line ultraviolet divergences are handled by renormalisation, if it is in the interior then they cancel by virtue of Ward's identity. Finally, one has to sum over all different postions of the fixed point.
If now the fixed point is in the interior part of the diagram, an insertion of the variable end into the initial state line before the basic interaction will produce a term

$$\begin{aligned}\bar{u}_{p'}\Gamma_2\frac{1}{\not{p}+\not{Q}-m}\gamma_\mu\frac{1}{\not{p}+\not{Q}-\not{k}-m}\Gamma_1\frac{1}{\not{p}-\not{k}-m}\gamma^\mu u_p = \\ \bar{u}_{p'}\Gamma_2\frac{1}{\not{p}+\not{Q}-m}\frac{2\not{p}-\not{k}}{k^2-2(k\cdot p)}\frac{1}{\not{p}+\not{Q}-\not{k}-m}\Gamma_1\frac{1}{\not{p}-\not{k}-m}u_p + K(k)\end{aligned} \tag{2.20}$$

with Γ_1 and Γ_2 being matrices representing the parts of the diagram before and after the fixed point, respectively, and $K(k)$ is, again, finite as $k \to 0$. Thus, Γ used in (2.3) is just the product

$$\Gamma_2\frac{1}{\not{p}+\not{Q}-m}\Gamma_1 \tag{2.21}$$

when k is set to zero. Furthermore, Γ_1 satisfies an indentity similar to (2.10). Thus, this case can be treated as before. Again, there will be a contribution coming from difference between $\Gamma_1(p-k)$ and $\Gamma_1(p)$ that has to be combined with all the contributions from graphs where the variable end of the virtual photon line terminates inside Γ_1 (Fig.2.3f). And again, this will only lead to a substitution of the form (2.12) leading to

$$\begin{aligned}\bar{u}_{p'}\Gamma_2\frac{1}{\not{p}+\not{Q}-m}\Bigg\{\frac{2\not{p}-\not{k}}{k^2-2(k\cdot p)}\left(1+\frac{1}{\not{p}+\not{Q}-\not{k}-m}\not{k}\right) \\ +\gamma_\mu\frac{1}{\not{p}+\not{Q}-\not{k}-m}\gamma^\mu - \frac{2\frac{m^2+(k\cdot p)}{m}}{k^2-2(k\cdot p)}\Bigg\}\frac{1}{\not{p}+\not{Q}-m}\Gamma_1 u_p\,.\end{aligned} \tag{2.22}$$

As before, all terms have to be analysed to determine their behaviour in the infrared limit. The first term equals (2.20) when k is set to zero. The second term equals Fig.2.3f where the photon is emitted and reabsorbed by the same internal line. The third term gives, upon integration, the mass renormalisation. Further, it can be seen that the second part of the

first term combined with the second term has the same structure as (2.13) multiplied by γ_μ from the left resulting in a contribution like (2.14) multiplied by γ_μ from the left. Analysing this new term shows that all of them are either finite or contribute to mass renormalisation. Thus, the curly bracket reduces to

$$\left\{ \frac{2(\not{p}-m)}{k^2-2(k\cdot p)} - \frac{\frac{m\not{k}+2(k\cdot p)}{m}}{k^2-2(k\cdot p)} + \frac{3\not{k}}{k^2-2(k\cdot(p+Q))+Q^2+2(p\cdot Q)} \right\} .$$

The first term is obviously infrared save by virtue of the Dirac equation. The second and the third term are infrared save due to cancellations. To see these it is convenient to use symmetry to make the replacements $\not{k} \to \frac{1}{m^2}\not{p}(k\cdot p)$ in the second term and $\not{k} \to (\not{p}+\not{Q})\frac{(k\cdot(p+Q))}{(p+Q)^2}$ in the third term. These then read

$$-\frac{\frac{1}{m^2}(\not{p}+2m)(k\cdot p)}{k^2-2(k\cdot p)} + \frac{\frac{3}{m^2}(\not{p}+\not{Q})(k\cdot(p+Q))}{k^2-2(k\cdot(p+Q))} .$$

Thus, by the same arguments as in (2.7), these contributions are finite as $k \to 0$. It is to note that it still contains an ultraviolet divergence necessary to cancel another ultraviolet divergence arising later.
There is one case still open for consideration, namely when the fixed point is on a final charged line. One of the graphs arising is shown in Fig.2.3a. Its contribution is

$$\bar{u}_{p'}\frac{2\not{p}-\not{k}}{k^2-2(k\cdot p)}\frac{1}{\not{p}'-\not{k}-m}\Gamma(p-k)u_p + K(k) . \tag{2.23}$$

By the same arguments as before this may be replaced by

$$\frac{(2p-k)\cdot(2p'-k)}{(k^2-2(k\cdot p))(k^2-2(k\cdot p'))}\bar{u}_{p'}\Gamma(p)u_p + K(k) . \tag{2.24}$$

After identifying and removing those parts that belong to the spurious charge renormalisation (they arise when $p = p'$) the sum over all results for photons being emitted and reabsorbed by the same fermion line is found to be

$$-\frac{1}{2}\left(\frac{2p_i^\mu - k^\mu}{k^2-2(k\cdot p_i)} - \frac{2p_i'^\mu - k^\mu}{k^2-2(k\cdot p_i')}\right)^2 , \tag{2.25}$$

where again gauge invariance is apparent.
Therefore, the contribution from emission and absorbtion of the virtual photon by the same charged line is

$$\frac{ie^2}{2(2\pi)^4k^2}\sum_i\left(\frac{2p_i^\mu - k^\mu}{k^2-2(k\cdot p_i)} - \frac{2p_i'^\mu - k^\mu}{k^2-2(k\cdot p_i')}\right)^2 \tag{2.26}$$

which has to be added to the previous result for emission and absorbtion by two distinct lines. Thus, the complete factorised matrix element for virtual photons reads

$$\int \mathrm{d}^4k\,[S(k)\mathcal{M} + K(k)] \tag{2.27}$$

with

$$S(k) = \frac{ie^2}{2(2\pi)^4 k^2}\left[\sum_i \left(\frac{2p_i^\mu - k^\mu}{k^2 - 2(k\cdot p_i)} - \frac{2p_i'^\mu - k^\mu}{k^2 - 2(k\cdot p_i')}\right)^2 \right.$$
$$\left. - 2\sum_{i<j}\left(\frac{2p_i^\mu - k^\mu}{k^2 - 2(k\cdot p_i)} + \frac{2p_i'^\mu + k^\mu}{k^2 + 2(k\cdot p_i')}\right)\left(\frac{2p_j^\mu + k^\mu}{k^2 + 2(k\cdot p_j)} + \frac{2p_j'^\mu - k^\mu}{k^2 - 2(k\cdot p_j')}\right)\right] \tag{2.28}$$

and $K(k)$ finite as $k \to 0$. $\mathcal{M}$ is the matrix element without that photon. Therefore, introducing

$$\alpha B = \int \mathrm{d}^4k\, S(k) \qquad \text{and} \qquad \beta = \int \mathrm{d}^4k\, K(k) \tag{2.29}$$

as the finite residue, the factorised matrix element reads

$$\alpha B\mathcal{M} + \beta\,. \tag{2.30}$$

The factorisation is similar for real photon emission or absorbtion, only differing in the fact that it occurs on the basis of the squared matrix element and $k^2 = 0$, i.e. the photon is on-shell. Therefore, the factorised squared matrix element in the soft limit is

$$\frac{e^2}{(2\pi)^3}\,\delta(k^2)\sum_i \tilde{R}^\mu(p_i, p_i', k)\tilde{R}_\mu(p_i, p_i', k)\,|\mathcal{M}|^2\,, \tag{2.31}$$

or, away from the soft limit keeping the residuals,

$$\int \mathrm{d}^4k\delta(k^2)\left[\tilde{S}(k)\,|\mathcal{M}|^2 + \tilde{K}(k)\right] \tag{2.32}$$

with

$$\tilde{S}(k) = \frac{e^2}{(2\pi)^3}\sum_i\left(\frac{p_i}{(p_i\cdot k)} - \frac{p_i'}{(p_i'\cdot k)}\right)^2 \tag{2.33}$$

and $\tilde{K}(k)$ being finite as $k \to 0$. Therefore, again, introducing

$$\alpha\tilde{B} = \int \mathrm{d}^4k\,\delta(k^2)\,\tilde{S}(k) \qquad \text{and} \qquad \tilde{\beta} = \int \mathrm{d}^4k\,\delta(k^2)\,\tilde{K}(k) \tag{2.34}$$

as the finite residue, the factorised squared matrix element reads

$$\alpha\tilde{B}\,|\mathcal{M}|^2 + \tilde{\beta}\,. \tag{2.35}$$

There is one set of diagrams not included in the preceding discussion: closed charged loops with four or more photon lines coupling to it. If those diagrams would contain divergences they would invalidate the decoupling of the factorisation for real and virtual photons necessary for the exponentiation shown later on. However, these diagrams do not give rise to infrared divergences and are part of the finite residue. To see this let one of the photon momenta go to zero, then the contribution from this diagram vanishes by virtue of the fact that a charged loop with an uneven number of gauge bosons attached to it gives zero. This

follows from the fact that this expression can always be obtained by differentiating the expression of one order less with respect to the loop momentum. The integral then is one of a perfect derivative and, thus, gives zero. An important exception are vacuum polarisation loops. Here it gives the proper charge renormalisation.

Finally, it has to be stressed again that in the formalism of Yennie, Frautschi and Suura the factorisation is only rigorously proven for matrix elements containing up to one hard interaction. As discussed, it is reasonable to use the same factorisation in more general cases as well.
When considering photons away from the soft limit it becomes more and more important to include non-infrared terms (typified by β and $\tilde{\beta}$). They are, of course, not general terms but process dependent. Nonetheless, when calculating them another kind of factorisation can be used, the factorisation in the limit of collinear or quasi-collinear emission, cf Sec. 4.

To summarise. It was shown explicitely that the matrix element and the squared matrix element factorise process independently upon insertion of a virtual and real photon, respectively, in every case except in between two hard interactions. In these cases, the factorisation can only argued but not proven in a general case. However, these results facilitate the successive insertion of one virtual or real photon after the other and, hence, the correction of the basic matrix elements to all orders in QED.

2.2 Extraction of Virtual Emission Singularities to All Orders

Now use of the factorisation shown in the preceding section can be made. First repeating the notation for the matrix element

$$\mathcal{M}_{n_R}^{n_V+\frac{1}{2}n_R},$$

where n_R and n_V are the numbers of real and virtual photons, respectively. Thus, $n_V + \frac{1}{2}n_R$ gives the order of α of the matrix element in relation to the undressed matrix element.
Due to the non-selfcoupling of the photons and the finiteness of radiation of charged loops in the limit $k \to 0$ the factorisation for real and virtual photons can be evaluated separately and independently. Now, considering only virtual photons, as depicted in Fig.2.5, and picking, because of their independence, $n_R = 0$ for simplicity,

$$\mathcal{M}_0 = \sum_{n_V=0}^{\infty} \mathcal{M}_0^{n_V}\,. \tag{2.36}$$

Using now the factorisation in the $k \to 0$ limit as follows

$$\mathcal{M}_0^0 = M_0^0 \tag{2.37}$$
$$\mathcal{M}_0^1 = \alpha B M_0^0 + M_0^1 \tag{2.38}$$
$$\mathcal{M}_0^2 = \frac{(\alpha B)^2}{2!} M_0^0 + \alpha B M_0^1 + M_0^2\,, \tag{2.39}$$

where the $M_0^{n_V}$ are the infrared subtracted finite remainders (formerly β) defined as

$$M_0^0 = \mathcal{M}_0^0 \tag{2.40}$$
$$M_0^1 = \mathcal{M}_0^1 - \alpha B M_0^0 \tag{2.41}$$
$$M_0^2 = \mathcal{M}_0^2 - \alpha B M_0^1 - \frac{(\alpha B)^2}{2!} M_0^0\,. \tag{2.42}$$

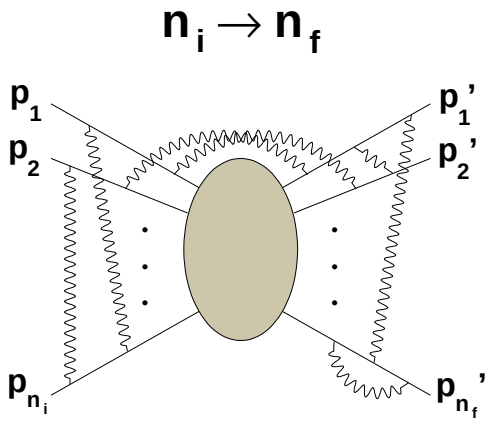

Figure 2.5: All virtual corrections to the basic matrix element

Thus, it holds

$$\mathcal{M}_0^{n_V} = \sum_{r=0}^{n_V} M_0^{n_V - r} \frac{(\alpha B)^r}{r!} \tag{2.43}$$

and for the IR subtracted matrix element

$$M_0^{n_V} = \mathcal{M}_0^{n_V} - \sum_{r=1}^{n_V} M_0^{n_V - r} \frac{(\alpha B)^r}{r!} \,. \tag{2.44}$$

After some rearrangement it follows that

$$\mathcal{M}_0 = \sum_{n_V} \mathcal{M}_0^{n_V} = \exp(\alpha B) \sum_{n_V=0}^{\infty} M_0^{n_V} \tag{2.45}$$

or

$$|\mathcal{M}_0|^2 = \exp(2\alpha B) \left| \sum_{n_V=0}^{\infty} M_0^{n_V} \right|^2 \,. \tag{2.46}$$

Since these derivations are independent of the number of emitted real photons, the generalisation to any number of emitted real photos is trivial, namely

$$|\mathcal{M}_{n_R}|^2 = \exp(2\alpha B) \left| \sum_{n_V=0}^{\infty} M_{n_R}^{n_V + \frac{1}{2} n_R} \right|^2 \,. \tag{2.47}$$

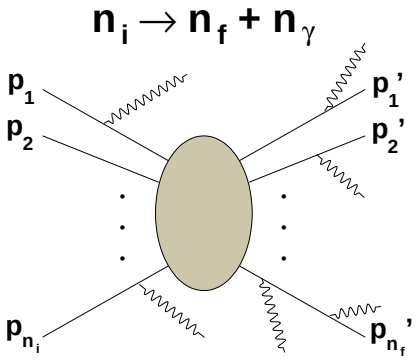

Figure 2.6: All real corrections to the basic matrix element

In this notation of the summed up virtual contribution the terms of different IR-behaviour are separated: while all the M_0^{nV} are IR-finite the term B contains the total singular behaviour. Its structure is:

$$\begin{aligned} B &= \frac{i}{8\pi^3}\int\frac{\mathrm{d}^4k}{k^2+i\epsilon}\left(\sum_{i=1}^{n_C}\frac{Z_i^2(2p_i-k)^2}{(k^2-2(k\cdot p_i))^2}\right. \\ &\qquad \left. -2\sum_{i<j}^{n_C}\frac{Z_iZ_j\theta_i\theta_j(2p_i\theta_i-k)\cdot(2p_j\theta_j+k)}{(k^2-2(k\cdot p_i)\theta_i)(k^2+2(k\cdot p_j)\theta_j)}\right) \qquad (2.48) \\ &= -\frac{i}{8\pi^3}\int\frac{\mathrm{d}^4k}{k^2+i\epsilon}\sum_{i<j}Z_iZ_j\theta_i\theta_j\left(\frac{2p_i\theta_i-k}{k^2-2(k\cdot p_i)\theta_i}+\frac{2p_j\theta_j+k}{k^2+2(k\cdot p_j)\theta_j}\right), \qquad (2.49) \end{aligned}$$

where $\sum\theta_i\mathrm{Z}_i = 0$ has been used. Inserting the matrix element with the extracted soft virtual singularities into the equation for the cross section gives

$$\begin{aligned} \sigma \sim \sum_{n_R=0}^{\infty}\frac{1}{n_R!}\int\mathrm{d}\Phi_{p_f}\mathrm{d}\Phi_k\,(2\pi)^4\,\delta^4\left(\sum p_i-\sum p_f-\sum k\right) \\ \times\exp(2\alpha B)\left|\sum_{n_V=0}^{\infty}M_{n_R}^{n_V+\frac{1}{2}n_R}\right|^2. \qquad (2.50) \end{aligned}$$

To emphasise again, the matrix element is now free of singularities due to virtual photons whose momentum tends to zero, they are extracted in the factor B. It still contains singularities due to soft real photons.

2.3 Exraction of Real Emission Singularities to All Orders

Because photons do not couple to photons, real emission can be considered exclusively, as depicted in Figure 2.6. For $k \to 0$ the matrix element of a single photon emission factorises

as shown in Section 2.1, Eq. 2.18.

$$|\mathcal{M}_1|^2 = -e^2 \left(\sum_{i=0}^{n_C} \frac{Z_i \theta_i p_i}{(p_i \cdot k)} \right)^2 |\mathcal{M}_0|^2 \equiv 2(2\pi)^3 \tilde{S}(k) \, |\mathcal{M}_0|^2 \tag{2.51}$$

and thus also

$$|M_1|^2 = 2(2\pi)^3 \tilde{S}(k) \, |M_0|^2 \ . \tag{2.52}$$

This factorisation in the IR limit can be used to define the completely IR finite quantities $\tilde{\beta}_{n_R}^{n_V+n_R}(k)$ for all k by

$$\frac{1}{2(2\pi)^3} \left| \sum_{n_V=0}^{\infty} M_1^{n_V+\frac{1}{2}} \right|^2 = \tilde{S}(k) \left| \sum_{n_V=0}^{\infty} M_0^{n_V} \right|^2 + \sum_{n_V=0}^{\infty} \tilde{\beta}_1^{n_V+1}(k) \tag{2.53}$$

and

$$\tilde{\beta}_1 = \sum_{n_V=0}^{\infty} \tilde{\beta}_1^{n_V+1}(k) = \frac{1}{2(2\pi)^3} \left| \sum_{n_V=0}^{\infty} M_1^{n_V+\frac{1}{2}} \right|^2 - \tilde{S}(k) \left| \sum_{n_V=0}^{\infty} M_0^{n_V} \right|^2 , \tag{2.54}$$

giving, up to $\mathcal{O}(\alpha)$,

$$\tilde{\beta}_1^1 = \frac{1}{2(2\pi)^3} M_1^{\frac{1}{2}} {M_1^{\frac{1}{2}}}^* - \tilde{S}(k) M_0^0 M_0^{0*} \, . \tag{2.55}$$

By analogy the $\tilde{\beta}_0^{n_V}$'s are defined,

$$\tilde{\beta}_0 = \sum_{n_V=0}^{\infty} \tilde{\beta}_0^{n_V} = \left| \sum_{n_V=0}^{\infty} M_0^{n_V} \right|^2 . \tag{2.56}$$

This can be generalised to higher real photon multiplicities.

$$\begin{aligned} \left(\frac{1}{2(2\pi)^3} \right)^{n_R} \left| \sum_{n_V=0}^{\infty} M_{n_R}^{n_V+\frac{1}{2}n_R} \right|^2 &= \tilde{\beta}_0 \prod_{i=1}^{n_R} \tilde{S}(k_i) \\ &+ \sum_{i=1}^{n_R} \frac{\tilde{\beta}_1(k_i)}{\tilde{S}(k_i)} \prod_{j=1}^{n_R} \tilde{S}(k_j) \\ &+ \sum_{\substack{i,j=1 \\ i \neq j}}^{n_R} \frac{\tilde{\beta}_2(k_i,k_j)}{\tilde{S}(k_i)\tilde{S}(k_j)} \prod_{l=1}^{n_R} \tilde{S}(k_l) \qquad (2.57) \\ &+ \cdots \\ &+ \sum_{i=1}^{n_R} \tilde{S}(k_i) \ \tilde{\beta}_{n_R-1}(k_1, \cdots, k_{i-1}, k_{i+1}, \cdots, k_{n_R}) \\ &+ \tilde{\beta}_{n_R}(k_1, \cdots, k_{n_R}) \qquad (2.58) \end{aligned}$$

As can be seen, formally the same thing happened as in the virtual part. The divergences are contained in the factors $\tilde{S}(k)$, while all $\tilde{\beta}_{n_R}$ are IR finite. Furthermore, strictly speaking, all $\tilde{\beta}_{n_R}$ are only defined if momentum conservation holds, namely $\sum p_i = \sum p_f + \sum k$. This

is important to keep in mind when they are inserted in the integral of the cross section where they are integrated over all possible final state momenta.
Now, this expression has to be put back into the equation for the cross section. For simplicity, to reduce the length of the formulae and to increase readability only terms up to $\mathcal{O}(\alpha)$ are taken, namely only the terms with $\tilde{\beta}_0^0$, $\tilde{\beta}_0^1$ and $\tilde{\beta}_1^1$.

$$\left(\frac{1}{2(2\pi)^3}\right)^{n_R}\left|M_{n_R}^{n_V+\frac{1}{2}n_R}\right|^2 = \left(\tilde{\beta}_0^0+\tilde{\beta}_0^1\right)\prod_{i=1}^{n_R}\tilde{S}(k_i)+\sum_{i=1}^{n_R}\frac{\tilde{\beta}_1^1(k_i)}{\tilde{S}(k_i)}\prod_{j=1}^{n_R}\tilde{S}(k_j)+\mathcal{O}(\alpha^2) \quad (2.59)$$

will be inserted to give the cross section as

$$\begin{aligned}\sigma_{n_R} &\sim \frac{1}{n_R!}\int \mathrm{d}\Phi_{p_f}\mathrm{d}\Phi_k(2\pi)^4\delta^4(\sum p_i-\sum p_f-\sum k)e^{2\alpha B}\\ &\quad\times\left\{\left[\tilde{\beta}_0^0+\tilde{\beta}_0^1\right]\prod_{i=1}^{n_R}\tilde{S}(k_i)+\sum_{i=1}^{n_R}\frac{\tilde{\beta}_1^1(k_i)}{\tilde{S}(k_i)}\prod_{j=1}^{n_R}\tilde{S}(k_j)\right\}+\mathcal{O}(\alpha^2)\end{aligned} \quad (2.60)$$

And, therefore, after expressing the δ-function as an exponential,

$$\begin{aligned}\sigma &= \sum_{n_R}\sigma_{n_R}\\ &\sim \sum_{n_R}\frac{1}{n_R!}\int \mathrm{d}\Phi_{p_f}e^{2\alpha B}\int \mathrm{d}y e^{iy(\sum p_i-\sum p_f)}\left(\int\frac{d^3k}{k}\tilde{S}(k)e^{-iyk}\right)^{n_R}\left[\tilde{\beta}_0^0+\tilde{\beta}_0^1\right]\\ &\quad+\sum_{n_R-1}\frac{1}{(n_R-1)!}\int \mathrm{d}\Phi_{p_f}e^{2\alpha B}\int \mathrm{d}y\frac{d^3K}{K}e^{iy(\sum p_i-\sum p_f-K)}\\ &\qquad\qquad\times\left(\int\frac{\mathrm{d}^3k}{k}\tilde{S}(k)e^{-iyk}\right)^{n_R-1}\tilde{\beta}_1^1(K)\\ &\quad+\mathcal{O}(\alpha^2)\end{aligned} \quad (2.61)$$

$$\begin{aligned}&= \int \mathrm{d}y\int d\Phi_{p_f}e^{2\alpha B}e^{iy(\sum p_i-\sum p_f)+\int\frac{d^3k}{k}\tilde{S}(k)e^{-iyk}}\\ &\qquad\qquad\times\left[\tilde{\beta}_0^0+\tilde{\beta}_0^1+\int\frac{d^3K}{K}e^{-iyK}\tilde{\beta}_1^1(K)\right]+\mathcal{O}(\alpha^2)\end{aligned} \quad (2.62)$$

As before, all singularities due to virtual photons are contained in B, while all singularities due to real emissions are incorporated in the integral over $\tilde{S}(k)$. To restore the momentum conserving δ-function the divergences have to be split off this integral. This can be done by simply subtracting the terms that are divergent for $k\to 0$. To this end, a small "soft" region Ω is defined together with an infrared-safe function $D(\Omega)$[1], such that

$$\begin{aligned}&\int\frac{\mathrm{d}^3k}{k}\,\tilde{S}(k)e^{-iyk}\\ &= \int\frac{\mathrm{d}^3k}{k}\left\{\tilde{S}(k)\left[\Big(1-\Theta(k,\Omega)\Big)+e^{-iyk}\Theta(k,\Omega)+\Big(e^{-iyk}-1\Big)\Big(1-\Theta(k,\Omega)\Big)\right]\right\}\\ &= 2\alpha\tilde{B}(\Omega)+D(\Omega)\end{aligned} \quad (2.63)$$

[1] Obviously $\Theta(k,\Omega)$ divides the phase space into two regions. While Ω comprises the region containing the infrared divergence, $(1-\Omega)$ is completely free of those divergences. Hence, $\Theta(k,\Omega)=1$ if $k\notin\Omega$ and zero otherwise. Thus, $D(\Omega)$ is IR save and $\tilde{B}(\Omega)$ contains the divergence.

where

$$\begin{aligned} D(\Omega) &= \int \frac{\mathrm{d}^3k}{k}\,\tilde{S}(k)\left[\left(e^{-iyk}-1\right)\left(1-\Theta(k,\Omega)\right)+e^{-iyk}\Theta(k,\Omega)\right] \\ &\xrightarrow{\Omega\to 0} \int \frac{\mathrm{d}^3k}{k}\,\tilde{S}(k)\,e^{-iyk}\,\Theta(k,\Omega) \end{aligned} \tag{2.64}$$

and

$$2\alpha\tilde{B}(\Omega) = \int \frac{\mathrm{d}^3k}{k}\,\tilde{S}(k)\,(1-\Theta(k,\Omega)) = \int\limits_{\Omega} \frac{\mathrm{d}^3k}{k}\,\tilde{S}(k)\,. \tag{2.65}$$

This definition of $\tilde{B}(\Omega)$ coincides with its previous schematic introduction in Eq. (2.34) when Ω comprises the whole photon phase space.

Reinserting this into the cross section gives

$$\begin{aligned} \sigma \sim \int \mathrm{d}y \int \mathrm{d}\Phi_{p_f} e^{2\alpha(B+\tilde{B}(\Omega))} e^{iy(\sum p_i - \sum p_f)+\int \frac{\mathrm{d}^3k}{k}\tilde{S}(k)e^{-iyk}\Theta(k,\Omega)} \\ \times \left(\tilde{\beta}_0^0+\tilde{\beta}_0^1+\int \frac{d^3K}{K}e^{-iyK}\tilde{\beta}_1^1\right)+\mathcal{O}(\alpha^2) \end{aligned} \tag{2.66}$$

After reexpansion of the exponentiated integral

$$\exp\left(\int \frac{\mathrm{d}^3k}{k}\tilde{S}(k)e^{-iyk}\Theta(k,\Omega)\right) = \sum_{n_R}\frac{1}{n_R!}\int \mathrm{d}\Phi_k \prod_{i=1}^{n_R}\tilde{S}(k_i)e^{-iyk_i}\Theta(k,\Omega) \tag{2.67}$$

for the $\tilde{\beta}_0^0$- and $\tilde{\beta}_0^1$-terms and

$$\exp\left(\int \frac{d^3k}{k}\tilde{S}(k)e^{-iyk}\Theta(k,\Omega)\right)$$

$$= \sum_{i=1}^{n_R}\sum_{n_R-1}\frac{1}{(n_R-1)!}\int \mathrm{d}\Phi_k \prod_{j\neq i}^{n_R}\tilde{S}(k_j)e^{-iyk_j}\Theta(k,\Omega) \tag{2.68}$$

$$= n_R\sum_{n_R-1}\frac{1}{(n_R-1)!}\int \mathrm{d}\Phi_k \prod_{j\neq i}^{n_R}\tilde{S}(k_j)e^{-iyk_j}\Theta(k,\Omega) \tag{2.69}$$

$$= \sum_{n_R-1}\frac{1}{n_R!}\int \mathrm{d}\Phi_k \prod_{j\neq i}^{n_R}\tilde{S}(k_j)e^{-iyk_j}\Theta(k,\Omega) \tag{2.70}$$

for the $\tilde{\beta}_1^1$-term, the δ-functions can be restored and the cross section reads

$$\begin{aligned}
\sigma \;\sim\; & \sum_{n_R} \frac{1}{n_R!} \int \mathrm{d}\Phi_{p_f} \mathrm{d}\Phi_k (2\pi)^4 \delta^4 \left(\sum p_i - \sum p_f - \sum k \right) e^{2\alpha(B+\tilde{B}(\Omega))} \\
& \qquad \times \prod_{i=1}^{n_R} \tilde{S}(k_i) \Theta(k,\Omega) \left[\tilde{\beta}_0^0 + \tilde{\beta}_0^1 \right] \\
& + \sum_{n_R-1} \frac{1}{n_R!} \int \mathrm{d}\Phi_{p_f} \mathrm{d}\Phi_k (2\pi)^4 \delta^4 \left(\sum p_i - \sum p_f - \sum k \right) e^{2\alpha(B+\tilde{B}(\Omega))} \\
& \qquad \times \prod_{i=1}^{n_R} \tilde{S}(k_i) \Theta(k,\Omega) \sum_{i=1}^{n_R} \frac{\tilde{\beta}_1^1(k_i)}{\tilde{S}(k_i)} \qquad (2.71) \\
= \; & \sum_{n_R} \frac{1}{n_R!} \int \mathrm{d}\Phi_{p_f} \mathrm{d}\Phi_k (2\pi)^4 \delta^4 \left(\sum p_i - \sum p_f - \sum k \right) e^{2\alpha(B+\tilde{B}(\Omega))} \\
& \qquad \times \prod_{i=1}^{n_R} \tilde{S}(k_i) \Theta(k,\Omega) \left[\tilde{\beta}_0^0 + \tilde{\beta}_0^1 + \sum_{i=1}^{n_R} \frac{\tilde{\beta}_1^1(k_i)}{\tilde{S}(k_i)} \right] + \mathcal{O}(\alpha^2) \,. \qquad (2.72)
\end{aligned}$$

The preceding calculations are general and identical for any squared matrix element integrated over all possible final state configurations. Thus, they are directly applicable to the case of interest in this work: particle decays. However, the quantity needed is not the cross section of the reaction but the decay rate of some particle. Consequently, the fully inclusive decay rate reads

$$\begin{aligned}
\Gamma \;=\; & \frac{1}{2M} \sum_{n_R} \frac{1}{n_R!} \int \mathrm{d}\Phi_{p_f} \mathrm{d}\Phi_k (2\pi)^4 \delta^4 \left(\sum p_i - \sum p_f - \sum k \right) e^{2\alpha(B+\tilde{B}(\Omega))} \\
& \qquad \times \prod_{i=1}^{n_R} \tilde{S}(k_i) \Theta(k,\Omega) \left[\tilde{\beta}_0^0 + \tilde{\beta}_0^1 + \sum_{i=1}^{n_R} \frac{\tilde{\beta}_1^1(k_i)}{\tilde{S}(k_i)} \right] + \mathcal{O}(\alpha^2) \,, \qquad (2.73)
\end{aligned}$$

wherein M is mass of the initial state, i.e. the decaying particle.
The explicit form of the infrared subtracted squared matrix elements up to $\mathcal{O}(\alpha)$ is

$$\begin{aligned}
\tilde{\beta}_0^0 &= M_0^0 M_0^{0\,*} \\
\tilde{\beta}_0^1 &= M_0^0 M_0^{1\,*} + M_0^1 M_0^{0\,*} \\
\tilde{\beta}_1^1 &= \frac{1}{2(2\pi)^3} \, M_1^{\frac{1}{2}} M_1^{\frac{1}{2}\,*} - \tilde{S}(k) \, M_0^0 M_0^{0\,*} \,. \qquad (2.74)
\end{aligned}$$

The whole factorisation scheme is independent of possible spin correlations in the undressed matrix element. Thus, the same result would be obtained if $|\mathcal{M}|^2$ would have had the form $\rho_{\alpha\beta} \mathcal{M}^\alpha \mathcal{M}^{\beta\,*}$ where $\rho_{\alpha\beta}$ is a spin density matrix. This parallels the fact that soft photon radiation (real and virtual) is blind regarding the spin of the line which emitted it.
In terms of spin correlated matrix elements the infrared safe squared matrix elements up to $\mathcal{O}(\alpha)$ read

$$\begin{aligned}
\tilde{\beta}_0^0 &= \rho_{\alpha\beta} \, \mathcal{M}_0^{0\alpha} \mathcal{M}_0^{0\beta\,*} \\
\tilde{\beta}_0^1 &= \rho_{\alpha\beta} \left(\mathcal{M}_0^{0\alpha} \mathcal{M}_0^{1\beta\,*} + \mathcal{M}_0^{1\alpha} \mathcal{M}_0^{0\beta\,*} - 2\alpha B \, \mathcal{M}_0^{0\alpha} \mathcal{M}_0^{0\beta\,*} \right) \\
\tilde{\beta}_0^1 &= \rho_{\alpha\beta} \left(\frac{1}{2(2\pi)^3} \mathcal{M}_1^{\frac{1}{2}\alpha} \mathcal{M}_1^{\frac{1}{2}\beta\,*} - \tilde{S}(k) \, \mathcal{M}_0^{0\alpha} \mathcal{M}_0^{0\beta\,*} \right) .
\end{aligned}$$

3 The Algorithm

3.1 The Master Formula

The basic, undressed matrix element (no additional photons) reads

$$2M\,\Gamma_0 = \int \mathrm{d}\Phi_q\,(2\pi)^4\delta^4(p_C + p_N - Q_C - Q_N)\,|\mathcal{M}|^2 \tag{3.1}$$

where the phase space element for the outgoing momenta $q \in \{Q_C,\, Q_N\}$ is given by

$$\mathrm{d}\Phi_q = \prod_{i=1}^{n} \frac{\mathrm{d}^3 q_i}{(2\pi^3)2q_i^0}\,. \tag{3.2}$$

Here, and in the following, the initial and final state momenta have been classified to whether the respective particles are charged or neutral: p_C denotes the sum of all charged, p_N the sum of all neutral initial state particle momenta while Q_C is the sum of all charged and Q_N is the sum of all neutral final state momenta. After QED corrections, the Q_C and Q_N will become P_C and P_N, respectively. K is the sum of all additional real, resolved Bremsstrahlungs-photons generated in the process, whereas photons already present in the core process are included in P_N and Q_N, respectively.
In the previous section the factorisation of infrared divergent terms and the construction of infrared-finite expressions for cross sections with all possible numbers of resolved photons has been discussed. In these expressions the universal, process-independent parts of the QED corrections have been separated and exponentiated, the residual process dependence and the effect of particle spins etc. has been absorbed in infrared-finite, subtracted terms $\tilde{\beta}$, cf. Eq. (2.72). With small changes in the notation this form of the decay rate thus reads

$$2M\,\Gamma \;=\; \sum_{n_\gamma} \frac{1}{n_\gamma!} \int \mathrm{d}\Phi\; e^{Y(\Omega)} \prod_{i=1}^{n_\gamma} \tilde{S}(k_i)\Theta(k_i,\Omega)\,\tilde{\beta}_0^0\,\mathcal{C}\,. \tag{3.3}$$

Here, the phase space has been separated into a phase space element for the particles of the "core" process and one for the additional n_γ resolved real photons,

$$\mathrm{d}\Phi = \mathrm{d}\Phi_p\,\mathrm{d}\Phi_k\,(2\pi)^4\delta\,(p_C + p_N - P_C - P_N - K)\,. \tag{3.4}$$

with

$$\mathrm{d}\Phi_p \;=\; \prod_{i=1}^{n} \frac{\mathrm{d}^3 p_i}{(2\pi)^3 2p_i^0} \tag{3.5}$$

$$\mathrm{d}\Phi_k \;=\; \prod_{i=1}^{n_\gamma} \frac{\mathrm{d}^3 k}{k^0} \tag{3.6}$$

Note that the factor $\frac{1}{2(2\pi)^3}$, missing in the photon phase space element, has already been incorporated in the eikonal factor $\tilde{S}(k)$, in accordance with the choice made in [2]. In the equation above, Eq. (3.3), the undressed matrix element $\tilde{\beta}_0^0$ has been factorised and the remainder of the perturbative expansion in α has been combined in the factor $\mathcal{C}$.

$$\mathcal{C} = 1 + \frac{1}{\tilde{\beta}_0^0}\left(\tilde{\beta}_0^1 + \sum_{i=1}^{n_\gamma}\frac{\tilde{\beta}_1^1(k_i)}{\tilde{S}(k_i)} + \mathcal{O}(\alpha^2)\right) \tag{3.7}$$

Furthermore, the YFS-Form-Factor has been introduced

$$Y(\Omega) = \sum_{i<j} Y_{ij}(\Omega) = \sum_{i<j} 2\alpha\left(B_{ij} + \tilde{B}_{ij}(\Omega)\right) \tag{3.8}$$

where the sum runs over all pairs of charged particles. The infrared factors B_{ij} and $\tilde{B}_{ij}$ are defined as

$$B_{ij} = -\frac{i}{8\pi^3} Z_i Z_j \theta_i \theta_j \int \mathrm{d}^4k \frac{1}{k^2}\left(\frac{2p_i\theta_i - k}{k^2 - 2(k\cdot p_i)\theta_i} + \frac{2p_j\theta_j + k}{k^2 + 2(k\cdot p_j)\theta_j}\right)^2 \tag{3.9}$$

$$\tilde{B}_{ij}(\Omega) = \frac{1}{4\pi^2} Z_i Z_j \theta_i \theta_j \int d^4k \delta(k^2)\left(1 - \Theta(k,\Omega)\right)\left(\frac{p_i}{p_i\cdot k} - \frac{p_j}{p_j\cdot k}\right)^2 . \tag{3.10}$$

They are the same quantities as defined in the last section, cf. Eqs. (2.30) and (2.34)/(2.65), generalised to arbitrary processes. Both contain the virtual and real infrared divergences, respectively. These divergences cancel according to the Kinoshita-Lee-Nauenberg theorem [5, 6]. Thus, each $Y_{ij}(\Omega)$ is guaranteed to be finite, which is explicitly shown in Appendix C. In the terms above, Z_i and Z_j are the charges of the particles i and j in terms of the positron charge e, and the signature factors $\theta = \pm 1$ for particles in the final or initial state, respectively. The symbol Θ, already defined at the end of section 2, refers to a phase space constraint with Ω denoting the soft, unresolvable region of photon radiation. Hence, $\Theta(k,\Omega) = 1$ if $k \notin \Omega$ and zero otherwise. If this division is done by defining an energy cut-off, the definition of Ω is not Lorentz-invariant and the frame in which this cut-off forms a flat hypersurface also needs to be specified. The advantage of splitting the photon phase space in that manner lies in the alleviation of integrating $\tilde{S}(k)$ over k. If the cut-off is defined in the frame the photon generation and momentum reconstruction will be done in[1] then the integration over the photon energy separates from the angular integration (see Appendix F), leading to yet another simplification of the calculation.
The eikonal factor $\tilde{S}(k)$ has already been introduced in the last section. It is defined as

$$\tilde{S}(k) = \sum_{i<j}\tilde{S}_{ij}(k) = \frac{\alpha}{4\pi^2}\sum_{i<j} Z_i Z_j \theta_i\theta_j\left(\frac{p_i}{p_i\cdot k} - \frac{p_j}{p_j\cdot k}\right)^2 . \tag{3.11}$$

However, despite all terms being finite in Eq. (3.3), it cannot be used straight away for Monte Carlo generation. This is because it is written in terms of the already corrected final state momenta p_i and not the original undressed momenta q_i. The problem here is that the undressed momenta are defined in an n-body phase space whereas the dressed momenta are part of an $(n+n_\gamma)$-body phase space. This necessitates a mapping procedure of the n-body

[1] In the algorithm presented here, this will be the rest frame of the multipole, i.e. the combined rest frame of all charged particles $p_C + P_C$.

onto the $(n + n_\gamma)$-body phase space. In principle, details of this mapping procedure are irrelevant as long as it respects the soft limit of photon radiation not altering the original kinematics, i.e. in this limit the momenta of the original particles in the $(n+n_\gamma)$-body phase space have to fall exactly onto those of the n-body phase space.

3.2 Phase Space Transformation

To solve this, consider the rest frame of all charged particles involved in the basic matrix element

$$P_M = p_C + P_C \,. \tag{3.12}$$

These particles form the multipole responsible for the Bremsstrahlung of the additional photons. In the rest frame of this multipole, a simple form of the mapping consists of a mere rescaling of the three-momenta of all final state particles by a common factor u such that the additional photons are accommodated. Clearly, the initial state momenta cannot be altered, because they have already been fixed when the basic matrix element was calculated. So, the task is to rewrite Eq. (3.4), explicitly in the rest frame of the multipole in question. The necessary transformations are detailed in the appendix, cf. App. D.1, here it suffices to give the result. It reads

$$\begin{aligned} \mathrm{d}\Phi &= \mathrm{d}\Phi_p \, \mathrm{d}\Phi_k \, (2\pi)^4 \delta \left(p_C + p_N - P_C - P_N - K\right) \\ &= \prod_{i=1}^{n} \left[\frac{\mathrm{d}^3 p_i}{(2\pi)^3 2p_i^0}\right] \prod_{i=1}^{n_\gamma} \left[\frac{\mathrm{d}^3 k}{k^0}\right] (2\pi)^4 \delta \left(p_C + p_N - P_C - P_N - K\right) \\ &= \mathrm{d}\Phi_p \, \mathrm{d}\Phi_k \, \frac{m_{M,p}^3}{M^2 (P_C^0 + P_N^0 + K^0)} \, (2\pi)^3 \delta^3(\vec{P}_M) \, (2\pi) \delta \left(P_M^0 - P_C^0 - p_C^0\right) \end{aligned} \tag{3.13}$$

In a similar fashion, the phase space related to the zeroth order uncorrected cross section can be transformed to

$$\begin{aligned} \mathrm{d}\Phi_0 &= (2\pi)^4 \mathrm{d}\Phi_q \, \delta^4 \left(p_C + p_N - Q_C - Q_N\right) \\ &= \frac{m_{M,q}^3}{M^2 (Q_C^0 + Q_N^0)} \, \mathrm{d}\Phi_q \, (2\pi)^3 \delta^3(\vec{Q}_M) \, (2\pi) \delta \left(Q_M^0 - Q_C^0 - p_C^0\right) \,. \end{aligned} \tag{3.14}$$

In both cases, $m_{M,p}$ ($m_{M,q}$) is the invariant mass of the uncorrected multipole and the vector components P_C^0 and P_N^0 (Q_C^0 and Q_N^0) are taken in the P_M (Q_M) rest frame. The Jacobian emerging in both cases will ultimately find its way into a correction weight in the Monte Carlo realisation of the method.

3.3 Mapping of Momenta

As mentioned before, the mapping procedure still has to be defined in detail to reconstruct the particles' momenta. The basic ideas of the mapping procedure suggested here are as follows: When representing all four-vectors in the rest frame of the multipole

- treat all final state momenta equally

- scale their three-momenta by a common factor u
- distribute the photon momenta
- assign the energy-component of every vector such that momentum conservation and all on-shell conditions are fullfilled

This will ultimately necessitate a change of the initial state momenta as well. However, since they are already fixed for the calculation of the basic matrix element this change will reduce to an alteration of the reconstruction frame during the reconstruction procedure.

However, closer examination reveals that the mapping paradigm above in fact enforces a different treatment for purely neutral and partially or fully charged initial state configurations. The reason is that the momenta of the newly generated Bremsstrahlungs photons need to be balanced. Furthermore, the phase space integral still has to be rewritten in terms of the undressed, original final state momenta defining the original matrix element and cross section without QED radiation. This will be addressed in the next sections, Sec. 3.3.1-3.3.2, where the case of decays, i.e. single initial state particles, either neutral or charged, will be discussed separately. Formally, of course, both treatments will yield identical results, since only the soft limit of photon emission is defined from first principles and because both treatments respect this limit.

3.3.1 Neutral Initial States: Final State Multipoles

The first case to be considered is the case of a neutral particle of mass M decaying into a final state with charged particles. The reconstruction paradigm above completely fixes the reconstruction procedure to a rescaling of all final state momenta, both charged and neutral, and balancing the summed photon momentum K by moving the frame of the multipole and, hence, of the initial state[2]. Denoting, again, with q_i the undressed and with p_i the dressed final state momenta, and denoting their respective sums by Q_C, Q_N, P_C and P_N, as declared earlier, and using K as the summed momentum of all Bremsstrahlungs photons, the reconstruction prescription reads as follows:

- The momenta of the Q_M rest frame

$$\begin{aligned} p_N^\mu &= \left(\sqrt{M^2+\vec{Q}_N^2}, \vec{Q}_N\right) \\ Q_C^\mu &= \left(Q_C^0, \vec{Q}_C = 0\right) \\ Q_N^\mu &= \left(Q_N^0, \vec{Q}_N\right) \end{aligned} \tag{3.15}$$

[2] Note that it is not possible to give any fraction of the photon momentum equally to all final states, while the multipole remains in its rest frame. It therefore is mandatory to balance the photon momentum with the initial state.

will be mapped onto

$$\begin{aligned} p_N^\mu \longrightarrow {p'_N}^\mu &= \left(\sqrt{M^2+(u\vec{Q}_N+\vec{K})^2}, u\vec{Q}_N+\vec{K} = u\vec{p}_N+\vec{K}\right) \\ P_C^\mu &= \left(P_C^0, u\vec{Q}_C = 0\right) \qquad (3.16) \\ P_N^\mu &= \left(P_N^0, u\vec{Q}_N\right) \qquad (3.17) \\ K^\mu &= \left(K^0, \vec{K}\right) \qquad (3.18) \end{aligned}$$

in the P_M rest frame.

- p_N and p'_N are the same physical vector but in different frames. The scaling parameter u now is determined by momentum conservation, i.e.

$$0 = \sqrt{M^2+\left(u\vec{Q}_N+\vec{K}\right)^2} - \sum_C \sqrt{m_i^2+u^2\vec{q}_i^2} - \sum_N \sqrt{m_i^2+u^2\vec{q}_i^2} - K^0\,, \qquad (3.19)$$

where the subscripts C and N in the sums indicate a summation over charged and neutral particles, respectively.

- The phase space element expressed in terms of the undressed final state momenta then reads

$$\begin{aligned} \mathrm{d}\Phi &= (2\pi)^4\,\mathrm{d}\Phi_q\,\mathrm{d}\Phi_k\,\delta^3\left(\vec{Q}_M\right)\delta\left(Q_M^0-Q_C^0-p_C^0\right)\frac{m_{M,p}^3}{M^2\left(P_C^0+P_N^0+K^0\right)} \\ &\quad\times u^{3n-4}\,\frac{\frac{\vec{p}_N^{\,2}}{p_N^0}-\sum_{C,N}\frac{\vec{q}_i^{\,2}}{q_i^0}}{\frac{\vec{p}'_N\vec{p}_N}{p'^0_N}-\sum_{C,N}\frac{\vec{p}_i\vec{q}_i}{p_i^0}}\;\prod_{i=1}^{n}\left[\frac{q_i^0}{p_i^0}\right]. \qquad (3.20) \end{aligned}$$

3.3.2 Charged Initial State: Mixed Multipoles

The other case of relevance in the framework of this publication is the decay of a charged particle of mass M, leading to multipoles containing both initial and final state particles emitting the photons. Again the paradigm above completely fixes the reconstruction procedure. Basically, the problem is to compensate the photon momentum after the final state momenta have been rescaled. This is achieved in the following way:

- The momenta of the Q_M rest frame

$$\begin{aligned} p_C^\mu &= \left(\sqrt{M^2+\vec{Q}_C^2}, -\vec{Q}_C\right) \\ Q_C^\mu &= \left(Q_C^0, \vec{Q}_C\right) \\ Q_N^\mu &= \left(Q_N^0, \vec{Q}_N = -2\vec{Q}_C\right) \qquad (3.21) \end{aligned}$$

will be mapped onto

$$\begin{aligned} p_C^\mu \longrightarrow p_c^{\mu\prime} &= \left(\sqrt{M^2+(u\vec{Q}_C-n_C\vec{\kappa})^2}, -u\vec{Q}_C+n_C\vec{\kappa}=u\vec{p}_C+n_C\vec{\kappa}\right) \\ P_C^\mu &= \left(P_C^0, u\vec{Q}_C-n_C\vec{\kappa}\right) \\ P_N^\mu &= \left(P_N^0, u\vec{Q}_N-n_N\vec{\kappa}=-2u\vec{Q}_C-n_N\vec{\kappa}\right) \\ K^\mu &= \left(K^0,\vec{K}\right) \end{aligned} \tag{3.22}$$

in the P_M rest frame. Here, n_C and n_N are the numbers of charged and neutral final state particles, respectively, and the abbreviation

$$\vec{\kappa}=\frac{1}{2n_C+n_N}\vec{K} \tag{3.23}$$

has been introduced for a more compact notation. Again, p_C and p'_C are the same physical vector represented in different frames, thus specifying the relation between the Q_M and the P_M rest frame. In the soft limit, i.e. for $K\to 0$, the scaling parameter $u\to 1$ and both vectors are identical, as required.

- In general, the scaling parameter is fixed through energy conservation as the solution of

$$\begin{aligned} 0 &= \sqrt{M^2+\left(u\vec{Q}_C-n_C\vec{\kappa}\right)^2}-\sum_C\sqrt{m_i^2+\left(u\vec{q}_i-\vec{\kappa}\right)^2} \\ &\quad -\sum_N\sqrt{m_i^2+\left(u\vec{q}_i-\vec{\kappa}\right)^2}-K^0\,. \end{aligned} \tag{3.24}$$

- The phase space integral rewritten in terms of the q_i reads

$$\begin{aligned} \mathrm{d}\Phi &= (2\pi)^4\,\mathrm{d}\Phi_q\,\mathrm{d}\Phi_k\,\delta^3\left(\vec{Q}_M\right)\delta\left(Q_M^0-Q_C^0-p_C^0\right)\frac{m_{M,p}^3}{M^2\left(P_C^0+P_N^0+K^0\right)} \\ &\quad\times u^{3n-4}\,\frac{\frac{\vec{p}_C^{\,2}}{p_C^0}-\sum_{C,N}\frac{\vec{q}_i^{\,2}}{q_i^0}}{\frac{\vec{p}'_C\vec{p}_C}{p_C^0}-\sum_{C,N}\frac{\vec{p}_i\vec{q}_i}{p_i^0}}\;\prod_{i=1}^n\left[\frac{q_i^0}{p_i^0}\right]. \end{aligned} \tag{3.25}$$

It is worth noting that this is identical to the case of a neutral particle in the initial state.

3.4 Event Generation

Having transformed the phase space integrals allows to write the full cross section including real and virtual QED radiation as

$$\begin{aligned} 2M\,\Gamma &= \sum_{n_\gamma}\frac{1}{n_\gamma!}\int\mathrm{d}\Phi_q\,\mathrm{d}\Phi_k(2\pi)^4\delta^3\left(\vec{Q}_M\right)\delta\left(Q_M^0-Q_C^0-p_C^0\right)\;\tilde{\beta}_0^0\,\mathcal{C}\,e^{Y(\Omega)} \\ &\quad\times\prod_{i=1}^{n_\gamma}\left[\tilde{S}(k_i)\Theta(k_i,\Omega)\right]\;\frac{m_{M,p}^3\,u^{3n-4}}{M^2\left(P_C^0+P_N^0+K^0\right)}\frac{\frac{\vec{p}^{\,2}}{p^0}-\sum_{C,N}\frac{\vec{q}_i^{\,2}}{q_i^0}}{\frac{\vec{p}'\vec{p}}{p'^0}-\sum_{C,N}\frac{\vec{p}_i\vec{q}_i}{p_i^0}}\prod_{i=1}^n\left[\frac{q_i^0}{p_i^0}\right] \end{aligned} \tag{3.26}$$

wherein p and p' now generally stand for the initial state particle.
The zeroth order differential cross section, which will be used by default in all decays in SHERPA can easily be extracted and, employing Eq.(3.14), reads

$$\begin{aligned}\Gamma &= \sum_{n_\gamma} \frac{1}{n_\gamma!} \int \mathrm{d}\Gamma_0 \, \mathrm{d}\Phi_k \, e^{Y(\Omega)} \prod_{i=1}^{n_\gamma} \left[\tilde{S}(k_i)\Theta(k_i,\Omega)\right] \\ &\times \frac{m_{M,p}^3}{m_{M,q}^3} \frac{Q_C^0 + Q_N^0}{P_C^0 + P_N^0 + K^0} \, u^{3n-4} \frac{\frac{\vec{p}^2}{p^0} - \sum_{C,N} \frac{\vec{q}_i^2}{q_i^0}}{\frac{\vec{p}'\vec{p}}{p'^0} - \sum_{C,N} \frac{\vec{p}_i\vec{q}_i}{p_i^0}} \prod_{i=1}^{n} \left[\frac{q_i^0}{p_i^0}\right] \mathcal{C} \,. \end{aligned} \tag{3.27}$$

Up to here no approximations have been made at all. In order to generate the corresponding distribution with Monte Carlo techniques, however, this form is not particularly useful. To simplify the generation therefor, hit-or-miss and reweighting techniques are used, demanding upper bounds for the various pieces:

- All higher orders are neglected, thus setting $\mathcal{C}$ to one.
- The maximum of all Jacobians is given for $K = 0$, coinciding with the leading-order phase space.
- The dependencies on the dressed momenta in the eikonal factors are removed by approximating these factors by those depending on the undressed variables from the generation.

The resulting crude distribution reads

$$\Gamma_{\mathrm{cr}} = \sum_{n_\gamma=0}^{\infty} \frac{1}{n_\gamma!} \int \mathrm{d}\Gamma_0 \, \mathrm{d}\Phi_k \, e^{Y(\omega)} \prod_{i=1}^{n_\gamma} \tilde{S}_q(k_i)\Theta(k_i,\Omega). \tag{3.28}$$

After executing all k-integrations giving

$$\int \prod_{i=1}^{n_\gamma} \frac{\mathrm{d}^3 k_i}{k_i^0} \tilde{S}_q(k_i)\Theta(k_i,\Omega) = \bar{n}^{n_\gamma} \tag{3.29}$$

the YFS-Form-Factor is estimated by

$$Y(\Omega) \approx -\bar{n} \tag{3.30}$$

for suitable choices of Ω [3]. Reinserting this into the cross section, the leading-order cross section can be seperated from the QED radiation,

$$\Gamma_{\mathrm{cr}} = \Gamma_0 \sum_{n_\gamma=0}^{\infty} \left[\frac{1}{n_\gamma!} e^{-\bar{n}} \bar{n}^{n_\gamma}\right] \tag{3.31}$$

The result is the undressed zeroth order cross section times a Poisson distribution with the average photon multiplicity $\bar{n}$. In this factorised state the photon distribution can be separated from the generation of the basic matrix element. If now the basic matrix element is assumed to be already generated it can be corrected for real and virtual photon emissions to all orders by generating the photon distribution as follows:

[3] In this publication (and in the code), this choice has been to limit the photon energies by setting an infrared energy cut-off of 0.1GeV.

1. Generate the number of photons according to the Poisson distribution with mean $\bar{n}$.
2. Generate each photon according to $\tilde{S}_q(k)$. This implies
   - that its energy k^0 is distributed according to
   $$\rho(k^0) \sim \frac{1}{k^0} \tag{3.32}$$
   - and that the azimutal and polar angles are distributed according to
   $$\rho(\theta,\, \phi) \sim \sum_{i<j} \left(\frac{p_i}{p_i \cdot e_k} - \frac{p_j}{p_j \cdot e_k} \right)^2 , \tag{3.33}$$
   where e_k is a null vector of unit length,
   $$e_k^\mu = \frac{1}{k^0} k^\mu \quad \text{with} \quad e_k^2 = 0\,. \tag{3.34}$$
   It is possible that more than one hard photon is created such that the total energy of all photons exceeds the decaying system's energy. Obviously, this has to be avoided to guarantee energy conservation. A simple way of achieving this is a mere veto on such situations, accompanied with a repetition of photon generation, starting from step 1.
3. Reconstruct the momenta.
4. Calculate and apply all weights. This yields a total weight, namely
   $$W = W_{\text{dipole}} \times W_{\text{YFS}} \times W_{\text{J,L}} \times W_{\text{J,M}} \times W_{\mathcal{C}}\,, \tag{3.35}$$
   where the individual weights are given by
   $$W_{\text{dipole}} = \prod_{i=1}^{n_\gamma} \frac{\tilde{S}(p_C, P_C, k_i)}{\tilde{S}(p_C, Q_C, k_i)} \tag{3.36}$$
   $$W_{\text{YFS}} = \exp\left(Y(p_C, P_C, \Omega) + \bar{n}\right) \tag{3.37}$$
   $$W_{\text{J,L}} = \frac{m_{M,p}^3}{m_{M,q}^3} \frac{Q_C^0 + Q_N^0}{P_C^0 + P_N^0 + K^0} \tag{3.38}$$
   $$W_{\text{J,M}} = u^{3n-4} \frac{\frac{\vec{p}^2}{p^0} - \sum_{C,N} \frac{\vec{q}_i^2}{q_i^0}}{\frac{\vec{p}'\vec{p}}{p'^0} - \sum_{C,N} \frac{\vec{p}_i \vec{q}_i}{p_i^0}} \prod_{i=1}^{n} \left(\frac{q_i^0}{p_i^0} \right) \tag{3.39}$$
   $$W_{\mathcal{C}} = \mathcal{C} \tag{3.40}$$
   Here, W_{dipole} corrects the emitting dipoles from the unmapped to the mapped momenta, W_{YFS} accounts for the exact YFS form factor, $W_{\text{J,L}}$ essentially denotes the Jacobian due to the Lorentz-transformation, $W_{\text{J,M}}$ is the weight due the momenta-mapping, and $W_{\mathcal{C}}$ incorporates higher-order corrections, where available.

   The maximum of the combined weight indeed is smaller than the maximal weight employed for generating the distribution, $W < W(K = 0)$. Hence application of the combined weight is just a realisation of a hit-or-miss method. The distribution obtained is now the exact distribution of (3.3) or (3.27).

4 Higher Order Corrections

In the last section, the procedure generating the QED corrections to cross sections, following Eq. (2.72), has been outlined. By construction, the algorithm yields exact all-orders results, if all matrix elements are known. This, however, is never the case. On the other hand, the dominant universal soft photon contributions, real and virtual, are included to all orders in the YFS-Form-Factor, Eq. (3.8). Thus, if the basic undressed matrix element only is known, i.e. if $\mathcal{C} = 1$, the photons will be solely generated according to a product of eikonal factors $\tilde{S}(k_i)$. Consequently, their distribution will be correct in the soft limit only. Away from this limit, exact matrix elements at a given order may be mandatory to yield satisfactory and sufficient accuracy. For most applications on decay matrix elements - the topic of this publication - it will be sufficient to implement the matrix element correction to the first order in α, i.e. for the emission of one additional real or virtual photon. It should be noted here that hard photon emission predominantly occurs in situations where potential emitters are characterised by a large energy-to-mass ratio and that in any case hard photon emissions tend to populate regions in phase space that are collinear w.r.t. the emitters. In contrast, large angle radiation has the tendency to be predominantly soft.

4.1 Approximations for Real Emission Matrix Elements $\tilde{\beta}_1^1$

As already explained, the vast majority of hard photon emissions deserving an improved description through corrections to the soft limit underlying the YFS approach occurs in the collinear region of emission phase space. In this region, the well-known collinear factorisation can be used to approximate $\tilde{\beta}_1^1$. This amounts to an inclusion of the leading collinear logarithms arising in this limit, which are incorporated for instance in the Altarelli-Parisi evolution equation [19] and corresponding splitting kernels.
Since masses are to be taken fully into account the quasi-collinear limit defined in [20, 21] replaces the more familiar collinear one. In this limit the matrix element factorises as

$$\sum_{\lambda_\gamma} \left|\mathcal{M}_1^{\frac{1}{2}}(p_i,k)\right|^2 \cong \begin{cases} e^2 Z_i^2 g^{(\text{out})}(p_i,k)\left|\mathcal{M}_0^0(p_i+k)\right|^2 & \text{if } i \in \text{F.S.} \\ e^2 Z_i^2 g^{(\text{in})}(p_i,k)\left|\mathcal{M}_0^0(x\cdot p_i)\right|^2 & \text{if } i \in \text{I.S.}. \end{cases} \tag{4.1}$$

Here the $g^{(\text{in,out})}(p_i,k)$ denote massive splitting functions. For instance, for the case of a fermion emitting a photon they are given by

$$g^{(\text{out})}(p_i,k) = \frac{1}{(p_i\cdot k)}\left(P_{ff}(z) - \frac{m_i^2}{(p_i\cdot k)}\right) \tag{4.2}$$

$$g^{(\text{in})}(p_i,k) = \frac{1}{x(p_i\cdot k)}\left(P_{ff}(x) - \frac{x\,m_i^2}{(p_i\cdot k)}\right), \tag{4.3}$$

where $x = \frac{p_i^0 - k^0}{p_i^0}$ and $z = \frac{p_i^0}{p_i^0 + k^0}$ are the fractions of the fermion energies kept after the emission of the photon, and where $P_{ff}(y)$ is the well-known Altarelli-Parisi splitting function

$$P_{ff}(y) = \frac{1+y^2}{1-y}\,. \tag{4.4}$$

These functions are given for unpolarised fermions.
While a final state splitting does not change any momentum of the hard process other than p_i, initial state radiation reduces the CM-energy of this process. This is in contradiction with the fact that, in principle, the hard process has already been fixed and it cannot be guaranteed that the responsible zeroth order matrix element is sufficiently insensitive to deviation of the order of $\mathcal{O}(x)$ on the c.m. energy. Specifying this to the case considered here, namely to particle decays, there are essentially two cases to be considered:

- If the combined mass of the decay products is small compared to the mass of the decaying particle, huge phase space is open for hard radiation. As was argued above, any hard emissions, which can be improved by matrix element corrections will predominantly be collinear and emitted from one of the final state particles. Thus, hard photons will stem from the outgoing particles and the error made by neglecting the effect of hard emissions in the initial state will be small. Essentially, in this case, the assumption of the matrix element to be invariant under alterations in the initial state momentum is valid.

- If, on the other hand, the offsprings together are roughly as massive as the decaying particle the probability of emission off the initial state is sizable. But in this case there is almost no phase space left for photon emissions at all, and, consequently, there is essentially no hard photon emission necessitating higher order corrections. Thus, in this case, the photon emission will be soft and therefore adequately described by the eikonal factors times the leading order cross section, $\tilde{\beta}_0^0$.

In [20] dipole splitting functions for massive fermions etc. have been derived, which reproduce the corresponding Altarelli-Parisi splitting functions in the collinear limit and exhibit the correct behaviour in the soft limit. These dipole splitting functions have been generalised further in [22] to incorporate also polarisation. Thus, in principle they could directly be used in the framework of the YFS formulation replacing the original eikonal factors. In the framework of this publication, however, they are employed as universal correction factors, reweighing explicit photon emission such that the correct collinear limit is recovered. Since they interpolate smoothly between both limits they already include the soft limit. Therefore, in the correction weights, these soft terms have to be subtracted because they are already accounted for in the original YFS eikonals. In addition, since the dipole splitting kernels refer to an emitter and a spectator forming the dipole, for each dipole two such terms have to be applied, such that the squared matrix element with the dipole terms approximating the photon emission reads

$$\left|\mathcal{M}_1^{\frac{1}{2}}\right|^2 \cong -e^2 \sum_{i\neq j} \left[Z_i Z_j \theta_i \theta_j g_{ij}(p_i, p_j, k) \left|\mathcal{M}_0^0\right|^2 \right] \tag{4.5}$$

$$\cong -e^2 \sum_{i<j} \left[Z_i Z_j \theta_i \theta_j \left(g_{ij}(p_i, p_j, k) + g_{ji}(p_j, p_i, k) \right) \left|\mathcal{M}_0^0\right|^2 \right]. \tag{4.6}$$

Here, charge conservation in the form $\sum Z_i\theta_i = 0$ has been used. The second particle in each massive splitting function g_{ij} denotes the spectator of the emission process and accounts for the recoil, thus ensuring four-momentum conservation. It should also be noted that the sum in the equations above runs over charged particles only.
In order to subtract the soft terms, it is useful to consider the soft and quasi-collinear limits of the dipole splitting kernels $g_{ij}(p_i,\, p_j,\, k)$:

$$g_{ij}(p_i,p_j,k) \overset{k\to 0}{\sim} \frac{1}{(p_i\cdot k)}\left(\frac{2(p_i\cdot p_j)}{(p_i\cdot k)+(p_j\cdot k)} - \frac{m_i^2}{(p_i\cdot k)}\right) \tag{4.7}$$

$$g_{ij}(p_i,p_j,k) \overset{p\cdot k\to 0}{\sim} g^{(\text{out/in})}\,. \tag{4.8}$$

Because the soft limit is universal and spin-independent, it is a straightforward exercise to define soft-subtracted dipole splitting kernels

$$\begin{aligned}\bar{g}_{ij}(p_i,p_j,k) &= g_{ij}(p_i,p_j,k) - g_{ij}^{(\text{soft})}(p_i,p_j,k)\\ &= g_{ij}(p_i,p_j,k) - \frac{1}{(p_i\cdot k)}\left(\frac{2(p_i\cdot p_j)}{(p_i\cdot k)+(p_j\cdot k)} - \frac{m_i^2}{(p_i\cdot k)}\right)\,.\end{aligned} \tag{4.9}$$

The soft-subtracted dipole splitting kernels $\bar{g}_{ij}$ now have the correct (finite) soft limit while retaining the original quasi-collinear limit of g_{ij} ((4.8)). Accordingly, the soft-subtracted matrix element can be approximated as

$$\tilde{\beta}_1^1 = -\frac{\alpha}{4\pi^2}\sum_{i<j} Z_iZ_j\theta_i\theta_j\left(\bar{g}_{ij}(p_i,p_j,k)+\bar{g}_{ji}(p_j,p_i,k)\right)\tilde{\beta}_0^0\,. \tag{4.10}$$

The exact form of the $g_{ij}(p_i,p_j,k)$ for different emitter-spectator configurations will be given in Appendix G.

4.2 Virtual Emission Correction $\tilde{\beta}_0^1$

These are the only virtual corrections occurring to level $\mathcal{O}(\alpha)$. They are at present only implemented for two special cases where such contributions give the highest corrections: Leptonic W [23] and Z [24] decays.

$$\begin{aligned}\tilde{\beta}_0^1 &= \tfrac{\alpha}{\pi}\left(\ln\tfrac{m_W}{m_l}+\tfrac{1}{2}\right)\tilde{\beta}_0^0 \qquad (W\to l\nu_l)\\ \tilde{\beta}_0^1 &= \tfrac{\alpha}{\pi}\left(2\ln\tfrac{m_Z}{m_l}-1\right)\tilde{\beta}_0^0 \qquad (Z\to l\bar{l})\end{aligned} \tag{4.11}$$

5 Exact Higher Order Matrix Elements

In order to achieve a higher precision than with the approximated matrix elements presented in the previous section, the implementation of full matrix elements is mandatory. It should be clear, however, that large differences with the approximated matrix elements above will occur only in non-singular regions of comparable hard, wide-angle emissions. Since the module presented in this publication, PHOTONS++, is embedded in the SHERPA framework it is easy to implement such infrared subtracted squared matrix element. To do so, some basic building blocks already present in the framework can be re-used to construct the neccessary, infrared-subtracted one-photon real emission matrix elements, which are then evaluated at momentum configurations generated by the algorithm of Section 3. These building blocks are generic parts in terms of which matrix elements in the helicity formalism of [10–12] can be created; they are listed in App. H. This has been done for a number of relevant matrix elements, see below. Before going into these details, however, it is worthwhile to stress that in order to achieve even higher precision, it is equally possible to implement even higher-order exact matrix elements.
In general, the infrared-subtracted squared matrix element including single real emission can be written as

$$\tilde{\beta}_1^1 \;=\; \frac{1}{2(2\pi)^3}\,\mathcal{M}_1^{\frac{1}{2}}\mathcal{M}_1^{\frac{1}{2}\,*} - \tilde{S}(k)\,\mathcal{M}_0^0\mathcal{M}_0^{0\,*}\;, \tag{5.1}$$

and it is only the amplitudes $\mathcal{M}$ that are process-specific and need to be listed for the different processes. It should be noted that the implementation of matrix elements containing loops is somewhat more involved since in those cases the integral has to be calculated analytically and the divergences must be cancelled before its value as function of the outer momenta can be implemented.

5.1 Decays $V \to \ell\bar{\ell}$

The leading order decay matrix element of the decay of a vector particle into a lepton anti-lepton pair (Fig.5.1) reads

$$\mathcal{M}_0^0 \;=\; \varepsilon_\mu^V(p,\lambda)\;\bar{u}(q_1,s_1)\,\Gamma^\mu\,v(q_2,s_2) \tag{5.2}$$

where $\Gamma^\mu = \Gamma^\mu(\gamma^\mu,\gamma^5)$ or, explicitely,

$$\Gamma^\mu = \gamma^\mu\,(c_L P_L + c_R P_R) = \gamma^\mu\left(c_L\frac{1-\gamma^5}{2} + c_R\frac{1+\gamma^5}{2}\right)\,. \tag{5.3}$$

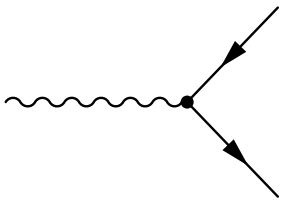

Figure 5.1: Leading Order $V \to \ell\bar{\ell}$ decay matrix element.

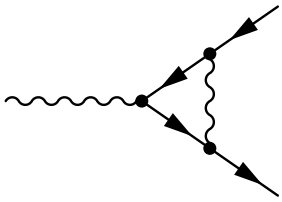

Figure 5.2: Diagram contributing to $\mathcal{M}_0^1$ in $V \to \ell\bar{\ell}$ decays.

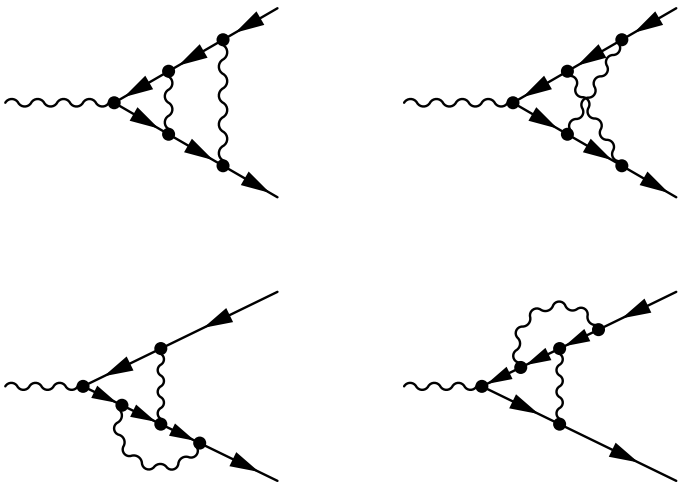

Figure 5.3: Diagrams contributing to $\mathcal{M}_0^2$ in $V \to \ell\bar{\ell}$ decays.

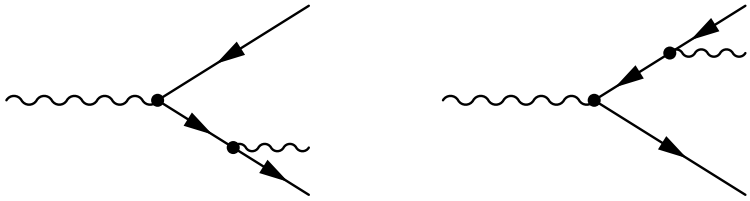

Figure 5.4: Diagrams contributing to $\mathcal{M}_1^{\frac{1}{2}}$ in $V \to \ell\bar{\ell}$ decays.

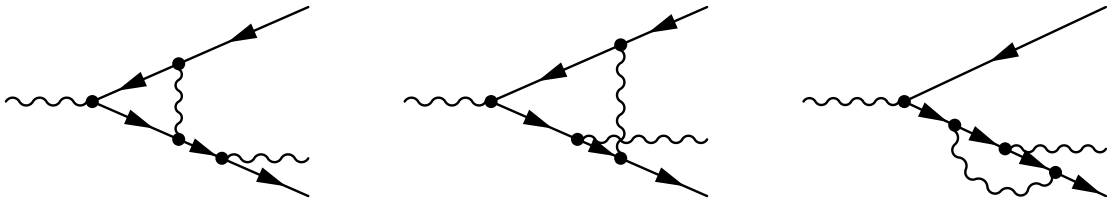

Figure 5.5: Diagrams contributing to $\mathcal{M}_1^{\frac{3}{2}}$ in $V \to \ell\bar{\ell}$ decays.

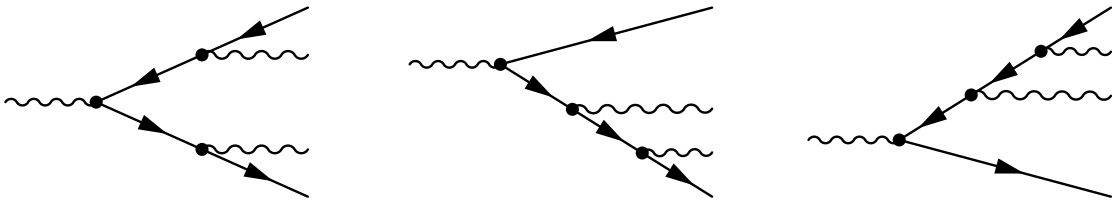

Figure 5.6: Diagrams contributing to $\mathcal{M}_2^1$ in $V \to \ell\bar{\ell}$ decays.

Process	c_L	c_R
$Z \to \ell\ell$	$\frac{ie}{2s_W c_W} 2s_W^2$	$\frac{ie}{2s_W c_W}(2s_W^2 - 1)$
$J/\psi \to \ell\ell$	$-ie$	$-ie$
$\Upsilon \to \ell\ell$	$-ie$	$-ie$

Table 5.1: Values of the coupling constants of different vector particles to the left- and right-handed leptonic currents.

The constants c_L and c_R depend on the coupling of the vector particle to the leptonic current, thus are process dependent (cf. Table 5.1). Hence, the infrared subtracted squared leading order matrix element is

$$\tilde{\beta}_0^0 = \sum_{\lambda, s_1, s_2} \mathcal{M}_0^0 \mathcal{M}_0^{0\,*} \,. \tag{5.4}$$

Although this leading order decay matrix element is factored out and part of the basic process assumed to be already generated, it is needed to calculate the relative size of the higher order matrix element as they occur in the correction weight

$$\mathcal{C} = 1 + \frac{1}{\tilde{\beta}_0^0}\left[\tilde{\beta}_0^1 + \sum_{i=1}^{n_\gamma} \frac{\tilde{\beta}_1^1(k_i)}{\tilde{S}(k_i)} + \tilde{\beta}_0^2 + \sum_{i=1}^{n_\gamma} \frac{\tilde{\beta}_1^2(k_i)}{\tilde{S}(k_i)} + \sum_{\substack{i,j=1 \\ i\neq j}}^{n_\gamma} \frac{\tilde{\beta}_2^2(k_i,k_j)}{\tilde{S}(k_i)\tilde{S}(k_j)} + \mathcal{O}(\alpha^3)\right] . \tag{5.5}$$

The first order, relative to the basic process, real emission matrix element as depicted in Figure 5.4 reads

$$\begin{aligned}\mathcal{M}_1^{\frac{1}{2}} = e\, \varepsilon_\mu^V(p,\lambda)\, \bar{u}(p_1,s_1) \Bigg[& \gamma^\nu \frac{\not{p}_1 + \not{k} + m}{(p_1+k)^2 - m^2} \Gamma^\mu \\ & - \Gamma^\mu \frac{\not{p}_2 + \not{k} - m}{(p_2+k)^2 - m^2} \gamma^\nu \Bigg] v(p_2,s_2)\, \varepsilon_\nu^{\gamma *}(k,\kappa)\end{aligned} \tag{5.6}$$

and

$$\tilde{\beta}_1^1 = \sum_{\substack{\lambda,\kappa \\ s_1,s_2}} \mathcal{M}_1^{\frac{1}{2}} \mathcal{M}_1^{\frac{1}{2}\,*} - \tilde{S}(k)\tilde{\beta}_0^0 \tag{5.7}$$

$$\tilde{\beta}_1^2 = \frac{1}{2(2\pi)^2} \sum_{\substack{\lambda,\kappa \\ s_1,s_2}} \left(M_1^{\frac{3}{2}} \mathcal{M}_1^{\frac{1}{2}\,*} + \mathcal{M}_1^{\frac{1}{2}} M_1^{\frac{3}{2}\,*} \right) - \tilde{S}(k)\tilde{\beta}_0^1 \tag{5.8}$$

where $M_1^{\frac{3}{2}}$ is the one-loop-one-emission virtually infrared subtracted matrix element.

The second order real emission matrix element (Figure 5.6) reads

$$\begin{aligned}
\mathcal{M}_2^1 &= e^2\,\varepsilon_\mu^V(p,\lambda)\,\bar{u}(p_1,s_1) \\
&\quad\Bigg[\gamma^\nu\frac{\not{p}_1+\not{k}_1+m}{(p_1+k_1)^2-m^2}\gamma^\sigma\frac{\not{p}_1+\not{k}_1+\not{k}_2+m}{(p_1+k_1+k_2)^2-m^2}\Gamma^\mu \\
&\quad+\Gamma^\mu\frac{\not{p}_2+\not{k}_2+\not{k}_1-m}{(p_2+k_2+k_1)^2-m^2}\gamma^\nu\frac{\not{p}_2+\not{k}_2-m}{(p_2+k_2)^2-m^2}\gamma^\sigma \\
&\quad-\gamma^\nu\frac{\not{p}_1+\not{k}_1+m}{(p_1+k_1)^2-m^2}\Gamma^\mu\frac{\not{p}_2+\not{k}_2-m}{(p_2+k_2)^2-m^2}\gamma^\sigma \\
&\quad+(k_1\leftrightarrow k_2)\Bigg] \\
&\quad v(p_2,s_2)\,\varepsilon_\nu^{\gamma *}(k_1,\kappa_1)\,\varepsilon_\sigma^{\gamma *}(k_2,\kappa_2)
\end{aligned} \tag{5.9}$$

and, thus,

$$\tilde{\beta}_2^2 = \left(\frac{1}{2(2\pi)^3}\right)^2 \sum_{\substack{\lambda,\kappa_1,\kappa_2\\ s_1,s_2}} \mathcal{M}_2^1\mathcal{M}_2^{1\,*} - \sum_{\substack{i,j=1\\ i\neq j}}^{2}\tilde{S}(k_i)\tilde{\beta}_1^1(k_j) - \tilde{S}(k_1)\tilde{S}(k_2)\tilde{\beta}_0^0\,. \tag{5.10}$$

When calculating these infrared subtracted squared matrix elements $\tilde{\beta}_{n_R}^{n_V+n_R}$ it is to be kept in mind that they are only defined if momentum conservation is fulfilled. Hence, a projection of all momenta in the $(n+n_\gamma)$-dimensional phase space, created by the first steps of the event generation procedure, onto the $(n+n_R)$-dimensional phase space of the infrared subtracted squared matrix element has to be made. If $n_\gamma \geq n_R$, this is a projection onto one of the edges of the higher dimensional phase space. In practise, this amounts to repeating the reconstruction procedure of Section 3.3 and only considering a n_R-dimensional subset of all n_γ photons. If, on the other hand, $n_\gamma < n_R$, then $\tilde{\beta}_{n_R}^{n_V+n_R} \equiv 0$.

All infrared subtracted squared matrix elements with $n_V = 0$ can in principle be calculated using the Helicity Formalism also used in SHERPA's AMEGIC++. To this end, all matrix elements have to be expressed in terms of X-, Y- or Z-functions (see App. H), e.g.

$$\mathcal{M}_0^0 = X\left(q_1,s_1;\varepsilon^V;q_2,\bar{s}_2;c_L,c_R\right) \tag{5.11}$$

$$\begin{aligned}
\mathcal{M}_1^{\frac{1}{2}} &= \frac{e}{2}\Bigg[\frac{1}{p_a^2-m^2}\left(1+\frac{m}{\sqrt{p_a^2}}\right)\sum_s X\left(p_1,s_1,\varepsilon^{\gamma *},p_a,s,1,1\right)X\left(p_a,s,\varepsilon^V,p_2,\bar{s}_2,c_L,c_R\right) \\
&\quad+\frac{1}{p_a^2-m^2}\left(1-\frac{m}{\sqrt{p_a^2}}\right)\sum_s X\left(p_1,s_1,\varepsilon^{\gamma *},p_a,\bar{s},1,1\right)X\left(p_a,\bar{s},\varepsilon^V,p_2,\bar{s}_2,c_L,c_R\right) \\
&\quad-\frac{1}{p_b^2-m^2}\left(1+\frac{m}{\sqrt{p_b^2}}\right)\sum_s X\left(p_1,s_1,\varepsilon^V,p_b,s,c_L,c_R\right)X\left(p_b,s,\varepsilon^{\gamma *},p_2,\bar{s}_2,1,1\right) \\
&\quad-\frac{1}{p_b^2-m^2}\left(1-\frac{m}{\sqrt{p_b^2}}\right)\sum_s X\left(p_1,s_1,\varepsilon^V,p_b,\bar{s},c_L,c_R\right)X\left(p_b,\bar{s},\varepsilon^{\gamma *},p_2,\bar{s}_2,1,1\right)\Bigg]
\end{aligned} \tag{5.12}$$

with $p_a = p_1 + k$ and $p_b = p_2 + k$, or

$$\begin{aligned}
\mathcal{M}_2^1 \;=\; & \frac{e^2}{4}\left\{ \frac{1}{(p_a^2-m^2)(p_b^2-m^2)}\left(1+\frac{m}{\sqrt{p_a^2}}\right)\left(1+\frac{m}{\sqrt{p_b^2}}\right)\right. \\
& \times \sum_{s_a,s_b} X\left(p_1,s_1;\varepsilon^{\gamma_2 *};p_a,s_a;1,1\right) X\left(p_a,s_a;\varepsilon^{\gamma_1 *};p_b,s_b;1,1\right) \\
& \qquad X\left(p_b,s_b;\varepsilon^{V};p_2,\bar{s}_2;c_L,c_R\right) \\
& + \frac{1}{(p_a^2-m^2)(p_b^2-m^2)}\left(1+\frac{m}{\sqrt{p_a^2}}\right)\left(1-\frac{m}{\sqrt{p_b^2}}\right) \\
& \times \sum_{s_a,s_b} X\left(p_1,s_1;\varepsilon^{\gamma_2 *};p_a,s_a;1,1\right) X\left(p_a,s_a;\varepsilon^{\gamma_1 *};p_b,\bar{s}_b;1,1\right) \\
& \qquad X\left(p_b,\bar{s}_b;\varepsilon^{V};p_2,\bar{s}_2;c_L,c_R\right) \\
& + \frac{1}{(p_a^2-m^2)(p_b^2-m^2)}\left(1-\frac{m}{\sqrt{p_a^2}}\right)\left(1+\frac{m}{\sqrt{p_b^2}}\right) \\
& \times \sum_{s_a,s_b} X\left(p_1,s_1;\varepsilon^{\gamma_2 *};p_a,\bar{s}_a;1,1\right) X\left(p_a,\bar{s}_a;\varepsilon^{\gamma_1 *};p_b,s_b;1,1\right) \\
& \qquad X\left(p_b,s_b;\varepsilon^{V};p_2,\bar{s}_2;c_L,c_R\right) \\
& + \frac{1}{(p_a^2-m^2)(p_b^2-m^2)}\left(1-\frac{m}{\sqrt{p_a^2}}\right)\left(1-\frac{m}{\sqrt{p_b^2}}\right) \\
& \times \sum_{s_a,s_b} X\left(p_1,s_1;\varepsilon^{\gamma_2 *};p_a,\bar{s}_a;1,1\right) X\left(p_a,\bar{s}_a;\varepsilon^{\gamma_1 *};p_b,\bar{s}_b;1,1\right) \\
& \qquad X\left(p_b,\bar{s}_b;\varepsilon^{V};p_2,\bar{s}_2;c_L,c_R\right) \\
& \left. + \cdots \right\}
\end{aligned} \tag{5.13}$$

wherein $p_a = p_1 + k_1$ and $p_b = p_1 + k_1 + k_2$. The bar over the fermionic spin label s signifies an anti-particle. In the expression for $\mathcal{M}_2^1$ only the first term has been written out explicitly and it can already be seen that the number of terms increases tremendously with the number of fermion propagators. Nonetheless, these expressions are easy to evaluate numerically. However, due to the lack of $M_1^{\frac{3}{2}}$, the second order infrared subtracted squared matrix elements $\tilde{\beta}_0^2$, $\tilde{\beta}_1^2$ and $\tilde{\beta}_2^2$ are not yet implemented in the code.

5.2 Decays $S/P \to \ell\bar{\ell}$

The leading order decay matrix element for the decay of a scalar/pseudo-scalar particle into a lepton anti-lepton pair (cf. Fig.5.1 with the initial state vector replaced by a scalar/pseudo-scalar) reads

$$\mathcal{M}_0^0 \;=\; \bar{u}(q_1,s_1)\,\Gamma\,v(q_2,s_2)\,, \tag{5.14}$$

where this time $\Gamma = \Gamma(1,\gamma^5)$ or, explicitely,

$$\Gamma = c_L P_L + c_R P_R = c_L \frac{1-\gamma^5}{2} + c_R \frac{1+\gamma^5}{2}\,. \tag{5.15}$$

Process	c_L	c_R
$\pi^0 \to \ell\ell$	$ieF_L(p)$	$ieF_R(p)$
$K_L \to \ell\ell$	$ieF_L(p)$	$ieF_R(p)$
$h^0 \to \ell\ell$	$-i\frac{m_\ell}{v}$	$-i\frac{m_\ell}{v}$

Table 5.2: Values of the coupling constants of different vector particles to the left- and right-handed leptonic currents for pseudo-scalar mesons and the Higgs boson. For the Higgs boson couplings the differentiation into couplings to left- and right-handed currents is physically incorrect, but as long $c_L = c_R$, $\Gamma = c_L = c_R$. $F_{L/R}(p)$ are the form factors the hadron decay module used for the leading order decay.

Again, the constants c_L and c_R depend on the coupling of the scalar to the left- and right-handed leptonic currents (see Fig.5.2). The first order real emission matrix element, corresponding to the graphs in Figure 5.4 with, again, the vector replaced by a scalar/pseudo-scalar, reads

$$\mathcal{M}_1^{\frac{1}{2}} = e\,\bar{u}(p_1,s_1)\left[\gamma^\sigma\frac{\not{p}_1+\not{k}+m}{(p_1+k)^2-m^2}\Gamma-\Gamma\frac{\not{p}_2+\not{k}-m}{(p_2+k)^2-m^2}\gamma^\sigma\right]v(p_2,s_2)\,\varepsilon_\sigma^{\gamma*}(k,\kappa)\,. \quad (5.16)$$

5.3 Decays $V^- \to \ell^- \bar{\nu}_\ell$

This type of decay differs from the one in Section 5.1 by the fact that now the decaying vector particle itself may radiate a photon. Nonetheless, the leading order decay matrix element (Fig. 5.7) has the same form as above

$$\mathcal{M}_0^0 = \varepsilon_\mu^V(p,\lambda)\,\bar{u}(q_1,s_1)\,\Gamma^\mu\,v(q_2,s_2)\,. \quad (5.17)$$

Again, $\Gamma^\mu = \Gamma^\mu(\gamma^\mu,\gamma^5)$ and has the form of Eq. (5.3). Explicite values for c_L and c_R are stated in Table 5.3.

Process	c_L	c_R
$W^- \to \ell^- \bar{\nu}_\ell$	$\frac{ie}{s_W\sqrt{2}}\,2s_W^2$	0
$D^{*-} \to \ell^- \bar{\nu}_\ell$	$ieF(p)$	0
$D_s^{*-} \to \ell^- \bar{\nu}_\ell$	$ieF(p)$	0

Table 5.3: Values of the coupling constants of different vector particles to the left- and right-handed leptonic currents. The couplings to the right-handed currents are of course absent, since in the standard model there are no currents involving right-handed neutrinos.

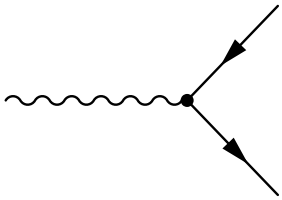

Figure 5.7: Leading Order $V^- \to \ell^- \bar{\nu}_\ell$ decay matrix element.

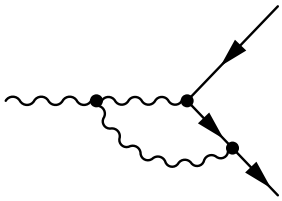

Figure 5.8: Diagram contributing to $\mathcal{M}_0^1$ in $V^- \to \ell^- \bar{\nu}_\ell$ decays in unitary gauge.

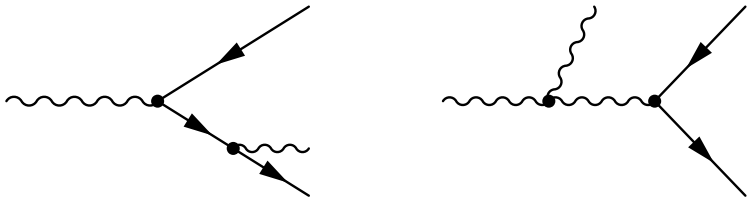

Figure 5.9: Diagrams contributing to $\mathcal{M}_1^{\frac{1}{2}}$ in $V^- \to \ell^- \bar{\nu}_\ell$ decays in unitary gauge.

The first order real emission matrix elements, depicted in Figure 5.9, is given in unitary gauge by

$$\begin{aligned}
\mathcal{M}_1^{\frac{1}{2}} &= e\,\varepsilon_\mu^V(p,\lambda)\;\bar{u}(p_1,s_1)\gamma^\sigma \frac{\not{p}_1+\not{k}+m_1}{(p_1+k)^2-m_1^2}\,\Gamma^\mu\, v(p_2,s_2)\;\varepsilon_\sigma^{\gamma *}(k,\kappa) \\
&\quad + e\,\varepsilon_\mu^V(p,\lambda)\;V^{\mu\nu\sigma}\frac{g_{\nu\rho}}{(p-k)^2-m_W^2}\;\bar{u}(p_1,s_1)\,\Gamma^\rho\, v(p_2,s_2)\;\varepsilon_\sigma^{\gamma *}(k,\kappa) \\
&\quad - e\,\varepsilon_\mu^V(p,\lambda)\;V^{\mu\nu\sigma}\frac{(p-k)_\nu (p-k)_\rho}{m_W^2\left((p-k)^2-m_W^2\right)}\;\bar{u}(p_1,s_1)\,\Gamma^\rho\, v(p_2,s_2)\;\varepsilon_\sigma^{\gamma *}(k,\kappa)\,, \quad (5.18)
\end{aligned}$$

wherein $V^{\mu\nu\sigma}$ is the triple vector coupling. With the momentum configuration of Figure 5.9 it is given by

$$V^{\mu\nu\sigma} = g^{\mu\nu}(-2p+k)^\sigma + g^{\mu\sigma}(p+k)^\nu + g^{\nu\sigma}(p-2k)^\mu \,. \tag{5.19}$$

For coding it into PHOTONS++ it again has to be written in terms of X-, Y- and Z-Functions. With the identities and definitions of Appendix H this is a straight forward task. Hereby the Lorentz-structure of $V^{\mu\nu\sigma}$ is written out explicitly. Thus,

$$\begin{aligned}
\mathcal{M}_1^{\frac{1}{2}} = {} & \frac{e}{2(q^2-m_1^2)}\left(1+\tfrac{m_1}{\sqrt{q^2}}\right)\sum_s X\left(p_1,s_1;\varepsilon^{\gamma*};q,s;1,1\right) X\left(q,s;\varepsilon^V;p_2,\bar{s}_2;c_L,c_R\right) \\
& + \frac{e}{2(q^2-m_1^2)}\left(1-\tfrac{m_1}{\sqrt{q^2}}\right)\sum_s X\left(p_1,s_1;\varepsilon^{\gamma*};q,\bar{s};1,1\right) X\left(q,\bar{s};\varepsilon^V;p_2,\bar{s}_2;c_L,c_R\right) \\
& + \frac{e}{(p-k)^2-m_V^2}\left(\varepsilon^{\gamma*}\cdot(-2p+k)\right) X\left(p_1,s_1;\varepsilon^V;p_2,\bar{s}_2;c_L,c_R\right) \\
& + \frac{e}{(p-k)^2-m_V^2}\left(\varepsilon^V\cdot\varepsilon^{\gamma*}\right) X\left(p_1,s_1;p+k;p_2,\bar{s}_2;c_L,c_R\right) \\
& + \frac{e}{(p-k)^2-m_V^2}\left(\varepsilon^V\cdot(p-2k)\right) X\left(p_1,s_1;\varepsilon^{\gamma*};p_2,\bar{s}_2;c_L,c_R\right) \\
& - \frac{e}{m_V^2\left((p-k)^2-m_V^2\right)}\left(\varepsilon^V\cdot(p-k)\right)\left(\varepsilon^{\gamma*}\cdot(-2p+k)\right) \\
& \qquad \times X\left(p_1,s_1;(p-k);p_2,\bar{s}_2;c_L,c_R\right) \\
& - \frac{e}{m_V^2\left((p-k)^2-m_V^2\right)}\left(\varepsilon^V\cdot\varepsilon^{\gamma*}\right)\left((p-k)\cdot(p+k)\right) \\
& \qquad \times X\left(p_1,s_1;(p-k);p_2,\bar{s}_2;c_L,c_R\right) \\
& - \frac{e}{m_V^2\left((p-k)^2-m_V^2\right)}\left(\varepsilon^V\cdot(p-2k)\right)\left(\varepsilon^{\gamma*}\cdot(p-k)\right) \\
& \qquad \times X\left(p_1,s_1;(p-k);p_2,\bar{s}_2;c_L,c_R\right) \,.
\end{aligned} \tag{5.20}$$

5.4 Decays $S^-/P^- \to \ell^-\bar{\nu}_\ell$

The leading order decay matrix element corresponds to the graph in Fig. 5.7 with the initial state vector replaced by a scalar. Thus,

$$\mathcal{M}_0^0 = \bar{u}(q_1,s_1)\,\Gamma\,v(q_2,s_2)\,, \tag{5.21}$$

wherein Γ is identical to the one of Section 5.2. The coupling constants c_L and c_R are given explicitly in Table 5.4.

The first order real emission matrix element, however, possesses a less entangled Lorentz-structure than in the charged vector decay. This is due to the simpler structure of the scalar-QED vertex used for the initial state emission. The full matrix element of the process thus reads

$$\begin{aligned}
\mathcal{M}_1^{\frac{1}{2}} = {} & e\,\bar{u}(p_1,s_1)\,\gamma^\sigma\frac{\not{p}_1+\not{k}+m}{(p_1+k)^2-m^2}\Gamma\,v(p_2,s_2)\,\varepsilon_\sigma^{\gamma*}(k,\kappa) \\
& + e\,\frac{1}{(p-k)^2-m_{p/S}^2}\left((2p-k)\cdot\varepsilon^{\gamma*}(k,\kappa)\right)\,\bar{u}(p_1,s_1)\,\Gamma\,v(p_2,s_2)\,.
\end{aligned} \tag{5.22}$$

It is to note that this decay matrix element is not yet implemented in PHOTONS++.

Process	c_L	c_R
$\pi^- \to \ell^- \bar{\nu}_\ell$	$ieF(p)$	0
$K^- \to \ell^- \bar{\nu}_\ell$	$ieF(p)$	0
$B^- \to \ell^- \bar{\nu}_\ell$	$ieF(p)$	0

Table 5.4: Values of the coupling constants of different vector particles to the left- and right-handed leptonic currents.

6 Results

In this section some of the results of the PHOTONS++ program, as it is implemented within the SHERPA framework, are presented. The focus lies on the central distribution produced by the preceding calculations, the total energy of **all** photons radiated per event in the rest frame of the decaying particle. In addition, angular distributions for dipole and multipole configurations will be shown.

6.1 Validation: Leptonic Heavy Gauge Boson Decays

The leptonic decays of W and Z bosons, $W \to l\nu_l$ and $Z \to l\bar{l}$, will play the central role in validating the accuracy of the PHOTONS++ implementation of the YFS approach. Before studying in more detail these processes and comparing the results obtained with PHOTONS++ with those from other codes, namely AMEGIC++ [10] and WINDEC [23], it is worthwhile to discuss one of the key distributions, namely the total energy radiated off the decay.

6.1.1 Radiated Photon Energy

The result for this distribution, namely the total energy radiated off the decay in form of photons, is presented in Figure 6.1. For both processes, i.e. for both leptonic Z and W decays, different leptons with different masses have been considered. Clearly, the most radiation is connected to final states involving electrons, being the lightest fermions taken into account, while radiation off heavier fermions is increasingly suppressed. One of the most prominent feature of every spectrum is the kink at around half the boson mass, which is due to a kinematic limit set on single photon emission. This kink gets washed out and moves to the left with increasing fermion mass, because the final state particles have to compensate for the three-momentum of the photons being emitted. Events surpassing this limit must have at least two hard photons, which are sufficiently separated in angle that they can recoil, at least partially, against each other. This gives some idea why this feature is absent in the W-decay spectra. There, the W-boson would have to emit a hard photon simultaneously to the charged lepton. This, however, is severely suppressed due to the high mass of the boson and, consequently, to the reduced average photon number, as compared to the Z-decay. Along the same line, such double hard photon emissions are decreasingly probable with rising lepton masses. However, since in the present state only approximated matrix elements up to $\mathcal{O}(\alpha)$ are included in the program these double emission are not described correctly yet.
In Fig. 6.1 also different treatment of higher order matrix elements are included: photons emitted solely according to the purely soft YFS eikonals (left panel) are contrasted with

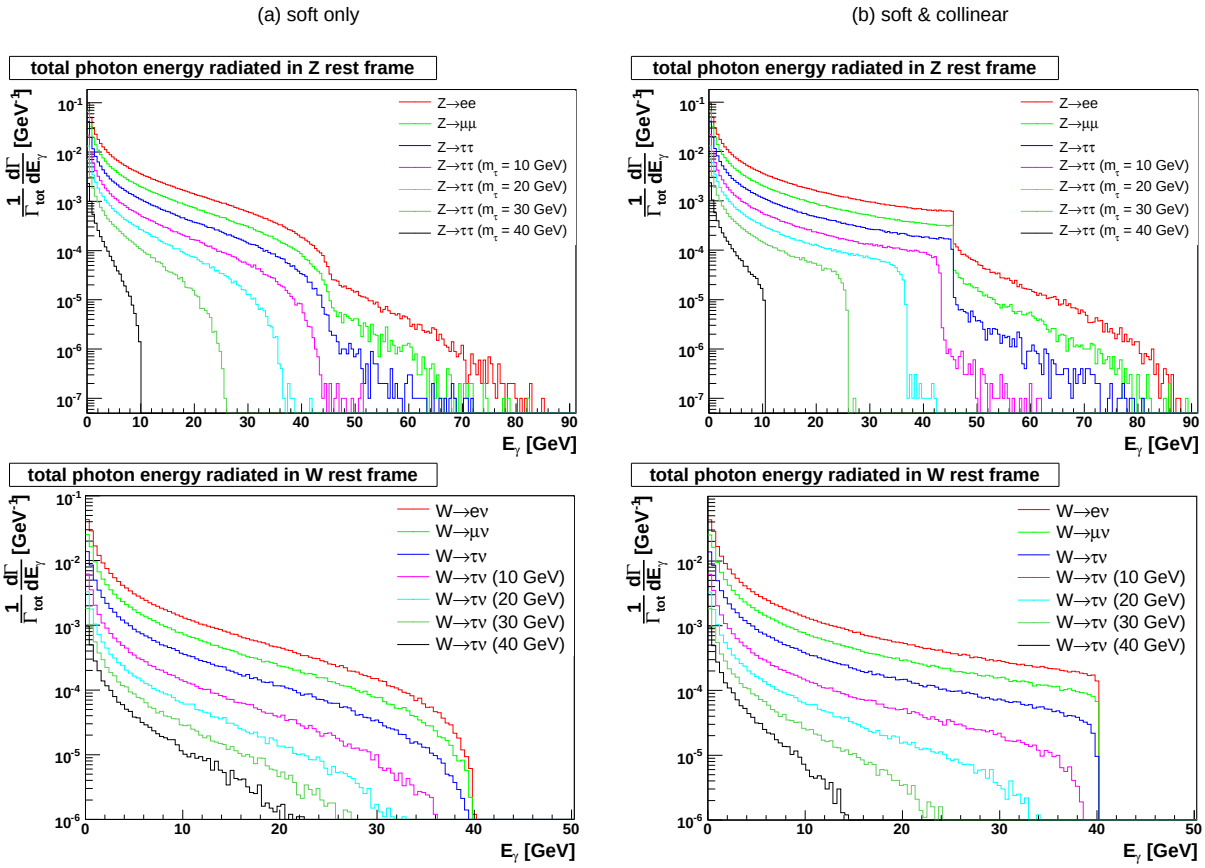

Figure 6.1: Photon radiation in leptonic decays of Z (upper panel) and W bosons (lower panel) for different leptons, including fictional heavy τ's in a range of masses. In the left panel, (a), $\mathcal{C} = 1$, i.e. photon generation according to the YFS form factor only is depicted, whereas in the right panel, (b), corrections up to $\mathcal{O}(\alpha)$ are included using the dipole splitting functions and the virtual corrections, cf. Sec. 4.2 and 4.1. All distributions are normalised on the total decay width of the decay into the respective lepton and lepton-neutrino pair. The infrared cut-off in all cases is set to 0.1GeV.

corrections due to the approximated matrix elements presented in Sec. 4.1. The former distribution, labelled with "soft", thus is correct in the soft limit but it is inadequate for the description of hard, collinear photon radiation. This, including virtual corrections of $\mathcal{O}(\alpha)$, is displayed in the panel labelled with "soft & collinear".

The inclusion of these corrections gives reasonably good results as long as most photons are soft or if complicated correlations of hard photons are not important.

6.1.2 Comparison with other Codes

After checking the physical sanity of the implementation in principle, results obtained with PHOTONS++ are now to be compared to those from other, established and dedicated Monte Carlo event generators capable of describing QED effects in the decays of W and Z bosons, in particular with the WINDEC package [23]. This program aims at the description of the production and decay of W-bosons in hadronic collisions. WINDEC performs the decay of the W-boson into lepton-neutrino pairs including QED corrections summed in the YFS-approach and corrected by exact $\mathcal{O}(\alpha)$ real emission and virtual correction matrix elements. They are obtained for the decay only in the narrow width approximation, i.e. only the $W \to \ell\nu$ decay is taken into account. Furthermore, in this section, the results of PHOTONS++ are compared with the exact, fixed order, one-photon emission results of the SHERPA-inherent matrix element generator AMEGIC++. However, comparisons with AMEGIC++ are only sensible when the average photon number of the process under consideration is low, i.e. when multiphoton emission gives a negligible contribution to the differential cross section. Additionally, it should be stressed that AMEGIC++ lacks virtual corrections and therefore comparisons are sensible for normalised distributions only.

A channel suited best for comparing all three generators is $W \to \tau\nu_\tau$. Besides the low average photon multiplicity (with an infrared cut-off of 0.1 GeV multiphoton events make up for less than 3% of all radiative events) virtual corrections merely amount to a 1% correction of the zeroth order cross section. Furthermore, as discussed earlier, the majority of multiphoton events will consist of at most one single hard photon and additional soft ones. Therefore, these events will be approximately described by the hard emission only.

It should be stressed at this point, however, that there is one fundamental difference in the comparison of the various results, related to the way the infrared cut-off is implemented: While in WINDEC the energy cut-off is applied in the rest frame of the decaying W, it is applied in the rest-frame of the decaying dipole in both PHOTONS++ and AMEGIC++.

The distributions generated by all three programs are shown in Fig. 6.2.

In general terms, the distributions agree reasonably well with each other. There is, however, a slight deviation in the region of large radiated energies, where WINDEC undershoots the results of the two other codes on the level of up to 10%. On the other hand, WINDEC exhibits an overshoot in the very low energy bins, for radiated energies around or smaller 5 GeV, which is due to the different frames in which the infrared cut-offs are applied. As already mentioned, in WINDEC this is defined in the W rest frame, hence resulting in a flat hypersurface in this frame. In contrast, in PHOTONS++ it is applied in the rest frame of the W-l-dipole. Subsequently the surface of the region cut off by this definition forms a directionally dependent hypersurface in the rest frame of the W (observable in Fig. 6.3 where the cut-off is set to 1GeV). The net result is that some photons having more than 0.1GeV in this frame had less than 0.1GeV in the rest frame of the dipole, and vice versa. Ultimately, different definitions of the infrared cut-off result in different behaviour in the vicinity of this cut-off in nearby frames. The differences are the larger the further both frames are apart. On the other hand, the differences at high photon energies most likely stem from different mapping procedures in both codes. The mapping procedure in PHOTONS++, cf. Sec. 3.3.2, does not require neutral particles, in this case the neutrino. It therefore ensures that the full phase space possible for the radiative decay can be mapped onto the leading order one. Otherwise, the masslessness of the neutrino may spoil this capacity.

Another feature to study is the dependence of the distributions on the choice of the infrared

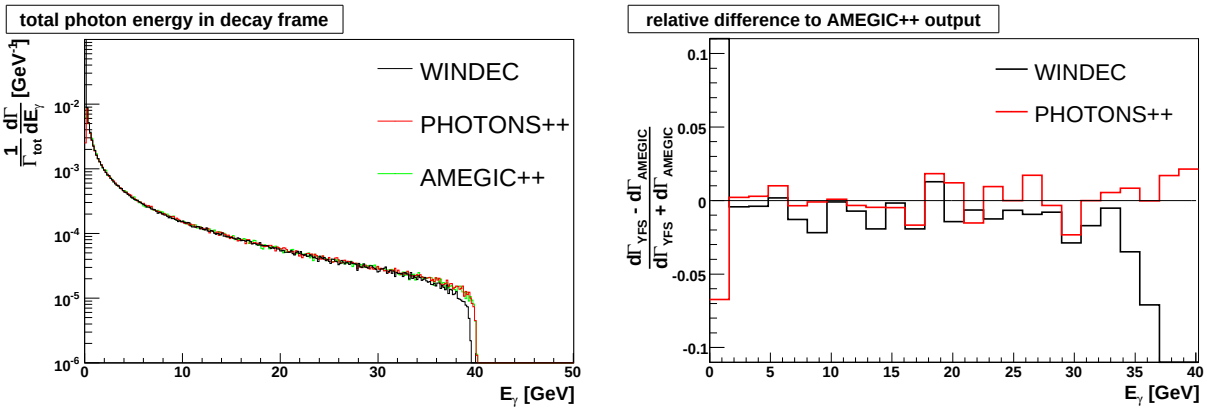

Figure 6.2: The total photon energy in the decay frame in $W \to \tau\nu_\tau$. In the left panel, (a), the distributions generated by WINDEC (black), PHOTONS++ (red) and AMEGIC++ (green) are depicted, where the latter has been rescaled with the true average photon multiplicity. In the right panel, the relative deviations of WINDEC (black) and PHOTONS++ (red) with respect to the rescaled matrix element result of AMEGIC++ are displayed.

cut-off ω. Its principal function is to separate the divergent region of real soft photon emission, which is exponentiated together with the virtual contributions, from the region of the phase space where resolvable photons will be generated. Accordingly, this cut-off sets a limit on the number of photons to be generated. In Figure 6.3 the results of this variation on the spectrum of the radiated photons' total energy are exhibited for two different final states, electrons (upper panel) and τ's (lower panel). In the case of the decays $W \to \tau\nu$ the two codes, PHOTONS++ (left panel) and WINDEC (right panel) show a similar behaviour: Varying the cutoffs between 1 MeV and 1 GeV yields stable results in large regions and especially also in the high-energy tail of the distribution, whereas differences appear only in the region of small energies, around 1-2 GeV. However, in the case of the decays $W \to e\nu$ there is some difference between the two codes. Varying the cutoff there yields still comparably stable results for PHOTONS++, but the results of WINDEC show a significant dependence on the cut-off of the order of around 10%. This is due to the fact that with decreasing fermion mass the effect of the infrared cutoff on the average photon number increases[1].

In order to choose an optimal value of the infrared cut-off ω there are different considerations to be taken into account: On the one hand an efficient generation is desirable, pushing ω as high as physically sensible, e.g. the detector level energy resolution on soft photons or decay products. Along the same lines it should be noted that all photons in the soft (unresolved) region will be assumed to yield a negligible combined momentum. Therefore, choosing a comparably large infrared cut-off will not have any effect on distributions involving the resolved Bremsstrahlung photons, but it will reduce the accuracy of results obtained for e.g. invariant masses of the primary decay products. This consideration clearly demands a smaller cut-off. On the other hand, when exponentiating the real soft photon emission

[1] In fact, this feature was one of the reasons for preferring the τ decay channel over the electron channel.

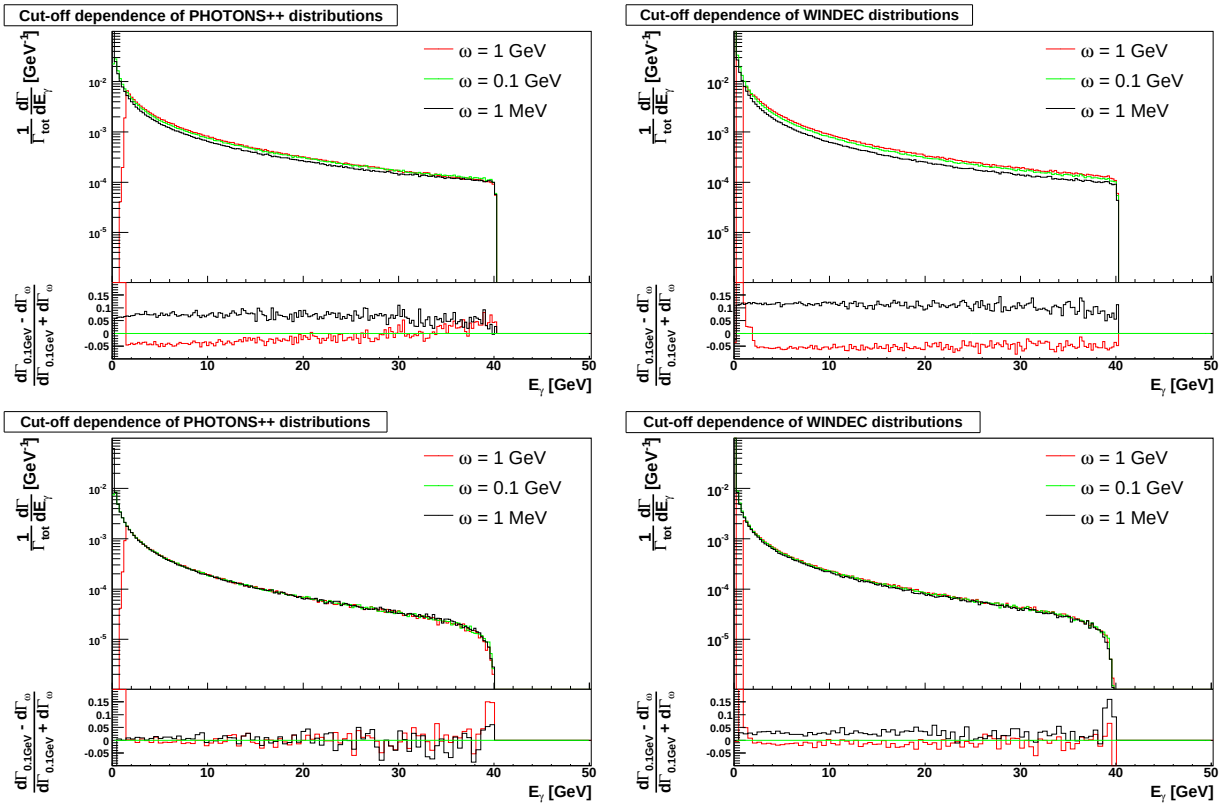

Figure 6.3: Dependence of the total energy of the radiated photons' on the infrared cut-off in PHOTONS++ (left panel) and WINDEC (right panel) for $W \to e\nu_e$ (upper panel) and $W \to \tau\nu_\tau$ decays (lower panel).

a factor $\int \frac{d^3k}{k^0}\tilde{S}(k)(e^{-iyk}-1)\Theta(\omega-k^0)$ has been neglected, which is strictly true only for $\omega \to 0$. Thus, some residual dependence is to be expected, even if infrared subtracted matrix element corrections were included to all orders. This dependence is of course minimised with small cut-offs.

6.1.3 Effects of Inclusion of Exact Matrix Elements

Including exact matrix elements, as discussed in Section 5, further improves the accuracy of the distributions. This is especially true away from the singular limits, where considerable differences emerge. This is exemplified in Fig. 6.6, where the angular distributions of photons in $Z \to \ell\bar{\ell}$ decays is depicted. Of course, there is also an effect on the differential decay rate. Fig. 6.6 shows that corrections obtained from the quasi-collinear approximation, i.e. from the approximate matrix element, overestimates the exact matrix element resulting in a increased differential decay rate. This is especially true in the region of very hard photon emission which, due to the angular constraints imposed by the emitter's mass, no longer fullfill the condition $(p \cdot k) \to 0$. Here the full matrix element exhibits some destructive interference between the two relevant diagrams which is of course absent in the treatment

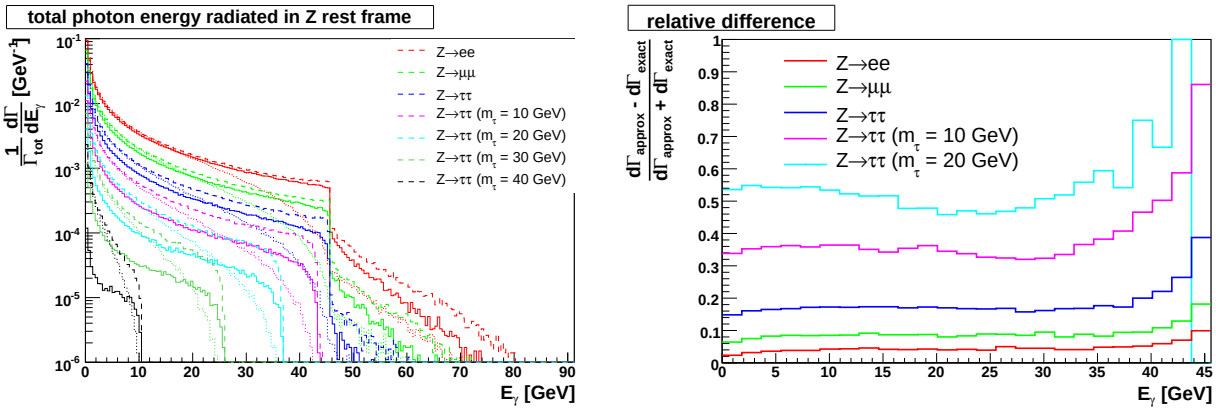

Figure 6.4: The total energy of all photons radiated in $Z \to \ell\bar{\ell}$. Left panel (a): The same plot as in Fig. 6.1(b), but this time the correction is done by using the **exact** matrix element (solid) instead of the **approximated** one (dashed). The distribution generated using the eikonals only is shown as a dotted line. Right panel (b): The relative difference of the distributions obtained using the exact and the approximated matrix elements. In both cases again different fermion masses have been used.

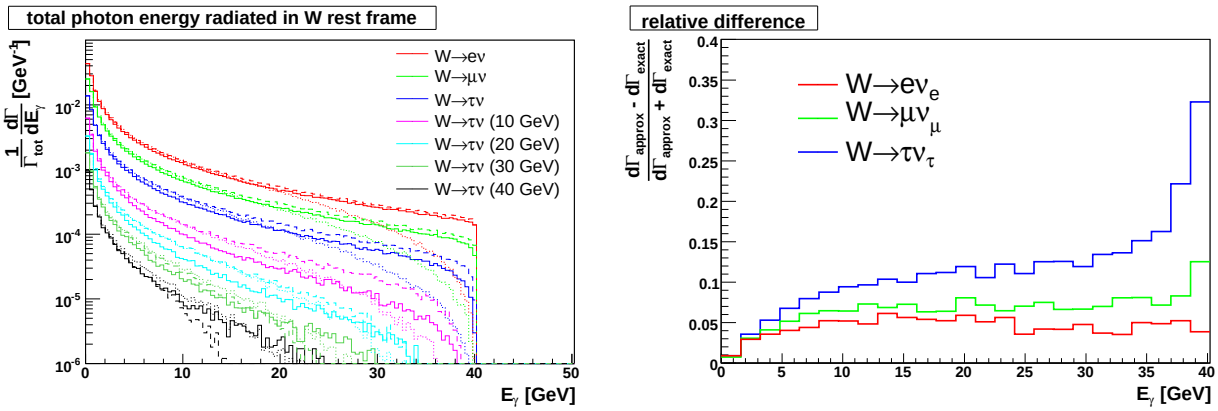

Figure 6.5: The total energy of all photons radiated in $W \to \ell\nu$. Left panel (a): The same plot as in Fig. 6.1(d), but this time the correction is done by using the **exact** matrix element (solid) instead of the **approximated** one (dashed). The distribution generated using the eikonals only is shown as a dotted line. Right panel (b): The relative difference of the distributions obtained using the exact and the approximated matrix elements. In both cases again different fermion masses have been used.

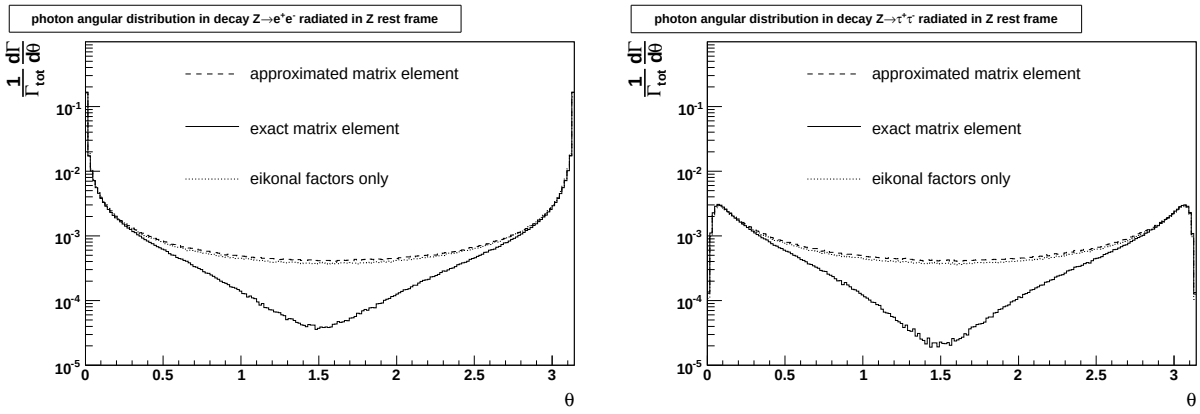

Figure 6.6: Angular distributions of the emitted photons in $Z \to \ell\bar{\ell}$, using exact and approximated matrix elements. In the left panel (a) and the right panel (b), the cases $Z \to ee$ and $Z \to \tau\tau$ are exhibited using the eikonals only (dotted lines) and corrections through exact (solid) and approximated matrix elements (dashed). In both plots the leptons sit at $\theta = 0$ and $\theta = \pi$.

through the dipole splitting kernels. This leads to a slightly earlier drop-off of the differential cross section w.r.t. radiated energy than with the approximated matrix elements.
Further, the absence of interference terms in both the eikonals and the quasi-collinear approximation lead to a depletion of radiation at large angles. Because of only small correlations between the energy of the photon radiated and its angular distribution this depletion leads to an almost constant decline in the differential cross section w.r.t. the photon energy. Of course this effect is small in the decay channel $Z \to e^+e^-$. However, the effect is increasing as the mass of the emitter is raised and a larger fraction of the radiation is radiated at large angles.

6.2 Other Channels

Finally, a short overview over other interesting cases is given. In principle, PHOTONS++ can handle any possible final state configuration in single particle decays independent of its charge. Thus, it is well suited to address all τ- and hadron decays, which will be the topic of this section.

6.2.1 J/Ψ decays to leptons

First of all, consider the case of $J/\Psi \to \ell\bar{\ell}$, which is topologically identical to leptonic Z-decay, but nonetheless very important for the calibration of detectors and as a background source of leptons. In Fig. 6.7 the decay channels $J/\psi \to e^+e^-$ and $J/\psi \to \mu^+\mu^-$ are investigated and the effect of $\mathcal{O}(\alpha)$ corrections is scrutinised. Again, the kinematic limit at half the mass of the decaying particle produces a visible and prominent kink. Due to the

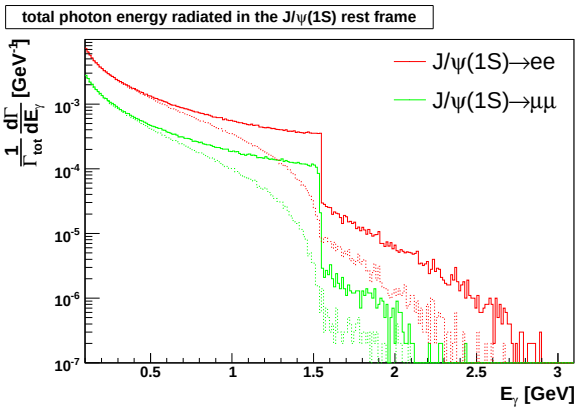

Figure 6.7: The total energy of the radiated photons in the rest frame of the decaying J/ψ vector meson for different lepton pairs (electrons in red, muons in green) in the final state. In the plot, $\mathcal{C} = 1$ (dotted) is contrasted with $\mathcal{C} = 1 + \tilde{\beta}_1^1/\tilde{\beta}_0^0$ (solid). In all cases, the distributions are normalised on the width of the inclusive decay into the respective lepton pair, and the infrared cut-off has been fixed to $\omega = 0.1$ GeV.

much smaller mass of the J/ψ compared to the Z mass, the effects of the higher muon mass is much more pronounced.

6.2.2 $B \to D^*+$ pions and Semileptonic B Decays

Another system to demonstrate the versatility of PHOTONS++ are B-decays because of its manyfold topologies in the final state. Exemplary, decays into a D^* accompanied with various numbers of charged and neutral π's have been chosen. The results are on display in Fig. 6.8, where the total radiated photon energy and the angular distribution of the photons are depicted. The orientation of the final state momenta has been chosen in such a way that configurations of the same multipole structure differing only by a neutral pion have a similar momentum distribution within the multipole, but still letting the π^0 have a non-vanishing effect. The most prominent feature in the distribution of the total energy of all photons in the B mesons restframe is the receding kinematic limit for the total energy, it is independent of the momentum layout within the multipole. It is due to the decreasing amount of phase space open for bremsstrahlung with an increasing number of pions. On the other hand, while the total energy available for the photon decreases, the amount of Bremsstrahlung increases with the number of charged particles involved. Switching from a dipole (two charged particles) to a quadrupole (four charged particles), the probability of double hard photon emission is increased due to favourable momentum configurations among the strongly radiating pions. Additionally, since the pions are spin-0, their photon distribution is generated exclusively by a product of eikonal factors. Furthermore, the angular distributions of the emitted photons are shown. There, the differential cross-section is integrated over energy and the azimuthal angle. For better interpretability these distributions are plotted in the rest frame of the multipole. The $D^*(2010)^-$ allways rests at $\theta = 0$. Due to its large mass, compared to the pions, very little radiation is emitted in its direction.

In contrast, all charged pions are plainly visible as peaks in the spectrum. However, their respective mass cones are hidden due to the azimuthal integration unless the pion sits at $\theta = \pi$, as is the case in the dipole configurations.
In Figure 6.9 semi-leptonic decays of B^0 and B^+ mesons are displayed. The resulting distributions are similar for e or μ being the lepton. This is because in both cases the bulk of the radiation is emitted off the lepton and the amount open for bremsstrahlung is of similar magnitude. Only the average photon multiplicity is noticeably affected by the difference in mass between the electron and the muon. Directly related to that is the increased number of multiple hard photon radiation in case of the electron. The τ-channel on the other hand presents itself differently due to the mass of the tau being comparable both to the mass of the B- and the D-meson. This not only leads to the near absence of soft bremsstrahlung above the infrared cut-off, as compared to the other semi-leptonic channels, it also results in a completely different radiation pattern: The bulk of the photons is radiated in-between both dipole particles and not primarily collinearly.

6.2.3 $\Delta^{++} \to p^+\pi^+$ Decays

A rather exotic decay for the purpose of this publication is the decay $\Delta^{++} \to p^+\pi^+$, due to its lack of neutral particles. This case is presented in Fig. 6.10, where the total energy and the angular distribution of the emitted photons are exhibited. However, this channel leaves only very little phase space open for photon radiation. Thus, collinear enhancement for the p^+ and the Δ^{++} should be negligible.

6.2.4 τ Decays

The leptonic τ decays are an example of a final state containing multiple neutral and massless particles. This has the effect, that the clear drop-off gets washed out as depicted in Figure 6.11. Because of the relatively small τ-mass and the considerable fraction of momentum carried by the neutrinos the effects of the different masses of the electron and the muon are plainly visible, in the photon energy spectrum as well as the angular distribution.

6.3 Numerical Stability and Precision in the Dead Cones of Ultra-Relativistic Particles

The dead cone of a massive particle is of size $\sim \frac{m}{E}$, cf. [28]. This leads to very small angles in case of highly relativistic charges such as electrons emitted from a decaying Z-boson. In this case the dead cone extends to $\theta \sim \frac{2m_e}{m_Z} \approx 1.12 \cdot 10^{-5}$. Figure 6.12 shows the dead cones of the charged leptons. As can be seen, they only scale with the mass of the lepton, as predicted. In case of the τ decay channel the depletion of radiation at large angles due to the inclusion of the interference terms in the exact matrix element is already visible.
Also the algorithm is numerically stable even for highly relativistic particles of very low mass.

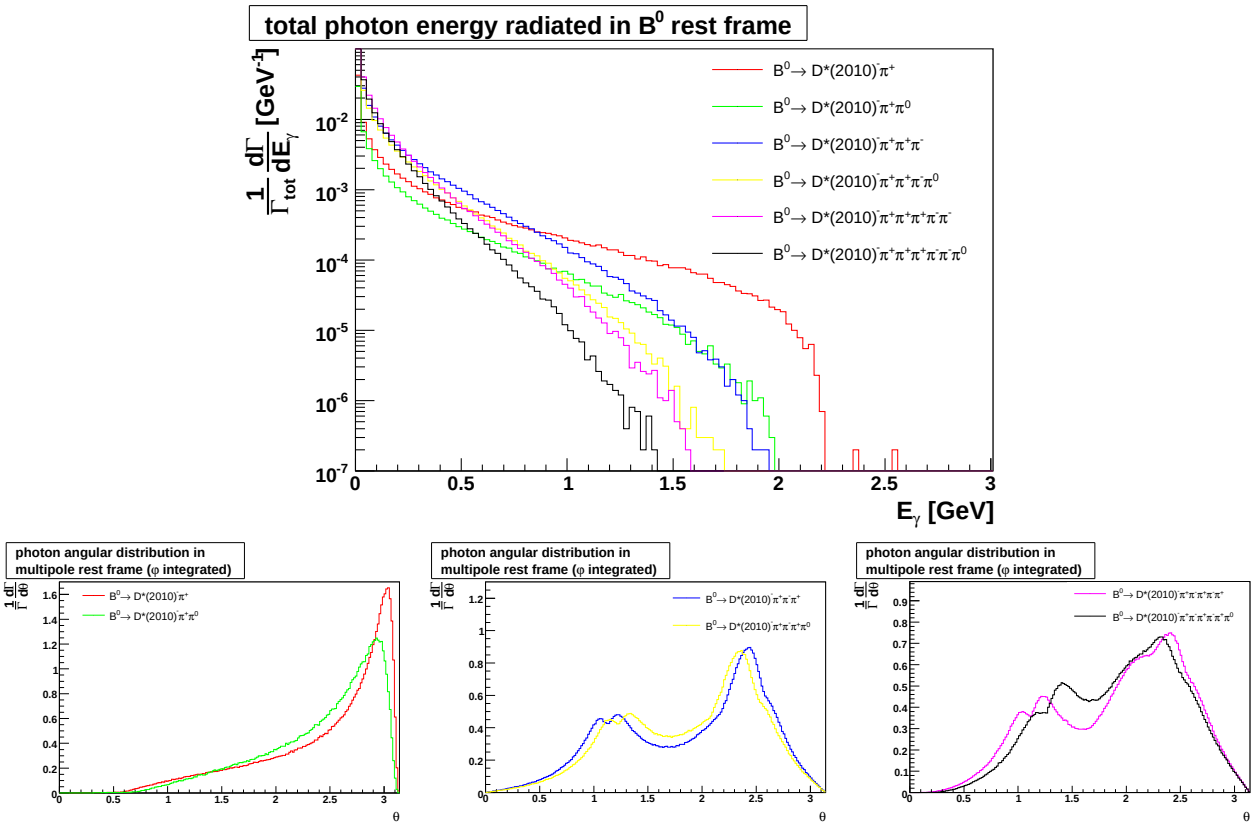

Figure 6.8: The total photon energy in the rest frame of the decaying B^0 meson for different numbers of pions in the final state (upper plot) and the angular distribution of this radiation in the multipole rest frame (lower panel). For the multi-body final states the same kinematic configuration have been used, as detailed in the text, to yield easily interpretable results. For identical multipoles similar final state momentum configurations with non-vanishing π^0 momentum have been chosen to increase comparability. The infrared cut-off in all cases has been set to $\omega = 1\text{MeV}$.

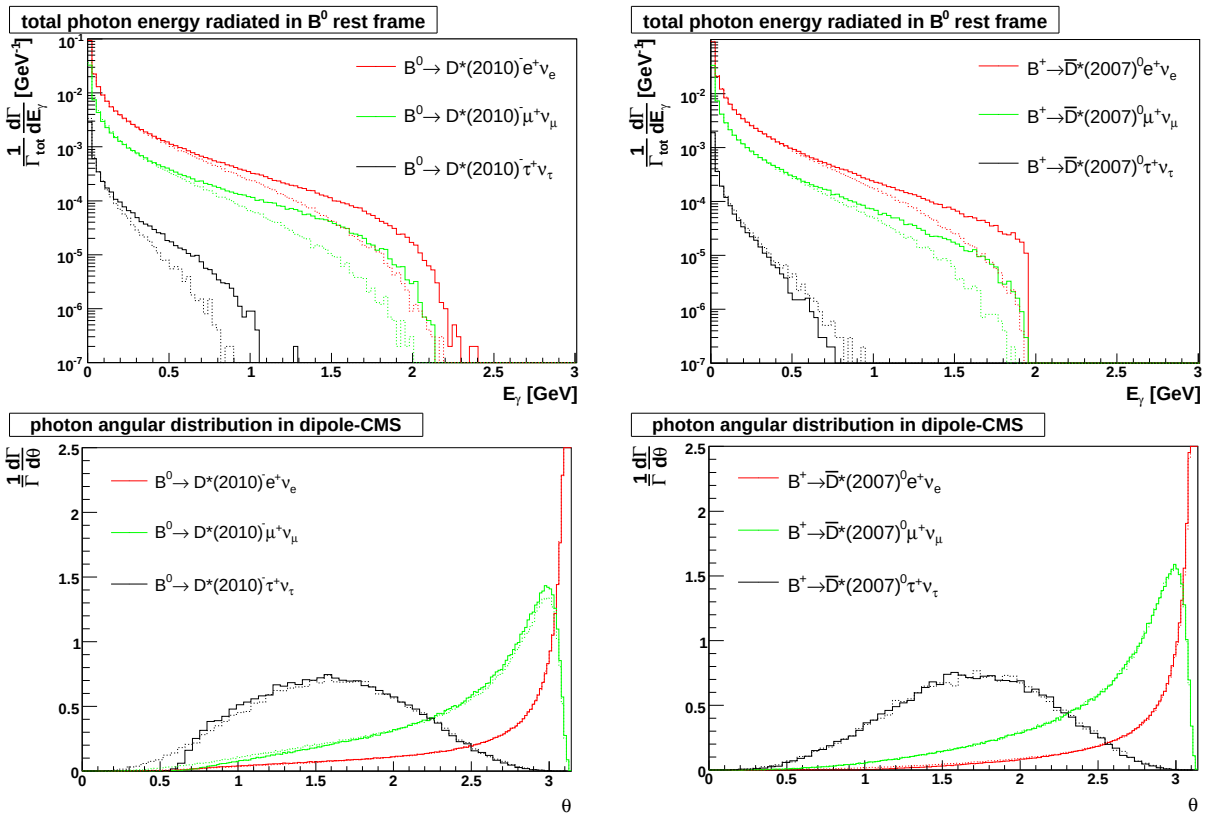

Figure 6.9: Semi-leptonic decays $B^{+,0} \to D^{*0,-}\ell\nu$ for different leptons and with different matrix element corrections. The solid line corresponds to the correction using the dipole splitting kernels, the dotted line to using the eikonals only. It is obvious that using the quasi-collinear approximation may lead to spurious results when the radiation pattern is not even close to this limit. Again, the infrared cut-off has been set to 1 MeV.

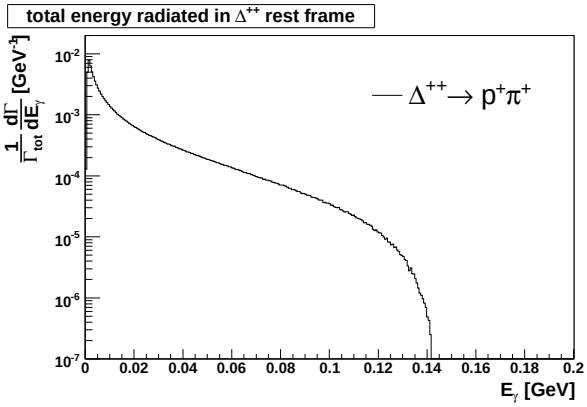

Figure 6.10: The total photon energy in $\Delta^{++} \to p^+\pi^+$ in the rest frame of the decaying Δ^{++} baryon is exhibited. The infrared cut-off was set to 1keV.

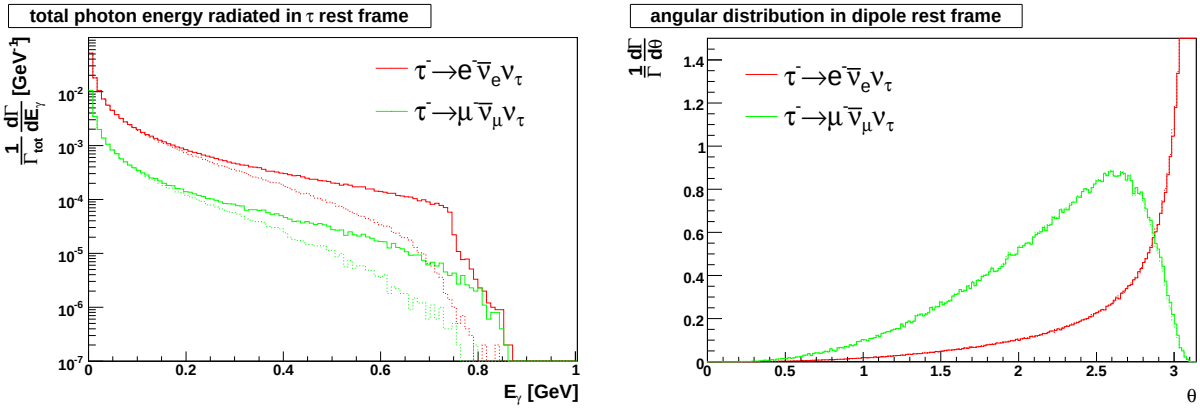

Figure 6.11: The total photon energy in $\tau^- \to \ell^- \bar{\nu}_\ell \nu_\tau$ in the rest frame of the decaying τ lepton is shown in the left panel. In the right panel the distribution of the photons' polar angle is shown. In both plots, the solid line shows the distribution corrected with the approximated matrix element and the dotted line the one using the eikonals only. The infrared cut-off has been set to 1 MeV.

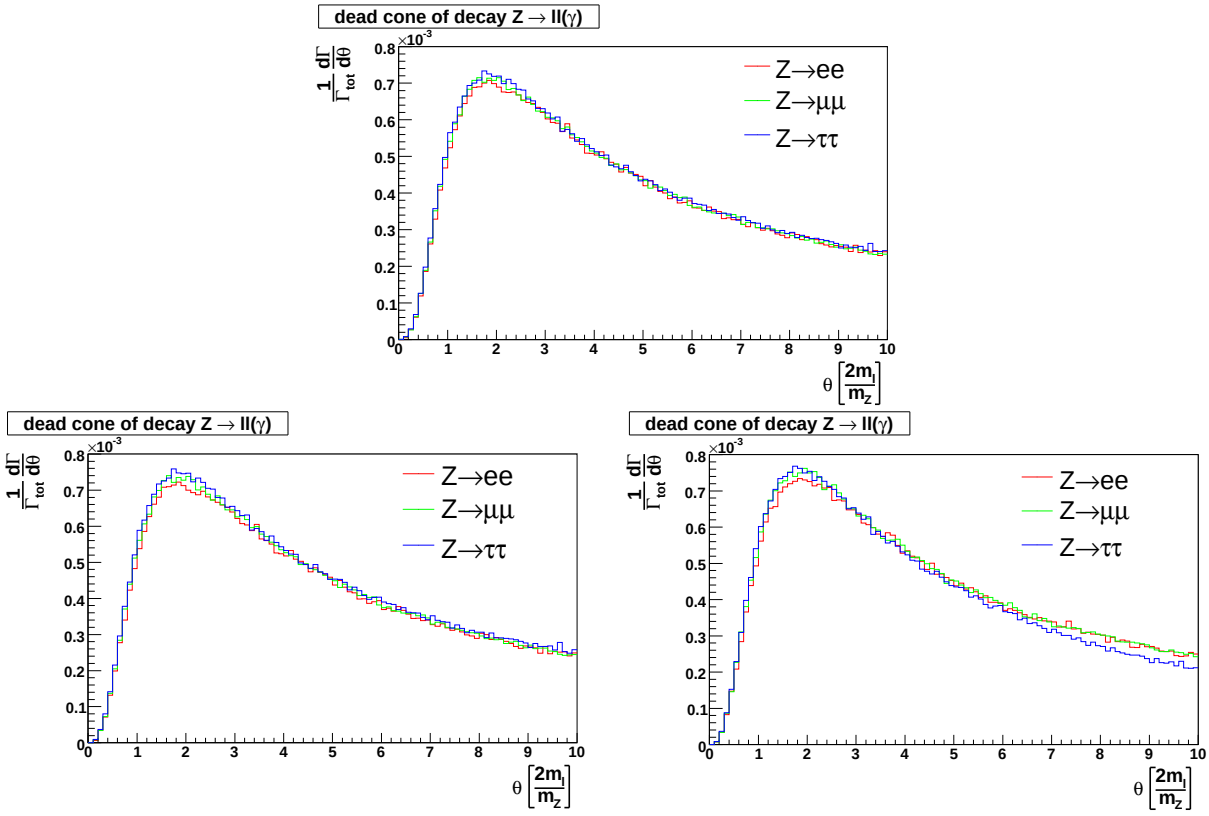

Figure 6.12: Dead cones of the charged leptons in $Z \to l\bar{l}$ decays. The left hand side shows the distributions corrected by the approximated matrix element, those on the right hand side is corrected by the exact matrix element. The one on the top is generated using the eikonals only. All distributions are normed to the total inclusive decay rate of the respective channel.

7 Conclusions

The result of this thesis, in relation to the implementation of the algorithm in the new module PHOTONS++, can be summarised in the following way:

1. The PHOTONS++ module was developed. It is constructed to correct all decay matrix elements of HADRONS++ [13, 14], the module handling most of the hadron decays in SHERPA[1], for soft QED radiation using the YFS-Formalism [2]. Higher order infrared subtracted squared matrix elements can systematically be included to correct for effects arising in non-singular regions. Per default, the first order infrared subtracted squared matrix element is approximated using the factorisation in the quasi-collinear limit [20, 22]. This has the advantage of a certain universality but lacks precision in many cases. PHOTONS++ is designed, however, to allow for easy incorporation of exact, process specific higher order infrared subtracted squared matrix elements.

2. PHOTONS++ is abled to treat any particle decay with an arbitrary final state configuration. All such decays can be grouped by the charge of the decaying particle. Thus, there are two distinct but intimately related algorithms for $Z_{dec.part.} = 0$ and $Z_{dec.part.} \neq 0$. However, it is not possible to treat all particle decays equally, as was shown in Section 3.3. As was shown, decays with multiple charged particle (multipoles) can be treated identically those with only two charged particles (dipoles). Nonetheless, all key routines are implemented twice to decrease processing time because in the dipole case, most of the integrals can be solved analytically.

3. The distributions obtained do have an acceptable dependence of the infrared cut-off. They also agree well with other generators dedicated to single channels and also employing the YFS-Formalism as their theoretical foundation. However, there are some differences that, nonetheless, agree with the expectation. Also, the inclusion of exact matrix elements for Z- and W-decays revealed inadequacies in approximating those matrix elements by the quasi-collinear approximation. Their origin is well understood and their quantity is within acceptable limits for physical cases. Despite this fact, the use of these approximated matrix element is mandatory if the universality of PHOTONS++ is not to be restricted.

Still, there is some work to be done to make PHOTONS++ more precise:

1. Further comparisons with other dedicated generators for different decay channels, such as HORACE [29], have to be made to further exclude the possibility of erroneous code. Although most programs do not employ the YFS-formalism but work at fixed order the difference should be small.

[1] All decay channels presently missing in HADRONS++ are handled by PYTHIA. Nonetheless, PHOTONS++ is abled to handle those in the same fashion.

2. Also decays involving multipoles should be checked qualitatively with programs like PHOTOS [30] which can handle more complicated final states. A direct agreement is not to be expected due different theoretical ansatzes and different handling of emissions off multipoles.

3. The not yet implemented matrix elements of Section 5 and further exact matrix elements have to be implemented for channels of interest to improve the accuracy of these decay modes.

4. For decay modes of particular interest, e.g. $Z \to \ell\bar{\ell}$, higher order matrix elements beyond $\mathcal{O}(\alpha)$ should be implemented. This also requires higher order loop calculations.

5. To further increase the number of decays that can be corrected by an exact matrix element some communication between HADRONS++ and PHOTONS++ has to be established to inform PHOTONS++ about which form factor model has been employed for the leading order hadronic decay.

6. General terms for $\tilde{\beta}_0^1$ will have to be implemented to correct consistently for any decay channel to $\mathcal{O}(\alpha)$.

This precision may not be of top priority at measurements at the LHC, except for the calibration channels. Nonetheless, it is of major importance for the data taking at present and future high precision machines, such as the e^+-e^--collider ILC. Furthermore, the Yennie-Frautschi-Suura Formalism is applicable to all matrix elements, production as well as decay. Thus, to achieve a consistent level of accuracy, also initial state radiation in the primary collisions should be included via the YFS-Formalism. However, the implementation developed here (Sec. 3) is insufficient for this task due to its construction as a correction tool and intrinsic assumption of negligible effect of the momentum shift in the initial state particles on the cross section/decay rate.

Appendix A Factorisation in the Soft Limit for Lines of Different Spins

The factorisation in the soft limit when the emitting line is a spin-$\frac{1}{2}$ fermion was already shown section 2.1. To show the factorisation for emissions off lines of different spins the procedure is similar. Starting with emissions off spin-0 bosons scalar QED will be used. The extension to scalar QED with formfactors is straight forward.

A.1 Emissions off Scalars

Now, using again Figs. 2.2, 2.3 and 2.4 as a representation of the basic interaction in which the additional photon line is to be inserted. If the charged line is a scalar, the matrix element of Fig. 2.2 contains a factor

$$\Gamma(p, q_i)\,. \tag{A.1}$$

Upon insertion of a photon into the initial state this will be modified to

$$\Gamma(p, \bar{q}_i)\frac{1}{(p-k)^2 - m^2}\,(p + p - k)_\mu \approx \Gamma(p, q_i)\frac{2p_\mu - k_\mu}{k^2 - 2(k\cdot p)}. \tag{A.2}$$

This directly corresponds to equation (2.6), but without any residuals. The further analysis proceeds as before, introducing some infrared finite terms along the line. These are only due to the approximation $\bar{q}_i \to q_i$ in the above matrix element fragment. No other terms appear away from the soft limit.

A.2 Emissions off Vectors

This factorisation is somewhat less easy to show in case of a charged vector line. Fig. 2.2 now contains a factor

$$\Gamma_{\mu\nu}(p, q_i)\,. \tag{A.3}$$

After the insertion of one photon into the initial state this factor, in Feynman gauge[1] , will have the form

$$\begin{aligned} & \Gamma_{\mu\rho}(p,\bar{q}_i)\frac{g^{\rho\sigma}}{(p-k)^2-m^2}\left[g_{\sigma\nu}(2p-k)_\tau+g_{\nu\tau}(-p-k)_\sigma+g_{\tau\sigma}(2k-p)_\nu\right] \\ \approx\ & \Gamma_{\mu\nu}(p,q_i)\frac{(2p-k)_\tau}{k^2-2(k\cdot p)} \\ & \qquad -\Gamma_{\mu\rho}(p,\bar{q}_i)\frac{1}{k_\lambda(k-2p)^\lambda}\left[g_{\nu\tau}k^\rho+2\delta^\rho_\tau k_\nu+g_{\nu\tau}p^\rho-\delta^\rho_\tau p_\nu\right] \qquad \text{(A.4)} \\ \overset{k\to 0}{=}\ & \Gamma_{\mu\nu}(p,q_i)\frac{(2p-k)_\tau}{k^2-2(k\cdot p)}\,. \qquad \text{(A.5)} \end{aligned}$$

The term $g_{\nu\tau}p^\rho-\delta^\rho_\tau p_\nu$ gives zero which can be seen easily when evaluating it in the rest frame of p. Hence, the soft limit of Eq.(2.8) is universal and independent of the spin of the emitting line.

[1] The choice of this gauge is both sufficient and beneficial. While giving the vector propagator in its simplest form, the additional gold stone boson that has to be considered is a scalar of the same mass. It thus shows the same factorisation as in the above case.

Appendix B Identities and Useful Formulae

B.1 Dimensional Regularisation

When calculating loops in Feynman graphs, divergent integrals are often encountered. In order to deduce the physical content of these terms it is necessary to identify and quantify their divergences. There are two basic types of divergence: infrared divergences occur as the momentum tends to zero, while ultraviolet divergences occur is it tends to infinity. Each integral has at most one type of divergence. Infrared divergences appearing within Feynman graphs involving loops of massless particles have to be cancelled with terms of opposite sign arising in Feynman graphs involving infinitely soft real emissions of those particles. In the case of Quantum Electro Dynamics, where this massless quantum is the photon, this is the major topic of this work. Ultraviolet divergences, on the other hand do not have such a counterpart. They have to be cancelled by counterterms and a renormalised theory emerges.

How to execute this extraction and cancellation of divergences is, however, not unambiguous. Nonetheless, if a theory is renormalisable, all divergences can be absorbed by mass, charge and wave function renormalisation.

B.1.1 The Idea

Considering the integral

$$I = \int \frac{\mathrm{d}^4 k}{(2\pi)^4} \frac{1}{k^2} \frac{1}{(k+p)^2 - m^2} \frac{1}{(k+q)^2 - m^2} \,, \tag{B.1}$$

as occurring in one loop Feynman amplitudes, it is to realise, that it is divergent as $k \to 0$. However, this is only the case in a 4 dimensional space-time. In a higher dimensional space-time this integral is finite. Thus, in the complex D-plain (D being the number of dimensions considered) the finite result at larger D's can be analytically continued to the divergent case $D = 4$. Then the divergence can be extracted and identified expanding the result in a Laurent series.

One of the major advantage of this dimensional regularisation scheme is that, besides not relying on an arbitrary cut-off, it completely preserves gauge invariance.

B.1.2 Integrals in D dimensions

The general starting point is the re-expression of the Feynman amplitudes in D dimensions. This basically amounts to substitution

$$\int \frac{\mathrm{d}^4k}{(2\pi)^4} \longrightarrow \mu^{4-D} \int \frac{\mathrm{d}^Dk}{(2\pi)^D} \tag{B.2}$$

in the divergent integrals (when $D = 4$). Herein μ is the regularisation scale introduced to preserve the dimension of the integral. It has to cancel when a finite result is extracted.
There are a few integrals available in D dimensions. Those of importance to this work read

$$\int \frac{\mathrm{d}^Dk}{(2\pi)^D} \frac{1}{(k^2-\Delta)^n} = \frac{i(-1)^n}{(4\pi)^{\frac{D}{2}}} \frac{\Gamma\left(n-\frac{D}{2}\right)}{\Gamma(n)} \Delta^{\frac{D}{2}-n} \tag{B.3}$$

and

$$\begin{aligned} &\int \frac{\mathrm{d}^{D-1}k}{(2\pi)^{D-1}} f(\kappa,\theta) \\ &= \frac{4}{(4\pi)^{\frac{D}{2}}\Gamma\left(\frac{D}{2}-1\right)} \int \mathrm{d}\kappa\, \kappa^{D-2} \int_{-1}^{1} \mathrm{d}c \left(1-c^2\right)^{\frac{D}{2}-2} f(\kappa,c)\,, \end{aligned} \tag{B.4}$$

where the D dimensional metric is taken to be Minkowskian with a $(D-1)$ dimensional Euklidian subspace, $\kappa = k^0$ and $c = \cos\theta$.

B.2 Feynman Parametrisation

When calculating amplitudes the denominator often is a product of a number of polynomials of the loop momentum. It is therefore convenient to combine them into a term of the form of (B.3). The following procedure to achieve this is called Feynman parametrisation. Another possible option is the Schwinger parametrisation.
If a and b are polynomials and α and β are real numbers, the following identity holds true:

$$\frac{1}{a^\alpha b^\beta} = \frac{\Gamma(\alpha+\beta)}{\Gamma(\alpha)\Gamma(\beta)} \int_0^1 \mathrm{d}y \frac{y^{\alpha-1}(1-y)^{\beta-1}}{[ay+b(1-y)]^{\alpha+\beta}}\,. \tag{B.5}$$

Of importance to this work are the following two identities deriving from the above one.

$$\frac{1}{ab} = \int_0^1 \mathrm{d}y \frac{1}{[(a-b)y+b]^2}\,, \tag{B.6}$$

$$\frac{1}{a^2b} = 2\int_0^1 \mathrm{d}y \frac{y}{[(a-b)y+b]^3}\,. \tag{B.7}$$

Also, the following similar identity will be used:

$$\frac{2}{(a\cdot b)(a\cdot c)} = \int_{-1}^{1} \mathrm{d}x \frac{1}{\left[\frac{1}{2}a\cdot((b+c)+x(b-c))\right]^2}\,, \tag{B.8}$$

wherein a, b and c are 4-vectors.

B.3 The Γ-Function

The Γ-Function is defined by the integral

$$\Gamma(z) \;=\; \int_0^\infty \mathrm{d}t\; t^{z-1}\, e^{-t} \tag{B.9}$$

for all complex z. This function has poles at all negative integers and at 0. Its basic relation

$$\Gamma(z+1) \;=\; z\,\Gamma(z) \tag{B.10}$$

relates it to the factorial and the identification

$$\Gamma(n+1) \;=\; n! \tag{B.11}$$

can be made for all postive integers n.

B.3.1 Important Expasions

Γ-Functions are often encountered in dimensional regularisation. When taking the limit $D \to 4$ ($\varepsilon \to 0$) the following expansions are of particular interest to the upcoming calculations.

$$\Gamma(\varepsilon) \;=\; \frac{1}{\varepsilon} - \gamma_E + \tfrac{1}{2}\left(\gamma_E^2 + \tfrac{1}{6}\pi^2\right)\varepsilon + \mathcal{O}(\varepsilon^2)\,, \tag{B.12}$$

$$\begin{aligned}\Gamma(1+\varepsilon) \;&=\; \varepsilon\,\Gamma(\varepsilon) \\ &=\; 1 - \gamma_E\varepsilon + \tfrac{1}{2}\left(\gamma_E^2 + \tfrac{1}{6}\pi^2\right)\varepsilon^2 + \mathcal{O}(\varepsilon^3)\,,\end{aligned} \tag{B.13}$$

$$\Gamma(1-\varepsilon) \;=\; 1 + \gamma_E\varepsilon + \tfrac{1}{2}\left(\gamma_E^2 + \tfrac{1}{6}\pi^2\right)\varepsilon^2 + \mathcal{O}(\varepsilon^3)\,. \tag{B.14}$$

B.4 The Dilogarithm

The Dilogarithm or Spence Function is defined via

$$\mathrm{Li}_2(x) \;=\; -\int_0^x \mathrm{d}t\,\frac{\ln(1-t)}{t}\,. \tag{B.15}$$

It has the following useful properities

$$\mathrm{Li}_2\,(0) \;=\; 0\,, \tag{B.16}$$

$$\mathrm{Li}_2\,(1) \;=\; \tfrac{1}{6}\pi^2\,, \tag{B.17}$$

$$\mathrm{Li}_2\,(-1) \;=\; -\tfrac{1}{12}\pi^2\,, \tag{B.18}$$

$$\mathrm{Li}_2\left(\tfrac{1}{2}\right) \;=\; \tfrac{1}{12}\pi^2 - \tfrac{1}{2}\ln^2 2\,. \tag{B.19}$$

Appendix C The YFS-Form-Factor

C.1 Cancellation of the Real and Virtual Divergences

Here, the cancellation of the virtual and real soft singularities will be made explicit and the YFS-Form-Factor will be calculated. Herein, whereever necessary, the focus will lie on the present case of interest.
As already defined in Sections 2 and 3 the YFS-Form-Factor

$$\begin{aligned} Y(\Omega) &= 2\alpha\left(\mathcal{R}e\ B + \tilde{B}(\Omega)\right) && \text{(C.1)}\\ &= 2\alpha\sum_{i<j}\left(\mathcal{R}e\ B(p_i,p_j) + \tilde{B}(p_i,p_j,\Omega)\right) && \text{(C.2)}\\ &\equiv 2\alpha\sum_{i<j}\left(\mathcal{R}e\ B_{ij} + \tilde{B}_{ij}(\Omega)\right) && \text{(C.3)} \end{aligned}$$

with the virtual infrared factor

$$B_{ij} = -\frac{i}{8\pi^3}Z_iZ_j\theta_i\theta_j\int\frac{\mathrm{d}^4k}{k^2}\left(\frac{2p_i\theta_i - k}{(k^2-2(k\cdot p_i)\theta_i} + \frac{2p_j\theta_j + k}{k^2+2(k\cdot p_j)\theta_j}\right)^2 \qquad \text{(C.4)}$$

and the real infrared factor

$$\tilde{B}_{ij}(\Omega) = \frac{1}{4\pi^2}Z_iZ_j\theta_i\theta_j\int\mathrm{d}^4k\,\delta(k^2)\,(1-\Theta(k,\Omega))\left(\frac{p_i}{(p_i\cdot k)} - \frac{p_j}{(p_j\cdot k)}\right)^2. \qquad \text{(C.5)}$$

As before, Z_i and Z_j are the charges of particles i and j in units of the positron charge, $\theta_{i,j} = +1\,(-1)$ if the respective particle is in the final state (initial state) and Ω is the region of the phase space wherein the photons are considered soft and unresolvable. $\Theta(k,\Omega) = 1$ if $k \notin \Omega$.

C.1.1 Calculation of the Real Emission Factor

The factor $\tilde{B}$ depends on the definition of Ω. It is convenient to divide the full photon phase space into Ω and $(1-\Omega)$ by specifying an isotropic hypersurface through a general energy cut-off in the frame of interest. Then,

$$\begin{aligned} \tilde{B}_{ij} &= \frac{1}{8\pi^2}Z_iZ_j\theta_i\theta_j\int_\Omega\frac{\mathrm{d}^3k}{k^0}\left[\frac{p_i}{k\cdot p_i} - \frac{p_j}{k\cdot p_j}\right]^2\\ &= \frac{1}{8\pi^2}Z_iZ_j\theta_i\theta_j\int_0^\omega\frac{\mathrm{d}^3k}{k^0}\left[\frac{p_i^2}{(p_i\cdot k)^2} + \frac{p_j^2}{(p_j\cdot k)^2} - 2\frac{(p_i\cdot p_j)}{(p_i\cdot k)(p_j\cdot k)}\right]. && \text{(C.6)} \end{aligned}$$

using identity (B.8) on the interference term to give $\int_{-1}^{1} \frac{dx}{(k\cdot p_x)^2} = \frac{2}{(p_i\cdot k)(p_j\cdot k)}$ with $p_x = \frac{1}{2}\left((p_i+p_j)+x(p_i-p_j)\right)$ this can be transformed into

$$\tilde{B}_{ij} = \frac{1}{8\pi^2} Z_i Z_j \theta_i \theta_j \int_0^\omega \frac{\mathrm{d}^3k}{k^0} \left[\frac{p_i^2}{(k\cdot p_x)^2}\bigg|_{x=1} + \frac{p_j^2}{(k\cdot p_x)^2}\bigg|_{x=-1} - (p_i\cdot p_j)\int_{-1}^{1} \frac{\mathrm{d}x}{(k\cdot p_x)^2} \right] \tag{C.7}$$

$$= \frac{1}{8\pi^2} Z_i Z_j \theta_i \theta_j \left[p_i^2\cdot \tilde{I}(1) + p_j^2 \cdot \tilde{I}(-1) - (p_i\cdot p_j)\int_{-1}^{1} dx \tilde{I}(x) \right] \tag{C.8}$$

with

$$\tilde{I}(x) = \int_0^\omega \frac{\mathrm{d}^3k}{k^0} \frac{1}{(k\cdot p_x)^2}\,. \tag{C.9}$$

Calculation of $\tilde{I}(x)$

This integral contains the divergence due to real soft photon emission. It thus has to be evaluated analytically and its divergences will be identified using dimensional regularisation. To that end, the integral is first transformed into an D-dimensional spacetime and then evaluated using (B.4),

$$\beta_x = \frac{\sqrt{(\vec{p}_1+\vec{p}_2)^2 + 2x(\vec{p}_1^{\,2}-\vec{p}_2^{\,2}) + x^2(\vec{p}_1-\vec{p}_2)^2}}{(E_1+E_2)+x(E_1-E_2)} \tag{C.10}$$

and $c=\cos\vartheta$.

$$\tilde{I}(x) = (2\pi)^3\mu^{4-D}\int_0^\omega \frac{\mathrm{d}^{D-1}k}{(2\pi)^{D-1}k^0}\frac{1}{(k\cdot p_x)^2} \tag{C.11}$$

$$= (2\pi)^3\mu^{4-D}\int_0^\omega \frac{\mathrm{d}^{D-1}k}{(2\pi)^{D-1}k^0}\frac{1}{k^{0^2}E_x^2(1-\beta_x c)^2} \tag{C.12}$$

$$= (2\pi)^3\mu^{4-D}\frac{4}{(4\pi)^{\frac{D}{2}}\Gamma\left(\frac{D}{2}-1\right)}\int_0^\omega \mathrm{d}\kappa\,\kappa^{D-5}\int_{-1}^{1}\mathrm{d}c\frac{(1-c^2)^{\frac{D}{2}-2}}{E_x^2(1-\beta_x c)^2} \tag{C.13}$$

with $\kappa = k^0 = |\vec{K}|$. Now, inserting $D=4+2\varepsilon$ and performing the κ-integration gives

$$\tilde{I}(x) = \frac{4(2\pi)^3\mu^{-2\varepsilon}}{(a\pi)^{2+\varepsilon}\Gamma(1+\varepsilon)}\int_0^\omega \mathrm{d}\kappa\,\kappa^{-1+2\varepsilon}\int_{-1}^{1}\mathrm{d}c\frac{(1-c^2)^\varepsilon}{E_x^2(1-\beta_x c)^2} \tag{C.14}$$

$$= \frac{2\pi}{(4\pi\mu^2)^\varepsilon\Gamma(1+\varepsilon)}\frac{(\omega^2)^\varepsilon}{2\varepsilon}\int_{-1}^{1}\mathrm{d}c\frac{(1-c^2)^\varepsilon}{E_x^2(1-\beta_x c)^2}\,. \tag{C.15}$$

Taking the limit $\varepsilon \to 0$ results in

$$\tilde{I}(x) = \pi\left(\frac{1}{\varepsilon} + \gamma_E + \ln\frac{\omega^2}{4\pi\mu^2}\right)\int_{-1}^{1}\frac{\mathrm{d}c}{E_x^2(1-\beta_x c)^2} + \pi\int_{-1}^{1}\mathrm{d}c\frac{\ln(1-c^2)}{E_x^2(1-\beta_x c)^2}\,. \tag{C.16}$$

Performing the integrals over c gives

$$\tilde{I}(x) = \frac{2\pi}{p_x^2}\left(\frac{1}{\varepsilon} + \gamma_E + \ln\frac{\omega^2}{4\pi\mu^2} + 2\ln 2 + \frac{1}{\beta_x}\ln\frac{1-\beta_x}{1+\beta_x}\right) \tag{C.17}$$

$$= \frac{4\pi}{p_x^2}\left(\frac{1}{2}\left(\frac{1}{\varepsilon} + \gamma_E + \ln\frac{\omega^2}{4\pi\mu^2} + \ln\frac{p_x^2}{E_x^2}\right) - \tilde{G}(x)\right)\,, \tag{C.18}$$

where

$$\tilde{G}(x) = \frac{1-\beta_x}{2\beta_x}\ln\frac{1+\beta_x}{1-\beta_x} + \ln\frac{1+\beta_x}{2} \tag{C.19}$$

has been introduced. This can now be reinserted into (C.8) giving

$$\tilde{B}_{ij} = \frac{Z_i Z_j \theta_i \theta_j}{2\pi}\left[\frac{1}{\varepsilon} + \gamma_E + \ln\frac{\omega^2}{4\pi\mu^2} + \frac{1}{2}\ln\frac{p_i^2 p_j^2}{E_i^2 E_j^2} - \tilde{G}(1) - \tilde{G}(-1) - \frac{(p_i\cdot p_j)}{4\pi}\int_{-1}^{1}\mathrm{d}x\tilde{I}(x)\right] \tag{C.20}$$

or, for purposes of brevity with the replacement $-\ln\lambda^2 = \frac{1}{\varepsilon} + \gamma_E - \ln(4\pi\mu^2)$,

$$\begin{aligned}\tilde{B}_{ij} = \frac{Z_i Z_j \theta_i \theta_j}{2\pi}\Bigg[&\ln\frac{\omega^2}{\lambda^2} + \ln\frac{m_i m_j}{E_i E_j} - \frac{(p_i\cdot p_j)}{2}\int_{-1}^{1}\mathrm{d}x\frac{\ln\frac{p_x^2}{\lambda^2}}{p_x^2} \\ &+ \frac{(p_i\cdot p_j)}{2}\int_{-1}^{1}\mathrm{d}x\frac{\ln\frac{E_x^2}{\omega^2}}{p_x^2} - \tilde{G}(1) - \tilde{G}(-1) \\ &+ (p_i\cdot p_j)\int_{-1}^{1}\mathrm{d}x\frac{\tilde{G}(x)}{p_x^2}\Bigg]\,.\end{aligned} \tag{C.21}$$

In this form all divergences are extracted and the remaining parameter integrals are finite as long as all particles involved are massive.

C.1.2 Calculation of the Virtual Emission Factor

The virtual emission factor reads

$$B_{ij} = -\frac{i}{8\pi^3}Z_i Z_j \theta_i \theta_j \int\frac{\mathrm{d}^4 k}{k^2}\left[\frac{2p_i\theta_i - k}{k^2 - 2k\cdot p_i\theta_i} + \frac{2p_j\theta_j + k}{k^2 + 2k\cdot p_j\theta_j}\right]^2\,. \tag{C.22}$$

Since B is strictly only defined by its behaviour in the soft limit it is possible to modify it by adding terms which vanish as $k \to 0$. For the following calculations it is useful to rewrite it as

$$\begin{aligned} B_{ij} &= -\tfrac{i}{8\pi^3} Z_i Z_j \theta_i \theta_j \int \frac{\mathrm{d}^4 k}{k^2} \left[\left(\frac{2p_i\theta_i}{k^2 - 2k\cdot p_i\theta_i} + \frac{2p_j\theta_j}{k^2 + 2k\cdot p_j\theta_j} \right)^2 \right. \\ &\qquad \left. - k^2 \left(\frac{1}{k^2 - 2k\cdot p_i\theta_i} - \frac{1}{k^2 + 2k\cdot p_j\theta_j} \right)^2 \right] \qquad \text{(C.23)} \\ &\equiv -\tfrac{i}{8\pi^3} Z_i Z_j \theta_i \theta_j \left[\left(4p_i^2 I_{ii} + 4p_j^2 I_{jj} + 8(p_i\cdot p_j)\theta_i\theta_j I_{ij} \right) \right. \\ &\qquad \left. - \left(J_{ii} + J_{jj} - 2J_{ij} \right) \right], \qquad \text{(C.24)} \end{aligned}$$

wherein the terms I_{ij}, I_{ii} and I_{jj} contain infrared divergences while and J_{ij}, J_{ii} and J_{jj} contain ultraviolet ones. Both have to be calculated, identified and dealt with.

Calculation of I_{ij}, I_{ii} and I_{jj}

The divergent terms now have to be calculated and the singularities have to be identified. Again, this will be done by using dimensional regularisation. After using identity (B.8) again with $p_x^{'} = \frac{1}{2}\left((p_i\theta_i - p_j\theta_j) + x(p_i\theta_i + p_j\theta_j)\right)$, this results in

$$\begin{aligned} I_{ij} &= \int \frac{\mathrm{d}^4 k}{k^2} \frac{1}{(k^2 - 2k\cdot p_i\theta_i)(k^2 + 2k\cdot p_j\theta_j)} \qquad \text{(C.25)} \\ &= (2\pi)^4 \mu^{4-D} \int \frac{\mathrm{d}^D k}{(2\pi)^D} \frac{1}{k^2(k^2 - 2k\cdot p_i\theta_i)(k^2 + 2k\cdot p_j\theta_j)} \qquad \text{(C.26)} \\ &= \frac{1}{2}(2\pi)^4 \mu^{4-D} \int \frac{\mathrm{d}^D k}{(2\pi)^D} \int_{-1}^{1} \mathrm{d}x \frac{1}{k^2(k^2 - 2k\cdot p_x^{'})^2}\,. \qquad \text{(C.27)} \end{aligned}$$

With identity (B.7) this can be cast in the form

$$I_{ij} = (2\pi)^4 \mu^{4-D} \int \frac{\mathrm{d}^D k}{(2\pi)^D} \int_{-1}^{1} \mathrm{d}x \int_{0}^{1} \mathrm{d}y \frac{y}{(k^2 - 2k\cdot p_x^{'} y)^3}\,, \qquad \text{(C.28)}$$

where the substitution $K = k - y p_x^{'}$ leads to

$$I_{ij} = (2\pi)^4 \mu^{4-D} \int \frac{\mathrm{d}^D K}{(2\pi)^D} \int_{-1}^{1} \mathrm{d}x \int_{0}^{1} \mathrm{d}y \frac{y}{(K^2 - p_x^{'2} y^2)^3}\,, \qquad \text{(C.29)}$$

which can be easily integrated using (B.3) with $\Delta = y^2 p_x^{'2}$. This yields

$$I_{ij} = -\frac{i(2\pi)^4}{(4\pi)^{\frac{D}{2}}} \mu^{4-D} \frac{\Gamma\left(3 - \frac{D}{2}\right)}{\Gamma(3)} \int_{-1}^{1} \mathrm{d}x \int_{0}^{1} \mathrm{d}y\, y (y^2 p_x^{'2})^{\frac{D}{2}-3}\,. \qquad \text{(C.30)}$$

Inserting $D = 4 + 2\varepsilon$, performing the y-integral and taking the limit $\varepsilon \to 0$ gives

$$I_{ij} = -\frac{i\pi^2}{2}\frac{1}{2\varepsilon}\frac{\Gamma(1-\varepsilon)}{(4\pi\mu^2)^\varepsilon}\int\limits_{-1}^{1}\mathrm{d}x\frac{(p_x'^2)^\varepsilon}{p_x'^2} \tag{C.31}$$

$$= -\frac{i\pi^2}{4}\left(\frac{1}{\varepsilon}+\gamma_E+\ln\frac{1}{4\pi\mu^2}\right)\int\limits_{-1}^{1}\frac{\mathrm{d}x}{p_x'^2} - \frac{i\pi^2}{4}\int\limits_{-1}^{1}\mathrm{d}x\frac{\ln p_x'^2}{p_x'^2}\,. \tag{C.32}$$

The calculation of I_{ii} and I_{jj} proceeds similarily, giving

$$I_{ii} = -\frac{i\pi^2}{2}\left(\frac{1}{\varepsilon}+\gamma_E+\ln\frac{1}{4\pi\mu^2}\right)\frac{1}{p_1^2} - \frac{i\pi^2}{2}\frac{\ln p_1^2}{p_1^2} \tag{C.33}$$

and

$$I_{jj} = -\frac{i\pi^2}{2}\left(\frac{1}{\varepsilon}+\gamma_E+\ln\frac{1}{4\pi\mu^2}\right)\frac{1}{p_2^2} - \frac{i\pi^2}{2}\frac{\ln p_2^2}{p_2^2}\,. \tag{C.34}$$

Therefore,

$$p_i^2 I_{ii} + p_j^2 I_{jj} + 2(p_i\cdot p_j)\theta_i\theta_j I_{ij}$$
$$= -i\pi^2\left(\ln\frac{m_i m_j}{\lambda^2}+\frac{1}{2}(p_i\cdot p_j)\theta_i\theta_j\int\limits_{-1}^{1}\mathrm{d}x\frac{\ln\frac{p_x'^2}{\lambda^2}}{p_x'^2}\right) \tag{C.35}$$

Calculation of J_{ii} , J_{ij} and J_{jj}

Using the same identities and substitutions as in the calculation of the I_{ij}

$$J_{ij} = \int \mathrm{d}^4k\frac{1}{(k^2-2k\cdot p_i\theta_i)(k^2+2k\cdot p_j\theta_j)} \tag{C.36}$$

$$= \frac{1}{2}(2\pi)^4\mu^{4-D}\int\frac{\mathrm{d}^Dk}{(2\pi)^D}\int\limits_{-1}^{1}\mathrm{d}x\frac{1}{(k^2-2k\cdot p_x')^2} \tag{C.37}$$

$$= \frac{i}{2}\frac{(2\pi)^4}{(4\pi)^{\frac{D}{2}}}\mu^{4-D}\frac{\Gamma\left(2-\frac{D}{2}\right)}{\Gamma(2)}\int\limits_{-1}^{1}\mathrm{d}x(p_x'^2)^{\frac{D}{2}-2}\,. \tag{C.38}$$

Only this time, because the J_{ij} are ultraviolet divergent, $D = 4 - 2\varepsilon$ is used, giving

$$J_{ij} = -\frac{i\pi^2}{2}\left(-\frac{1}{\varepsilon}+\gamma_E+\ln\frac{1}{4\pi\mu^2}\right)\int\limits_{-1}^{1}\mathrm{d}x - \frac{i\pi^2}{2}\int\limits_{-1}^{1}\mathrm{d}x\ln p_x'^2\,. \tag{C.39}$$

Similarily

$$J_{ii} = -i\pi^2\left(-\frac{1}{\varepsilon}+\gamma_E+\ln\frac{p_i^2}{4\pi\mu^2}\right) \tag{C.40}$$

and

$$J_{jj} = -i\pi^2\left(-\frac{1}{\varepsilon}+\gamma_E+\ln\frac{p_j^2}{4\pi\mu^2}\right) \tag{C.41}$$

can be obtained. Thus,

$$J_{ii}+J_{jj}-2J_{ij} = -4i\pi^2\left(-\frac{1}{4}\int\limits_{-1}^{1}\mathrm{d}x\ln\frac{p_x'^2}{m_1m_2}\right). \tag{C.42}$$

As can be seen , all ultraviolet divergences cancel leaving a finite contribution. Thus, the virtual emission factor reads

$$\begin{aligned} B_{ij} = -\frac{1}{2\pi}Z_iZ_j\theta_i\theta_j\Bigg[&\ln\frac{m_1m_2}{\lambda^2}+\frac{1}{2}(p_1\cdot p_2)\theta_1\theta_2\int\limits_{-1}^{1}\mathrm{d}x\frac{\ln\frac{p_x'^2}{\lambda^2}}{p_x'^2}\\ &+\frac{1}{4}\int\limits_{-1}^{1}\mathrm{d}x\ln\frac{p_x'^2}{m_1m_2}\Bigg], \end{aligned} \tag{C.43}$$

where the remaining divergences are contained explicitly in $-\ln\lambda^2$. It is to note that all ultraviolet divergences have cancelled and only infrared ones remain.

Recombination to the YFS-Form-Factor

The YFS-Form-Factor equals the real part of the sum of both soft emission factors. This sum reads and

$$\begin{aligned} &B_{ij}+\tilde{B}_{ij}\\ &= -\frac{Z_iZ_j\theta_i\theta_j}{2\pi}\Bigg[\ln\frac{E_iE_j}{\omega^2}+\frac{(p_i\cdot p_j)}{2}\left(\theta_i\theta_j\int\limits_{-1}^{1}\mathrm{d}x\frac{\ln\frac{p_x'^2}{\lambda^2}}{p_x'^2}+\int\limits_{-1}^{1}\mathrm{d}x\frac{\ln\frac{p_x^2}{\lambda^2}}{p_x^2}\right)\\ &\quad-\frac{(p_i\cdot p_j)}{2}\int\limits_{-1}^{1}\mathrm{d}x\frac{\ln\frac{E_x^2}{\omega^2}}{p_x^2}+\frac{1}{4}\int\limits_{-1}^{1}\mathrm{d}x\ln\frac{p_x'^2}{m_1m_2}\\ &\quad+\tilde{G}(1)+\tilde{G}(-1)-(p_i\cdot p_j)\int\limits_{-1}^{1}dx\frac{\tilde{G}(x)}{p_x^2}\Bigg] \end{aligned} \tag{C.44}$$

wherein the divergences are evidently not yet generally cancelled. To see that they in fact do cancel the parameter integrals have to be performed.

C.1.3 The Parameter Integrals

Here the complete solutions to analytically integrable parameter integrals of Eq. (C.44) are given. In the following, using the invariance of $Y(\Omega)$ under the interchange of $p_i \leftrightarrow p_j$, the labels p_i and p_j are chosen such that $E_j \geq E_i$. It is useful to define

$$x_{1,2} = -\frac{p_i^2-p_j^2\pm 2\sqrt{(p_i\cdot p_j)^2-p_i^2p_j^2}}{(p_i-p_j)^2} \tag{C.45}$$

as the roots of p_x^2 and

$$x'_{1,2} = -\frac{p_i^2 - p_j^2 \pm 2\sqrt{(p_i \cdot p_j)^2 - p_i^2 p_j^2}}{(p_i + p_j)^2} \tag{C.46}$$

as those of $p_x'^2$ in case of $\theta_i\theta_j = +1$, satisfying $x_{1,2} \notin [-1,1]$ and $x'_{1,2} \in (-1,1)$, respectively. It holds that $x_1, x'_2 > 0$ and $x_2, x'_1 < 0$ if $(p_i - p_j)^2 < 0$ and $0 < x_1 < x_2$ and $0 < x'_1 < x'_2$ if $(p_i - p_j)^2 > 0$. These differences in the relations between x_1 and x_2 necessitate the differentiation of distinct cases in the calculations.

Cancellation of the Last Divergence

The integral that has to be evaluated first is

$$\theta_i\theta_j \int_{-1}^{1} \mathrm{d}x \frac{\ln \frac{p_x'^2}{\lambda^2}}{p_x'^2} + \int_{-1}^{1} \mathrm{d}x \frac{\ln \frac{p_x^2}{\lambda^2}}{p_x^2}\,. \tag{C.47}$$

It still contains some parts of the infrared divergences of the real and virtual emission factors that need to cancel in order for the YFS-Form-Factor to be finite.
In the case that one particle is in the initial state while the other is in the final state, i.e. $\theta_i\theta_j = -1$, $p_x'^2 = p_x^2$. Thus, the sum of both integrals vanishes identically.
If on the other hand both particles are in either the initial state or the final state and, thus, $\theta_i\theta_j = +1$, the first integral can be transformed into

$$\int_{-1}^{1} \mathrm{d}x \frac{\ln \frac{p_x'^2}{\lambda^2}}{p_x'^2} = -\int_{-1}^{1} \mathrm{d}y \frac{\ln \frac{p_y^2}{\lambda^2}}{p_y^2} + \int_{-1}^{1} \mathrm{d}y \frac{\ln y^2}{p_y^2} + \int_{-\infty}^{\infty} \mathrm{d}y \frac{\ln \frac{p_y^2}{\lambda^2}}{p_y^2} \tag{C.48}$$

using the substitution $y = \frac{1}{x}$ and shifting the poles of $p_x'^2$ off the real axis $x'_1 - i\varepsilon$ and $x'_2 + i\varepsilon$. Furthermore, the branches of the logarithm have to be chosen such, that $\mathcal{I}m \ln \frac{p_x'^2}{\lambda^2} = 0$ at $x = \pm 1$.
It can already be seen that the first term cancels in the full expression (C.47). However, there is still a divergent integral left. This can be evaluated, with the poles of p_y^2 being at $z_1^{-1} = x_1'^{-1} + i\epsilon$ and $z_2^{-1} = x_2'^{-1} - i\epsilon$, $z_1^{-1}, z_2^{-1} \notin [-1;1]$, giving

$$\int_{-\infty}^{\infty} \mathrm{d}y \frac{\ln \frac{p_y^2}{\lambda^2}}{p_y^2} = \frac{1}{A}\int_{-\infty}^{\infty} dy \frac{\ln \frac{A}{\lambda^2} + \ln(z_1 y - 1) + \ln(z_2 y - 1)}{(z_1 y - 1)(z_2 y - 1)} \tag{C.49}$$

$$= \frac{2\pi i}{A(z_2 - z_1)} \left(\ln \frac{A}{\lambda^2} + \ln\left(1 - \frac{z_2}{z_1}\right) + \ln\left(1 - \frac{z_1}{z_2}\right) \right) \tag{C.50}$$

$$= \frac{2\pi i}{A(x'_2 - x'_1)} \left(\ln\left(\frac{A}{\lambda^2} \left| \frac{(x'_1 - x'_2)^2}{x'_1 x'_2} \right| \right) - i\pi\Theta(x'_1 x'_2) \right) \tag{C.51}$$

where the short hand notation $A = \frac{1}{4}(p_i + p_j)^2$ has been used. However, only the real part of this integral finds it way into the YFS-Form-Factor and its contribution

$$\mathcal{R}e \int_{-\infty}^{\infty} \mathrm{d}y \frac{\ln \frac{p_y^2}{\lambda^2}}{p_y^2} = \frac{2\pi^2}{A(x'_2 - x'_1)}\Theta(x'_1 x'_2) \tag{C.52}$$

is completely finite.
The last integral is easy to evaluate and yields

$$\int_{-1}^{1} \mathrm{d}y \frac{\ln y^2}{p_y^2} = \frac{8}{(p_i-p_j)^2(y_1-y_2)} \int_{-1}^{1} \mathrm{d}y \ln y \left(\frac{1}{y-y_1} - \frac{1}{y-y_2}\right) \tag{C.53}$$

$$= \frac{8}{(p_i-p_j)^2(y_1-y_2)} \left[\ln y_1 \left(\mathrm{Li}_2\left(\tfrac{y_1-1}{y_1}\right) - \mathrm{Li}_2\left(\tfrac{y_1+1}{y_1}\right)\right) - \ln y_2 \left(\mathrm{Li}_2\left(\tfrac{y_2-1}{y_2}\right) - \mathrm{Li}_2\left(\tfrac{y_2+1}{y_2}\right)\right)\right] . \tag{C.54}$$

The Second Integral of the Virtual Contribution

This integral reads

$$\mathcal{R}e\left(\int_{-1}^{1} \mathrm{d}x \ln \frac{p_x'^2}{m_i m_j}\right) .$$

Again, a differentiation according to the sign of $\theta_i\theta_j$ is necessary. If $\theta_i\theta_j = +1$, then the range of integration contains poles of the integrand at $x'_{1,2}$. In this case, however, no shifting off the real axis is necessary. It can be shown by carefully taking separate limits on both sides of the singularities that the integral over them is completely finite. It yields

$$\int_{-1}^{1} \mathrm{d}x \ln \frac{p_x'^2}{m_i m_j} = 2\ln\frac{(p_1+p_2)^2}{4m_i m_j} + \int_{-1}^{1} \mathrm{d}x \ln\left(x - x_1'\right) + \int_{-1}^{1} \mathrm{d}x \ln\left(x - x_2'\right) . \tag{C.55}$$

With

$$\int_{-1}^{1} dx \ln\left(x - x_i'\right) = i\pi(1+x_i') + \ln\left(1-x_i'^2\right) - x_i \ln\frac{1-x_i'}{1+x_i'} - 2 \tag{C.56}$$

this gives

$$\int_{-1}^{1} \mathrm{d}x \ln \frac{p_x'^2}{m_1 m_2} = 2\ln\frac{(p_i+p_j)^2}{4m_i m_j} + \ln\left[\left(1-x_1'^2\right)\left(1-x_2'^2\right)\right] - x_1 \ln\frac{1-x_1'}{1+x_1'} - x_2' \ln\frac{1-x_2'}{1+x_2'} - 4 + i\pi\left(2 + x_1' + x_2'\right) \tag{C.57}$$

Similarly obtainable is the solution for $\theta_i\theta_j = -1$. Only the analogue to (C.56) needs less care since, here, there are no poles within the range of integration. Thus, the solution reads

$$\int_{-1}^{1} \mathrm{d}x \ln \frac{p_x^2}{m_i m_j} = 2\ln\frac{|(p_i-p_j)^2|}{4m_i m_j} + \ln\left[(1-x_1^2)(1-x_2^2)\right] - x_1 \ln\left|\frac{1-x_1}{1+x_1}\right| - x_2 \ln\left|\frac{1-x_2}{1+x_2}\right| - 4 . \tag{C.58}$$

Evidently, the case $(p_i - p_j)^2 = 0$, as is the case in leptonic W-decays, has to be treated separately. p_x^2 is linear in x and has the root $x_p = -\frac{p_i^2+p_j^2}{p_i^2-p_j^2}$. Subsequently, the integral yields

$$\int_{-1}^{1} \mathrm{d}x \ln \frac{p_x^2}{m_i m_j} = 2 \ln \frac{|p_i^2 - p_j^2|}{2 m_i m_j} + \int_{-1}^{1} \mathrm{d}x \ln(x - x_p) \tag{C.59}$$

$$= 2 \ln \frac{|p_i^2 - p_j^2|}{2 m_i m_j} + \ln|1 - x_p^2| - x_p \ln \left| \frac{1 - x_p}{1 + x_p} \right| - 2 \,. \tag{C.60}$$

The case $m_i = m_j$ is kinematically not possible in decay matrix elements.

The First Integral of the Real Contribution

The last integral that is generally solveable analytically differentiates even more cases. The easiest to solve is the case of $E_i = E_j$, as it is occurring in leptonic Z-decays. Here, E_x is independent of x, thus giving

$$\int_{-1}^{1} \mathrm{d}x \frac{\ln \frac{E_x^2}{\omega^2}}{p_x^2} = 2 \ln \frac{E_i + E_j}{2\omega} \int_{-1}^{1} \frac{\mathrm{d}x}{p_x^2} \tag{C.61}$$

$$= \frac{8}{(x_1 - x_2)(p_i - p_j)^2} \ln \frac{E_i + E_j}{2\omega} \ln \left| \frac{(1 - x_1)(1 + x_2)}{(1 + x_1)(1 - x_2)} \right| . \tag{C.62}$$

with

$$\int_{-1}^{1} \frac{\mathrm{d}x}{p_x^2} = \frac{4}{(x_1 - x_2)(p_i - p_j)^2} \int_{-1}^{1} \mathrm{d}x \left(\frac{1}{x - x_1} - \frac{1}{x - x_2} \right) \tag{C.63}$$

$$= \frac{4}{(x_1 - x_2)(p_i - p_j)^2} \ln \left| \frac{(1 - x_1)(1 + x_2)}{(1 + x_1)(1 - x_2)} \right| . \tag{C.64}$$

For all other dipoles three distinct cases appear. This differentiation has to be done because of changing signs of different terms inside the logarithm in-between the different realms. With the above choice $E_j > E_i$ the integral simplifies to

$$\int_{-1}^{1} \mathrm{d}x \frac{\ln \frac{E_x}{\omega}}{p_x^2} = \int_{-1}^{1} \mathrm{d}x \frac{\ln \left[\frac{1}{2}(E_j - E_i) \right]}{p_x^2} + \frac{4}{(x_1 - x_2)(p_i - p_j)^2} \int_{-1}^{1} \mathrm{d}x \left(\frac{1}{x - x_1} - \frac{1}{x - x_2} \right) \ln(x_E - x) \,, \tag{C.65}$$

where $E_x = \frac{1}{2}\left[(E_i + E_j) + x(E_i - E_j)\right] = \frac{1}{2}(E_j - E_i)\,(x_E - x)$ with $x_E = -\frac{E_i+E_j}{E_i-E_j} > 1$. The following cases now differentiate between the different relations of x_1, x_2 and x_E towards each other.

A: $(p_i - p_j)^2 < 0$. This is the most straight forward case. x_1 and x_2 are of opposite sign, i.e. $x_1 > 1$ and $x_2 < -1$. The integral containing x_2 can safely be executed since it does not contain any poles.

$$\int_{-1}^{1} \mathrm{d}x \frac{\ln(x_E - x)}{x - x_2} = \int_{-1-x_2}^{1-x_2} \mathrm{d}y \frac{\ln(x_E - x_2 - y)}{y} \tag{C.66}$$

$$= \ln(x_E - x_2) \ln\left|\frac{1-x_2}{1+x_2}\right| + \int_{-1-x_2}^{1-x_2} \mathrm{d}y \frac{\ln\left(1 - \frac{y}{x_E - x_2}\right)}{y}, \tag{C.67}$$

where $y = x - x_2$. And further, with $z = \frac{y}{x_E - x_2}$,

$$\int_{-1-x_2}^{1-x_2} \mathrm{d}y \frac{\ln\left(1 + \frac{y}{x_2 - x_E}\right)}{y} = \int_{-\frac{1+x_2}{x_E - x_2}}^{\frac{1-x_2}{x_E - x_2}} \mathrm{d}z \frac{\ln(1-z)}{z} \tag{C.68}$$

$$= \mathrm{Li}_2\left(-\tfrac{1+x_2}{x_E - x_2}\right) - \mathrm{Li}_2\left(\tfrac{1-x_2}{x_E - x_2}\right). \tag{C.69}$$

Thus

$$\int_{-1}^{1} \mathrm{d}x \frac{\ln(x_E - x)}{x - x_2} = \ln(x_E - x_2) \ln\left|\frac{1-x_2}{1+x_2}\right| + \mathrm{Li}_2\left(-\tfrac{1+x_2}{x_E - x_2}\right) - \mathrm{Li}_2\left(\tfrac{1-x_2}{x_E - x_2}\right). \tag{C.70}$$

For the integral containing x_1 a different parametrisation is necessary because $x_1 - x_E$ may very well fall within the range of integration. A convenient choice is $E_x = E_i(1 + \zeta(1-x))$ with $\zeta = -\frac{E_i - E_j}{2E_i}$. In a second step the substitution $y = \frac{1+\zeta(1-x)}{1+\zeta(1-x_1)}$ is used.

$$\int_{-1}^{1} \mathrm{d}x \frac{\ln E_x}{x - x_1} = \int_{-1}^{1} \mathrm{d}x \frac{\ln E_i \left(1 + \zeta(1-x)\right)}{x - x_1} \tag{C.71}$$

$$= \ln E_i \ln\left|\frac{1-x_1}{1+x_1}\right| + \int_{-1}^{1} \mathrm{d}x \frac{\ln\left(1 + \zeta(1-x)\right)}{x - x_1} \tag{C.72}$$

and

$$\int_{-1}^{1} \mathrm{d}x \frac{\ln\left(1 + \zeta(1-x)\right)}{x - x_1} = -\int_{\frac{1+2\zeta}{y_1}}^{\frac{1}{y_1}} \mathrm{d}y \frac{y_1}{\zeta} \frac{\ln(y y_1)}{-\frac{y y_1 - 1}{\zeta} + 1 - x_1} \tag{C.73}$$

$$= \int_{\frac{1+2\zeta}{y_1}}^{\frac{1}{y_1}} \mathrm{d}y \frac{\ln y_1 + \ln y}{y - 1} \tag{C.74}$$

$$= \ln y_1 \ln\left|\frac{1-y_1}{1-y_1+2\zeta}\right| + \mathrm{Li}_2\left(\tfrac{y_1 - 1 - 2\zeta}{y_1}\right) - \mathrm{Li}_2\left(\tfrac{y_1 - 1}{y_1}\right), \tag{C.75}$$

with $y_1 = 1 + \zeta(1 - x_1)$. Thus, the full integral yields in this realm of momentum configurations

$$\begin{aligned}
&\int_{-1}^{1} \mathrm{d}x \frac{\ln \frac{E_x^2}{\omega^2}}{p_x^2} \\
&= \frac{8}{(x_1 - x_2)(p_i - p_j)^2} \left[\ln \frac{E_i}{\omega} \ln \left| \frac{1 - x_1}{1 + x_1} \right| + \ln |y_1| \ln \left| \frac{1 - x_1}{1 + x_1} \right| \right. \\
&\qquad - \ln \frac{(1 + x_2)E_i + (1 - x_2)E_j}{2\omega} \ln \left| \frac{1 - x_2}{1 + x_2} \right| \\
&\qquad + \mathrm{Li}_2 \left(-\tfrac{\zeta(1+x_1)}{y_1} \right) - \mathrm{Li}_2 \left(\tfrac{\zeta(1-x_1)}{y_1} \right) \\
&\qquad \left. - \mathrm{Li}_2 \left(-\tfrac{1+x_2}{x_E - x_2} \right) + \mathrm{Li}_2 \left(\tfrac{1-x_2}{x_E - x_2} \right) \right] . \qquad \text{(C.76)}
\end{aligned}$$

B: $(p_i - p_j)^2 > 0$. In this configuration of the momenta $x_2 > x_E > x_1 > 1$. In consequence, the solution to the integral containing x_1 is still valid. However, the one containing x_2 has to be redone, only this time $x_2 - x_E$ may fall within the range of integration, too. Thus a different parametrisation is needed. Choosing this to be similar to the case involving x_1 from above, namely $E_x = E_j(1 + \xi(1 + x))$ with $\xi = \frac{E_i - E_j}{2E_j}$, the integral yields

$$\begin{aligned}
\int_{-1}^{1} \mathrm{d}x \frac{E_x}{x - x_2} &= \int_{-1}^{1} \mathrm{d}x \frac{\ln E_2 \left(1 + \xi(1 + x)\right)}{x - x_2} && \text{(C.77)} \\
&= \ln E_2 \ln \left| \frac{1 - x_2}{1 + x_2} \right| + \int_{-1}^{1} \mathrm{d}x \frac{(1 + \xi(1 + x))}{x - x_2} && \text{(C.78)}
\end{aligned}$$

with the substitution $\frac{1-y}{y} = -\frac{1+\xi(1+x)}{1+\xi(1+x_2)}$ the integral can be solved, giving

$$\begin{aligned}
\int_{-1}^{1} \mathrm{d}x \frac{(1 + \xi(1 + x))}{x - x_2} &= - \int_{\frac{y_2}{y_2 - 1}}^{\frac{y_2}{y_2 - 1 - 2\xi}} \mathrm{d}y \frac{\ln(-y_2) + \ln \left(\frac{1-y}{y} \right)}{y} && \text{(C.79)} \\
&= \ln |y_2| \ln \left| \frac{y_2 - 1}{y_2 - 1 - 2\xi} \right| \\
&\quad + \tfrac{1}{2} \ln^2 \frac{y_2}{y_2 - 1 - 2\xi} - \tfrac{1}{2} \ln^2 \frac{y_2}{y_2 - 1} \\
&\quad - \mathrm{Li}_2 \left(\tfrac{y_2}{y_2 - 1} \right) + \mathrm{Li}_2 \left(\tfrac{y_2}{y_2 - 1 - 2\xi} \right) , && \text{(C.80)}
\end{aligned}$$

wherein $y_2 = 1 + \xi(1 + x_2)$. Thus, the full result is

$$\begin{aligned}
&\int_{-1}^{1} \mathrm{d}x \frac{\ln \frac{E_x^2}{\omega^2}}{p_x^2} \\
&= \frac{8}{(x_1 - x_2)(p_i - p_j)^2} \left[\ln \frac{E_i}{\omega} \ln \left| \frac{1 - x_1}{1 + x_1} \right| + \ln |y_1| \ln \left| \frac{1 - x_1}{1 + x_1} \right| \right. \\
&\qquad + \tfrac{1}{2} \ln^2 \left| \frac{y_2}{\xi(1 + x_2)} \right| - \tfrac{1}{2} \ln^2 \left| \frac{y_2}{\xi(1 - x_2)} \right| \\
&\qquad - \ln \frac{E_j}{\omega} \ln \left| \frac{1 - x_2}{1 + x_2} \right| + \ln |y_2| \ln \left| \frac{1 - x_2}{1 + x_2} \right| \\
&\qquad + \mathrm{Li}_2 \left(-\tfrac{\zeta(1+x_1)}{y_1} \right) - \mathrm{Li}_2 \left(\tfrac{\zeta(1-x_1)}{y_1} \right) \\
&\qquad \left. - \mathrm{Li}_2 \left(-\tfrac{y_2}{\xi(1-x_2)} \right) + \mathrm{Li}_2 \left(\tfrac{y_2}{\xi(1+x_2)} \right) \right] . \qquad \text{(C.81)}
\end{aligned}$$

C: $(p_i - p_j)^2 = 0$. With the definitions for x_E and x_p from above it allways holds that $x_E > x_p > 1$, thus

$$\begin{aligned}
\int_{-1}^{1} \mathrm{d}x \frac{\ln E_x^2}{p_x^2} &= 2 \int_{-1}^{1} \mathrm{d}x \frac{\ln \frac{1}{2}(E_2 - E_1)(x_E - x)}{\frac{1}{2}(p_2^2 - p_1^2)(x_p - x)} && \text{(C.82)} \\
&= \frac{4}{p_2^2 - p_1^2} \left(\ln \frac{1}{2}(E_2 - E_1) \ln \left| \frac{x_p + 1}{x_p - 1} \right| + \int_{-1}^{1} dx \frac{\ln(x_E - x)}{x_p - x} \right) && \text{(C.83)}
\end{aligned}$$

and, with the substitution $y = x_p - x$,

$$\begin{aligned}
\int_{-1}^{1} \mathrm{d}x \frac{\ln(x_E - x)}{x_p - x} &= - \int_{x_p+1}^{x_p-1} \mathrm{d}y \frac{\ln(x_e - x_p + y)}{y} && \text{(C.84)} \\
&= \ln(x_E - x_p) \ln \left| \frac{x_p + 1}{x_p - 1} \right| - \int_{x_p+1}^{x_p-1} \mathrm{d}y \frac{\left(1 + \frac{y}{x_E - x_p}\right)}{y} && \text{(C.85)} \\
&= \ln(x_E - x_p) \ln \left| \frac{x_p + 1}{x_p - 1} \right| + \mathrm{Li}_2 \left(\tfrac{x_p - 1}{x_p - x_E} \right) - \mathrm{Li}_2 \left(\tfrac{x_p + 1}{x_p - x_E} \right) . && \text{(C.86)}
\end{aligned}$$

Thus, the full result reads in this case

$$\begin{aligned}
&\int_{-1}^{1} \mathrm{d}x \frac{\ln \frac{E_x^2}{\omega^2}}{p_x^2} && \text{(C.87)} \\
&= \frac{4}{p_j^2 - p_i^2} \left[\ln \frac{E_j - E_i}{2\omega} \ln \left| \frac{1 + x_p}{1 - x_p} \right| + \ln(x_E - x_p) \ln \left| \frac{1 + x_p}{1 - x_p} \right| \right. \\
&\qquad \left. + \mathrm{Li}_2 \left(\tfrac{x_p - 1}{x_p - x_E} \right) - \mathrm{Li}_2 \left(\tfrac{x_p + 1}{x_p - x_E} \right) \right] .
\end{aligned}$$

The Second Integral of the Real Contribution

This is the integral

$$\int_{-1}^{1} \mathrm{d}x \frac{\tilde{G}_{12}(x)}{p_x^2} \tag{C.88}$$

is only solvable analytically in certain cases when either the dipole is its rest frame or in the rest frame of one of its constituents. In all other cases the integral has to be solved numerically. This, however, is harmless since the integrand is well behaved. Two special cases where analytical solutions can be obtained shall be discussed here.
A: A dipole of equal mass in its rest frame. Then, with $\beta = \frac{|\vec{p}_i|}{E_i} = \frac{|\vec{p}_j|}{E_j}$,

$$\beta_x = \beta|x| \tag{C.89}$$

and, with $E = E_i = E_j$,

$$p_x^2 = E^2\left(1-\beta^2 x^2\right) . \tag{C.90}$$

Inserting this into Eq. (C.88) yields

$$\begin{aligned}
&\int_{-1}^{1} \mathrm{d}x \frac{\tilde{G}_{12}(x)}{p_x^2} \\
&= \int_{-1}^{1} \mathrm{d}x \frac{1-\beta|x|}{2\beta|x|E^2(1-\beta^2x^2)} \ln\frac{1+\beta|x|}{1-\beta|x|} + \int_{-1}^{1} \frac{\mathrm{d}x}{E^2(1-\beta^2x^2)} \ln\frac{1+\beta|x|}{2} && \text{(C.91)}\\
&= \frac{1}{\beta E^2}\int_0^{\beta} \mathrm{d}y \frac{1-y}{y(1-y^2)} \ln\frac{1+y}{1-y} + \frac{2}{\beta E^2}\int_0^{\beta} \frac{\mathrm{d}y}{1-y^2} \ln\frac{1+y}{2} , && \text{(C.92)}
\end{aligned}$$

where $y = \beta x$ for $x > 0$ and $y = -\beta x$ for $x < 0$ have been substituted. These integrals now give

$$\begin{aligned}
&2\int_0^{\beta} \frac{\mathrm{d}y}{1-y^2} \ln\frac{1+y}{2} \\
&= \tfrac{1}{2}\ln^2\frac{1+\beta}{2} - \ln\frac{1-\beta}{2}\ln\frac{1+\beta}{2} + \tfrac{\pi^2}{12} - \mathrm{Li}_2\left(\tfrac{1+\beta}{2}\right) && \text{(C.93)}
\end{aligned}$$

and

$$\begin{aligned}
&\int_0^{\beta} \mathrm{d}y \frac{1-y}{y(1-y^2)} \ln\frac{1+y}{1-y} \\
&= \int_0^{\beta} \frac{\mathrm{d}y}{y(1+y)} \ln\frac{1+y}{1-y} && \text{(C.94)}\\
&= \ln\frac{1-\beta}{2}\ln\frac{1+\beta}{2} + \ln 2\ln(1+\beta) - \tfrac{1}{2}\ln^2 2 - \tfrac{1}{2}\ln^2(1+\beta) - \tfrac{\pi^2}{12} \\
&\quad + \mathrm{Li}_2\left(\tfrac{1-\beta}{2}\right) - \mathrm{Li}_2\left(-\beta\right) + \mathrm{Li}_2\left(\beta\right) . && \text{(C.95)}
\end{aligned}$$

Thus, the full integral reads

$$\begin{aligned}
&\int_{-1}^{1} \mathrm{d}x \frac{\tilde{G}(x)}{p_x^2} \\
&= \frac{1}{\beta E^2}\left[\tfrac{1}{2}\ln^2\frac{1+\beta}{2} + \ln 2\ln(1+\beta) - \tfrac{1}{2}\ln^2 2 - \tfrac{1}{2}\ln^2(1+\beta)\right. \\
&\qquad \left. + \mathrm{Li}_2\left(\tfrac{1-\beta}{2}\right) - \mathrm{Li}_2\left(\tfrac{1+\beta}{2}\right) + \mathrm{Li}_2(\beta) - \mathrm{Li}_2(-\beta)\right]. \qquad \text{(C.96)}
\end{aligned}$$

This result also gives a good approximation if both dipole constituents are of different mass but highly relativistic.

B: The other case analytically solveable which is of particular interest is the scenario of the leptoic W-decay. Here $m_j \gg m_i$ and $(p_i - p_j)^2 = 0$. The momenta in the rest frame of the dipole are

$$\begin{aligned}
p_W &\cong m_W\left(\tfrac{3}{\sqrt{8}}, 0, 0, \tfrac{1}{\sqrt{8}}\right) \qquad \text{(C.97)} \\
p_l &\cong m_W\left(\tfrac{1}{\sqrt{8}}, 0, 0, -\tfrac{1}{\sqrt{8}}\right). \qquad \text{(C.98)}
\end{aligned}$$

This leads to

$$\begin{aligned}
\beta_x &= \frac{|x|}{2-x} \\
p_x^2 &= \tfrac{1}{2}m_W^2\,[1-x]\,. \qquad \text{(C.99)}
\end{aligned}$$

Thus, the integral reads

$$\begin{aligned}
&\int_{-1}^{1} dx \frac{\tilde{G}(x)}{p_x^2} \\
&= \frac{2}{m_W^2}\int_0^1 dx\left[\frac{1}{x}\ln\frac{1}{1-x} + \frac{1}{1-x}\ln\frac{1}{2-x}\right] \\
&\quad + \frac{2}{m_W^2}\int_0^1 dx\left[\frac{1}{x(1+x)}\ln(1+x) + \frac{1}{1+x}\ln\frac{1+x}{2+x}\right] \qquad \text{(C.100)} \\
&= \frac{2}{m_W^2}\left[\mathrm{Li}_2(1) - \mathrm{Li}_2(-1) + \mathrm{Li}_2(-2) - \mathrm{Li}_2(-1) + \mathrm{Li}_2(-1)\right] \qquad \text{(C.101)} \\
&= \frac{2}{m_W^2}\left[\tfrac{3}{12}\pi^2 + \mathrm{Li}_2(-2)\right] \qquad \text{(C.102)}
\end{aligned}$$

C.2 Various Limits

C.2.1 The High Energy Dipole

If the multipole consists of only two particles in the final state, e.g. for decays of the type $Z \to \ell\bar{\ell}$, then the YFS-Form-Factor can be solved analytically in the rest frame of the dipole.

In the high-energy limit, given by $E_i \gg m_i$ for both QED corrected charged particles, the critical term above, Eq. (C.88), can be written as

$$(p_i \cdot p_j) \int_{-1}^{1} \mathrm{d}x \frac{\tilde{G}(x)}{p_x^2} \;\cong\; \tfrac{1}{6}\pi^2 \,. \tag{C.103}$$

Therefore, in this case, the full YFS form factor reads

$$\begin{aligned} Y(p_i, p_j, \omega) \;\cong\; -\frac{\alpha}{\pi} Z_i Z_j \theta_i \theta_j \Bigg[\left(1 - \ln \frac{2(p_i \cdot p_j)}{m_i m_j}\right) \ln \frac{E_i E_j}{\omega^2} + \ln \frac{E_i}{E_j} \ln \frac{m_i}{m_j} - \tfrac{1}{2} \ln^2 \frac{E_i}{E_j} \\ + \tfrac{1}{2} \ln \frac{(p_i\theta_i + p_j\theta_j)^2}{m_i m_j} - 1 - \tfrac{\pi^2}{6} \Bigg] \,, \end{aligned} \tag{C.104}$$

This result in the high-energy limit agrees with the result stated in [2].

C.2.2 Leptonic W-Boson Decay

A similar, but different case occurs for the decay of a charged particle into a final state involving only one charged particle, e.g. the case of W-decays, $W \to \ell\nu_\ell$. Then, in the corresponding dipole's rest frame neither $m_W \ll E_W$ nor $(p_i\theta_i + p_j\theta_j)^2 < 0$ and therefore this case is different from the one above. In this case

$$Y_W(\omega) \;=\; \frac{\alpha}{\pi} \left[2 \left(1 - \ln \frac{m_W}{m_l}\right) \ln \frac{m_W}{\omega\sqrt{8}} + \ln \frac{m_W}{m_l} - \tfrac{1}{2} + \tfrac{3}{2} \ln 2 - \tfrac{3}{12}\pi^2 \right] . \tag{C.105}$$

This result of course differs from the result in [23] since both results are given in different Lorentz-frames. Also, if in this process a photon is radiated, then $(p_W - p_l)^2 = 2(p_\nu \cdot p_\gamma) > 0$ and the YFS-Form-Factor takes a different a form.

Appendix D Transforming the Phase Space Elements

This section details the phase space manipulations necessary for the implementation of the YFS algorithm in form of a computer code.

D.1 Rewriting the Phase Space Element in other Frames

As discussed in Sec. 3.2, the phase space integral with the phase space element

$$\begin{aligned} \mathrm{d}\Phi &= \mathrm{d}\Phi_p \, \mathrm{d}\Phi_k \, (2\pi)^4 \delta \left(p_C + p_N - P_C - P_N - K \right) \\ &= \prod_{i=1}^{n} \left[\frac{\mathrm{d}^3 p_i}{(2\pi)^3 2 p_i^0} \right] \prod_{i=1}^{n_\gamma} \left[\frac{\mathrm{d}^3 k}{k^0} \right] (2\pi)^4 \delta \left(p_C + p_N - P_C - P_N - K \right) , \end{aligned} \tag{D.1}$$

has to be transformed to explicitly be in the chosen frame, the multipole rest frame. This can be achieved by using the identities

$$\begin{aligned} 1 &= \frac{2}{M^2} \int \mathrm{d}^4(p_C + p_N) \, \mathrm{d}^4 P_C \, \mathrm{d}m^2_{M,p} \, \delta \left(\frac{1}{M} (\vec{p}_C + \vec{p}_N) \right) \delta((p_C + p_N)^2 - M^2) \\ &\quad \times \delta^4 \left(P_C + P_N - \sum p_i \right) \delta((p_C + P_C)^2 - m^2_{M,p}) \, \Theta \left((p_C + p_N)^0 \right) . \end{aligned} \tag{D.2}$$

and

$$1 = \frac{2}{m^4_{M,p}} \int \mathrm{d}^4 x \, \delta \left(\frac{x^2}{m^2_{M,p}} - 1 \right) \delta^3 \left(\frac{1}{m_{M,p}} L^{-1} (p_C + P_C) \right) . \tag{D.3}$$

Here, $m_{M,p}$ is the invariant mass of the multipole $P_M = p_C + P_C$ and M is the invariant mass of the initial state $p_C + p_N$. As before, p_C and p_N and P_C and P_N are the sums of the initial and final state charged and neutral particles' momenta. The first identity basically amounts to extending the integration to an integration over the full phase space including the initial particles. The second identity, taken from [17], involves a Lorentz-transformation, denoted by L^{-1}, being the boost into the rest frame of x. Applying this boost on the phase space integral of course is a valid operation, since the full expression at this point is formulated in a Lorentz-invariant way. The result of this Lorentz-transformation, after inserting both

identities, reads

$$\begin{aligned}
\mathrm{d}\Phi &= (2\pi)^4 \mathrm{d}\Phi_p \mathrm{d}\Phi_k \int \mathrm{d}^4(p_C + p_N)\, \mathrm{d}^4 P_C\, \mathrm{d}m^2_{M,p}\, \mathrm{d}^4 x\, \frac{2}{M^2} \frac{2}{m^4_{M,p}} \\
&\quad \times \delta^4(p_C + p_N - P_C - P_N - K) \\
&\quad \times \delta^3\left(L(p_C + p_N)\right)\, \delta((p_C + p_N)^2 - M^2)\, \delta^4\left(P_C + P_N - \sum p_i\right) \\
&\quad \times \delta((p_C + P_C)^2 - m^2_{M,p})\, \Theta\left((p_C + p_N)^0\right) \\
&\quad \times \delta\left(\frac{x^2}{m^2_{M,p}} - 1\right) \delta^3\left(\frac{1}{m_{M,p}}(\vec{p}_C + \vec{P}_C)\right).
\end{aligned} \tag{D.4}$$

Reordering and using the identity

$$\delta\left(\frac{x^2}{m^2_{M,p}} - 1\right) = \int \mathrm{d}M^2 \delta\left(\frac{x^2}{M^2} - 1\right) \delta(M^2 - m^2_{M,p}) \tag{D.5}$$

yields

$$\begin{aligned}
\mathrm{d}\Phi &= (2\pi)^4 \mathrm{d}\Phi_p \mathrm{d}\Phi_k \int \mathrm{d}^4(p_C + p_N)\, \mathrm{d}^4 P_C\, \mathrm{d}m^2_{M,p} \frac{2}{M^2} \frac{2}{m_{M,p}} \\
&\quad \times \delta^4(p_C + p_N - P_C - P_N - K) \\
&\quad \times \delta^3(\vec{p}_C + \vec{P}_C)\, \delta((p_C + p_N)^2 - M^2)\, \delta^4\left(P_C + P_N - \sum p_i\right) \\
&\quad \times \delta((p_C + P_C)^2 - m^2_{M,p})\, \Theta\left((p_C + p_N)^0\right) \\
&\quad \times \int \mathrm{d}^4 x\, \mathrm{d}M^2\, \delta\left(\frac{x^2}{M^2} - 1\right) \delta^3\left(\frac{1}{M} L(p_C + p_N)\right) \delta(M^2 - m^2_{M,p}).
\end{aligned} \tag{D.6}$$

The last line can be further simplified by using the identity of Eq. (D.3) again and by integrating over M^2. Now, the other integrations can be performed, first over $(p+p_N)$, then over P and finally over $m^2_{M,p}$. This results in

$$\mathrm{d}\Phi = (2\pi)^4 \mathrm{d}\Phi_p \mathrm{d}\Phi_k \frac{2m^3_{M,p}}{M^2}\, \delta^3(2\sum \vec{p}_i - \vec{P}_N + \vec{K} - \vec{p}_N)\, \delta\left(\left(\sum p_i + K\right)^2 - M^2\right), \tag{D.7}$$

where $m^2_{M,p} = (p_C + P_C)^2 = (2\sum p_i - P_N + K - p_N)^2 = P^2_M$ is the invariant mass of the QED-corrected multipole.
Finally, the identity

$$\delta\left(\left(\sum p_i + K\right)^2 - M^2\right) = \frac{1}{2(P^0_C + P^0_N + K^0)} \delta(P^0_M - P^0_{M,0}) \tag{D.8}$$

will be used, where $P^0_{M,0} = P^0_C + p^0_C = m_{M,p}$ and where all zero-components are taken in the rest frame of $P_M = p_C + P_C$. Therefore,

$$\mathrm{d}\Phi = (2\pi)^4 \frac{m^3_{M,p}}{M^2(P^0_C + P^0_N + K^0)}\, \mathrm{d}\Phi_p\, \mathrm{d}\Phi_k\, \delta^3(\vec{P}_M)\, \delta\left(P^0_M - P^0_C - p^0_C\right). \tag{D.9}$$

The phase space element $\mathrm{d}\Phi$ has thus been explicitly rewritten in the rest frame of the multipole, at the cost of a Jacobian.

Similarly, the zeroth order uncorrected cross section can be transformed to

$$\begin{aligned} \mathrm{d}\Phi_0 &= (2\pi)^4 \mathrm{d}\Phi_q \, \delta^4 \left(p_C + p_N - Q_C - Q_N\right) \\ &= (2\pi)^4 \frac{m_{M,q}^3}{M^2(Q_C^0 + Q_N^0)} \, \mathrm{d}\Phi_q \, \delta^3(\vec{Q}_M) \, \delta\left(Q_M^0 - Q_C^0 - p_C^0\right) . \end{aligned} \tag{D.10}$$

where $m_{M,q}$ is the invariant mass of the uncorrected multipole and the Q_C^0 and Q_N^0 are taken in the Q_M rest frame.

D.2 Rewriting the Phase Space Element in Terms of the Undressed Momenta

In both cases the manipulations can be done in close analogy to the unitary algorithm of [18]. The necessary manipulations are easiest done backwards, starting with the phase space integral in terms of the q_i and defining $n = n_C + n_N$ to be the number of final state particles.

D.2.1 Mixed Multipoles

In this case the starting point reads

$$\begin{aligned} &\int \prod_{i=1}^{n} \frac{\mathrm{d}^3 q_i}{2q_i^0} \, \delta^3(\vec{Q_M}) \delta(Q_M^0 - Q_C^0 - p_C^0) \\ &\quad = \int \prod_{i=1}^{n} \left[\mathrm{d}^4 q_i \, \delta\left(q_i^2 - m_i^2\right) \Theta(q_i^0)\right] \, \delta^3 \left(\sum_C \vec{q}_i + \vec{p}_C\right) \, \delta\left(Q_M^0 - \sum_C q_i^0 - p_C^0\right) . \end{aligned} \tag{D.11}$$

This can be recast into a better form by inserting the identity

$$\begin{aligned} 1 &= \int \prod_{i=1}^{n} \left[\mathrm{d}^4 p_i \, \delta^3 \left(\vec{p}_i - u\vec{q}_i + \frac{1}{2n_C + n_N}\vec{K}\right) \, \delta\left(p_i^0 - \sqrt{\vec{p}_i^2 + m_i^2}\right)\right] \\ &= \int \prod_{i=1}^{n} \left[\mathrm{d}^4 p_i \, \delta^3 \left(\vec{p}_i - u\vec{q}_i + \vec{\kappa}\right) \, \delta\left(p_i^0 - \sqrt{\vec{p}_i^2 + m_i^2}\right)\right] \end{aligned} \tag{D.12}$$

with the abbreviation

$$\vec{\kappa} = \frac{\vec{K}}{2n_C + n_N} , \tag{D.13}$$

by using the definition of u written as

$$\begin{aligned} 1 = \int \mathrm{d}u \, \delta \Bigg[&\sqrt{M^2 + \left(u \sum_C \vec{q}_i - n_C \vec{\kappa}\right)^2} \\ &- \sum_{C,N} \sqrt{m_i^2 + (u\vec{q}_i - \vec{\kappa})^2} - K^0 \Bigg] \left(\frac{\vec{p}_C' \vec{p}_C}{p_C'^0} - \sum_{C,N} \frac{\vec{p}_i \vec{q}_i}{p_i^0} \right) \end{aligned} \tag{D.14}$$

and by expressing the δ-function fixing Q_M^0 in terms of the kinematically relevant variables q_i^0 and p_C^0. This then yields

$$\begin{aligned}
&\int \prod_{i=1}^{n} \frac{\mathrm{d}^3 q_i}{2q_i^0}\, \delta^3(\vec{Q}_M)\delta(Q_M^0 - Q_C^0 - p_C^0) \\
&= \int \mathrm{d}u \prod_{i=1}^{n} \left[\mathrm{d}^4 q_i\, \mathrm{d}^4 p_i\, \delta\left(q_i^2 - m_i^2\right) \Theta(q_i^0)\, \delta^3\left(\vec{p}_i - u\vec{q}_i + \vec{\kappa}\right) \delta\left(p_i^0 - \sqrt{\vec{p}_i^{\,2} + m_i^2}\right)\right] \\
&\quad \times \delta\left(\sqrt{M^2 + \left(u\sum_C \vec{q}_i - n_C\vec{\kappa}\right)^2} - \sum_{C,N} \sqrt{m_i^2 + \left(u\vec{q}_i - \vec{\kappa}\right)^2} - K^0\right) \\
&\quad \times \delta^3\left(\sum_C \vec{q}_i + \vec{p}_C\right)\, \delta\left(\sqrt{M^2 + \left(\sum_C \vec{q}_i\right)^2} - \sum_{C,N} q_i^0\right) \times \left[\frac{\vec{p}_C'\vec{p}_C}{p_C'^0} - \sum_{C,N} \frac{\vec{p}_i\vec{q}_i}{p_i^0}\right]
\end{aligned} \tag{D.15}$$

Integrating over $\mathrm{d}^3 q_i$ and $\mathrm{d}q_i^0$, using $\delta\left(x^2 - x_0^2\right)\Theta(x) = \frac{1}{2x_0}\delta(x - x_0)$, and integrating over u yields

$$\begin{aligned}
&\int \prod_{i=1}^{n} \frac{\mathrm{d}^3 q_i}{2q_i^0}\, \delta^3(\vec{Q_M})\delta(Q_M^0 - Q_C^0 - p_C^0) \\
&= \int \mathrm{d}u \prod_{i=1}^{n} \left[\mathrm{d}^4 p_i \delta\left(p_i^0 - \sqrt{\vec{p}_i^{\,2} + m_i^2}\right) \frac{1}{u^3} \frac{1}{2\sqrt{\frac{1}{u^2}\left(\vec{p}_i + \vec{\kappa}\right)^2 + m_i^2}}\right] \\
&\quad \times \delta^3\left(\frac{1}{u}\left[\sum_C \vec{p}_i + n_C\vec{\kappa} + u\vec{p}_C\right]\right) \\
&\quad \times \delta\left(\sqrt{M^2 + \frac{1}{u^2}\left[\sum_C \vec{p}_i + n_C\vec{\kappa}\right]^2} - \sum_{C,N} \sqrt{m_i^2 + \frac{1}{u^2}\left[\vec{p}_i + \vec{\kappa}\right]^2}\right) \\
&\quad \times \delta\left(\sqrt{M^2 + \left[\sum_C \vec{p}_i\right]^2} - \sum_{C,N} \sqrt{m_i^2 + \vec{p}_i^{\,2}} - K^0\right) \times \left[\frac{\vec{p}_C'\vec{p}_C}{p_C'^0} - \sum_{C,N} \frac{\vec{p}_i\left(\vec{p}_i + \vec{\kappa}\right)}{up_i^0}\right]. \\
&= \int \prod_{i=1}^{n} \left[\mathrm{d}^4 p_i \delta\left(p_i^0 - \sqrt{\vec{p}_i^{\,2} + m_i^2}\right) \frac{1}{u^3} \frac{1}{2\sqrt{\frac{1}{u^2}\left(\vec{p}_i + \vec{\kappa}\right)^2 + m_i^2}}\right] \\
&\quad \times u^3\delta^3\left(\sum_C \vec{p}_i + \vec{p}_C'\right) \delta\left(\sqrt{M^2 + \left[\sum_C \vec{p}_i\right]^2} - \sum_{C,N} \sqrt{m_i^2 + \vec{p}_i^{\,2}} - K^0\right) \\
&\quad \times \left[\frac{\vec{p}_C'\vec{p}_C}{p_C'^0} - \sum_{C,N} \frac{\vec{p}_i\left(\vec{p}_i + \vec{\kappa}\right)}{up_i^0}\right] \left[\frac{u}{\frac{\vec{p}_C^{\,2}}{p_C^0} - \sum_{C,N} \frac{\vec{q}_i^{\,2}}{q_i^0}}\right],
\end{aligned} \tag{D.16}$$

where in the integration over u the second last δ-function of the line above has been used. Furthermore, in this transformation, an identity similar to (D.14), arising when defining u

in terms of p_i, has been employed. A rearrangement of terms and a suitable transformation of the last δ-function in terms of P_M yields

$$\begin{aligned}
&\int \prod_{i=1}^{n} \frac{\mathrm{d}^3 q_i}{2q_i^0}\, \delta^3(\vec{Q_M})\delta(Q_M^0 - Q_C^0 - p_C^0) \\
&= \int \prod_{i=1}^{n} \left[\mathrm{d}^4 p_i \delta\left(p_i^2 - m_i^2\right) \Theta(p_i^0) \frac{1}{u^3} \frac{\sqrt{\vec{p}_i^{\,2} + m_i^2}}{\sqrt{\frac{1}{u^2}\left(\vec{p}_i + \vec{\kappa}\right)^2 + m_i^2}} \right] \\
&\quad \times u^4 \delta^3\left(\sum_C \vec{p}_i + \vec{p}_C'\right) \delta\left(p_C'^0 - P_C^0 - P_N^0 - K^0\right) \frac{\frac{\vec{p}_C' \vec{p}_C}{p_C'^0} - \sum_{C,N} \frac{\vec{p}_i \vec{q}_i}{p_i^0}}{\frac{\vec{p}_C^{\,2}}{p_C^0} - \sum_{C,N} \frac{\vec{q}_i^{\,2}}{q_i^0}} \\
&= \int \prod_{i=1}^{n} \left[\mathrm{d}^4 p_i \delta\left(p_i^2 - m_i^2\right) \Theta(p_i^0) \right] \delta^3\left(\vec{P}_M\right) \delta\left(P_M^0 - P_C^0 - p_C'^0\right) \\
&\quad \times \frac{1}{u^{3n-4}} \frac{\frac{\vec{p}_C' \vec{p}_C}{p_C'^0} - \sum_{C,N} \frac{\vec{p}_i \vec{q}_i}{p_i^0}}{\frac{\vec{p}_C^{\,2}}{p_C^0} - \sum_{C,N} \frac{\vec{q}_i^{\,2}}{q_i^0}} \prod_{i=1}^{n} \left[\frac{p_i^0}{q_i^0}\right] . \qquad \text{(D.17)}
\end{aligned}$$

Here, the identity

$$q_i^0 = \sqrt{\frac{1}{u^2}\left(\vec{p}_i + \vec{\kappa}\right)^2 + m_i^2} \qquad \text{(D.18)}$$

has been used. Reversing the procedure allows to express the phase space element through the undressed final state momenta as

$$\begin{aligned}
\mathrm{d}\Phi &= (2\pi)^4\, \mathrm{d}\Phi_q\, \mathrm{d}\Phi_k\, \delta^3\left(\vec{Q}_M\right) \delta\left(Q_M^0 - Q_C^0 - p_C^0\right) \frac{m_M^3}{M^2\left(P_C^0 + P_N^0 + K^0\right)} \\
&\quad \times u^{3n-4} \frac{\frac{\vec{p}_C^{\,2}}{p_C^0} - \sum_{C,N} \frac{\vec{q}_i^{\,2}}{q_i^0}}{\frac{\vec{p}_C' \vec{p}_C}{p_C'^0} - \sum_{C,N} \frac{\vec{p}_i \vec{q}_i}{p_i^0}} \prod_{i=1}^{n} \left[\frac{q_i^0}{p_i^0}\right] . \qquad \text{(D.19)}
\end{aligned}$$

D.2.2 Final State Multipoles

The transformation will be done using the same techniques as above. Starting from

$$\int \prod_{i=1}^{n} \frac{\mathrm{d}^3 q_i}{2q_i^0}\, \delta^3(\vec{Q}_M)\delta(Q_M^0 - Q_C^0) \qquad \text{(D.20)}$$

$$= \int \prod_{i=1}^{n} \left[\mathrm{d}^4 q_i \delta(q_i^2 - m_i^2)\Theta(q_i^0) \right] \delta^3\left(\sum_C \vec{q}_i\right) \delta\left(Q_M^0 - \sum_C q_i^0\right) \qquad \text{(D.21)}$$

Again, similar identities to (D.12) and (D.14) will be used, but due to the different mapping scheme they now read

$$1 = \int \prod_{i=1}^{n} \left[\mathrm{d}^4 p_i\, \delta^3(\vec{p_i} - u\vec{q_i})\, \delta\left(p_i^0 - \sqrt{\vec{p_i}^{\,2} + m_i^2}\right) \right] \qquad \text{(D.22)}$$

and

$$1 = \int \mathrm{d}u\, \delta \left[\sqrt{M^2 + \left(u \sum_N \vec{q}_i + \vec{K} \right)^2} - \sum_{C.N} \sqrt{m_i^2 + u^2 \vec{q}_i^2} - K^0 \right] \left(\frac{\vec{p}'_N \vec{p}_N}{p'^0_N} - \sum_{C,N} \frac{\vec{p}_i \vec{q}_i}{p_i^0} \right) \quad \text{(D.23)}$$

And, as before, the δ-function over Q_M^0 is expressed in the kinematically relevant variables q_i^0. This then yields

$$\begin{aligned}
&\int \prod_{i=1}^{n} \frac{\mathrm{d}^3 q_i}{2q_i^0}\, \delta^3(\vec{Q}_M) \delta(Q_M^0 - Q_C^0) \\
&= \int \mathrm{d}u \prod_{i=1}^{n} \left[\mathrm{d}^4 q_i \mathrm{d}^4 p_i\, \delta(q_i^2 - m_i^2) \Theta(q_i^0)\, \delta^3(\vec{p_i} - u\vec{q_i})\, \delta\left(p_i^0 - \sqrt{\vec{p_i}^2 + m_i^2} \right) \right] \\
&\quad \times \delta \left(\sqrt{M^2 + \left(u \sum_N \vec{q}_i + \vec{K} \right)^2} - \sum_{C,N} \sqrt{m_i^2 + u^2 \vec{q}_i^2} - K^0 \right) \\
&\quad \times \delta^3 \left(\sum_C \vec{q}_i \right) \delta \left(\sqrt{M^2 + \left(\sum_N \vec{q}_i \right)^2} - \sum_{C,N} q_i^0 \right) \times \left[\frac{\vec{p}'_N \vec{p}_N}{p'^0_N} - \sum_{C,N} \frac{\vec{p}_i \vec{q}_i}{p_i^0} \right] \qquad \text{(D.24)}
\end{aligned}$$

Integrating over $\mathrm{d}^4 q_i$ and u yields

$$\begin{aligned}
&\int \prod_{i=1}^{n} \frac{\mathrm{d}^3 q_i}{2q_i^0}\, \delta^3(\vec{Q}_M) \delta(Q_M^0 - Q_C^0) \\
&= \int \mathrm{d}u \prod_{i=1}^{n} \left[\mathrm{d}^4 p_i \delta \left(p_i^0 - \sqrt{\vec{p_i}^2 + m_i^2} \right) \frac{1}{u^3} \frac{1}{2\sqrt{\frac{1}{u^2}\vec{p_i}^2 + m_i^2}} \right] \delta^3 \left(\frac{1}{u} \sum_C \vec{p}_i \right) \qquad \text{(D.25)} \\
&\quad \times \delta \left(\sqrt{M^2 + \frac{1}{u^2} \left[\sum_N \vec{p}_i \right]^2} - \sum_{C,N} \sqrt{\frac{1}{u^2} \vec{p_i}^2 + m_i^2} \right) \qquad \text{(D.26)} \\
&\quad \times \delta \left(\sqrt{M^2 + \left[\sum_N \vec{p}_i + \vec{K} \right]^2} - \sum_{C,N} \sqrt{m_i^2 + \vec{p}_i^2} - K^0 \right) \times \left[\frac{\vec{p}' \vec{p}}{p'^0} - \sum_{C,N} \frac{\vec{p}_i^2}{u p_i^0} \right] \qquad \text{(D.27)} \\
&= \int \prod_{i=1}^{n} \left[\mathrm{d}^4 p_i \delta(p_i^2 - m_i^2) \Theta(p_i^0) \frac{1}{u^3} \frac{\sqrt{\vec{p_i}^2 + m_i^2}}{\sqrt{\frac{1}{u^2}\vec{p_i}^2 + m_i^2}} \right] u^3\, \delta^3 \left(\sum_C \vec{p}_i \right) \qquad \text{(D.28)} \\
&\quad \times \delta \left(\sqrt{M^2 + \left[\sum_N \vec{p}_i + \vec{K} \right]^2} - \sum_{C,N} \sqrt{m_i^2 + \vec{p}_i^2} - K^0 \right) \\
&\quad \times \left[\frac{\vec{p}' \vec{p}}{p'^0} - \sum_{C,N} \frac{\vec{p}_i^2}{u p_i^0} \right] \left[\frac{u}{\frac{\vec{p}^2}{p^0} - \sum_{C,N} \frac{\vec{q}_i^2}{q_i^0}} \right] \qquad \text{(D.29)}
\end{aligned}$$

where, again, the second last δ-function has been used in the integration over u. Additionally, an identity similar to (D.23), arising when defining u in terms of p_i, has been used. Rearranging terms leads to

$$\begin{aligned}
&\int \prod_{i=1}^{n} \frac{\mathrm{d}^3 q_i}{2q_i^0}\, \delta^3(\vec{Q}_M)\delta(Q_M^0 - Q_C^0) \\
&= \int \prod_{i=1}^{n} \left[\mathrm{d}^4 p_i\, \delta(p_i^2 - m_i^2)\Theta(p_i^0)\, \frac{1}{u^3}\, \frac{\sqrt{\vec{p}_i^{\,2} + m_i^2}}{\sqrt{\frac{1}{u^2}\vec{p}_i^{\,2} + m_i^2}} \right] \\
&\quad \times u^4\, \delta^3(\vec{P}_C)\, \delta\left(p_N'^0 - P_C^0 - P_N^0 - K^0\right)\, \frac{\frac{\vec{p}'_N \vec{p}_N}{p_N'^0} - \sum_{C,N} \frac{\vec{p}_i \vec{q}_i}{p_i^0}}{\frac{\vec{p}_N^{\,2}}{p_N^0} - \sum_{C,N} \frac{\vec{q}_i^{\,2}}{q_i^0}} \qquad \text{(D.30)} \\
&= \int \prod_{i=1}^{n} \left[\mathrm{d}^4 p_i\, \delta(p_i^2 - m_i^2)\Theta(p_i^0) \right]\, \delta^3(\vec{P_M})\, \delta(P_M^0 - P_C^0) \\
&\quad \times \frac{1}{u^{3n-4}}\, \frac{\frac{\vec{p}'_N \vec{p}_N}{p_N'^0} - \sum_{C,N} \frac{\vec{p}_i \vec{q}_i}{p_i^0}}{\frac{\vec{p}_N^{\,2}}{p_N^0} - \sum_{C,N} \frac{\vec{q}_i^{\,2}}{q_i^0}} \prod_{i=1}^{n} \left[\frac{p_i^0}{q_i^0} \right] \qquad \text{(D.31)}
\end{aligned}$$

where the identity

$$q_i^0 = \sqrt{\tfrac{1}{u^2}\vec{p}_i^{\,2} + m_i^2} \qquad \text{(D.32)}$$

has been used. Reversing the procedure allows to express the phase space element through the undressed final state momenta as

$$\begin{aligned}
\mathrm{d}\Phi &= \mathrm{d}\Phi_q\, \mathrm{d}\Phi_k\, (2\pi)^4\, \delta^3(\vec{Q}_M)\, \delta(Q_M^0 - Q_C^0)\, \frac{m_M^3}{M^2(P^0 + P_N^0 + K^0)} \\
&\quad \times u^{3n-4}\, \frac{\frac{\vec{p}_N^{\,2}}{p_N^0} - \sum_{C,N} \frac{\vec{q}_i^{\,2}}{q_i^0}}{\frac{\vec{p}'_N \vec{p}_N}{p_N'^0} - \sum_{C,N} \frac{\vec{p}_i \vec{q}_i}{p_i^0}} \prod_{i=1}^{n} \left[\frac{q_i^0}{p_i^0} \right] . \qquad \text{(D.33)}
\end{aligned}$$

Appendix E Monte Carlo Techniques

In this Section a number of Monte Carlo techniques are presented. These techniques are used in the code to produce random numbers according to a certain probability density function (PDF) and to facilitate Monte Carlo integration.

E.1 Sampling Random Numbers According to a Given Probability Density

For many Monte Carlo integration procedures random numbers distributed according to certain PDF's are needed. Assuming a random number generator producing uniformly distributed samples on the interval $[0,1]$ is available[1] , this uniform distribution can be bent into other distributions according to the given PDF's.

E.1.1 The Inverse Transform Method

The Inverse Transform Method is a possibility to create samples according to a such a given PDF.
Let ξ be a uniform distributed number on the interval $[0,1]$ and ζ is desired to have the PDF $f(x)$ (i.e. the distribution function $F(\zeta) = \int_a^\zeta \mathrm{d}x\, f(x)$) on $[a,b]$. Then inverting $F(\zeta) = \xi$ gives the correct distribution for ζ.

E.1.2 The Acception-Rejection Method

This is a commonly used means of generating random numbers on distributions that cannot be obtained by the inverse transform method.
Let ζ be a variable which is to be sampled according to the PDF $f(x)$ on $[a,b]$, which cannot be obtained by inverse transform. Let further be $g(x) \geq f(x)\, \forall x \in [a,b]$, which can be inverted by the inverse transform method. Then ζ can be generated according to $f(x)$ by the following method:

1. Take two samples ξ_1 and ξ_2 from the standard equidistribution.
2. Solve the generalisation of the basic inverse transform method for ζ:

$$\int_a^\zeta \mathrm{d}x\, g(x) \;=\; \xi_1 \int_a^b \mathrm{d}x\, g(x)\,. \tag{E.1}$$

[1] It is indispensable that this random number generator produces highly independent samples.

3. If $\xi_2\, g(\zeta) \leq f(\zeta)$ then accept ζ as a sample from f. Otherwise, reject this ζ and restart from the top of the algorithm.

The resulting sample ζ is then distributed according to the PDF $f(x)$. There are other specialised algorithms especially for Gaussian distributions, but since they are of no importance to this work they will not be discussed here.

E.2 Monte Carlo Integration

There are various methods that can be used in numerical integrations. Their applicability varies with the peak structure of the integrand and the complexity of the range of integration. Monte Carlo methods compute quantities as the expectation value of some random variable. In many cases such a random variable can be found, although it is not generally possible to do this. Then an estimate of its expectation value is made taking samples of the random variable. Consequently, the result is approximate only.
Only procedures relevant to this work are discussed. However, there are plenty of other techniques, e.g. Markov Chain Monte Carlos, which may possibly increase speed and accuracy of the methods currently used.

E.2.1 Rectangle Method

This is the most straight forward method. It is a direct implementation of the Riemannian defintion of the integral.
In one dimension the range of integration is divided into N subintervals of equal size and the integral of each of those intervals is approximated by a rectangle using the interval length as its base and any value of the integrand within the interval as its height,

$$\int_a^b \mathrm{d}x\, f(x) \;=\; \lim_{N\to\infty} \sum_{i=0}^{N-1} (x_i - x_{i+1}) f(\tilde{x}_i)\,, \tag{E.2}$$

with $x_0 = a$ and $x_N = b$. $\tilde{x}_i \in [x_i, x_{i+1}]$. Usually this value is taken either at the centre or one of both ends of the interval. Nonetheless, all such choices converge as $N \to \infty$.
For one dimensional integrals this method requires little CPU-time as compared to other methods with the same N. However, when the integrand is peaked it requires a large increase in N to keep a certain level of accuracy.
Additionally, although the generalisation to higher dimensional integrals is straight forward, the number of intervals grows as N^D, rendering this method impractical for integrations in such spaces. Nonetheless, it is useful for low dimensional integrations of unpeaked functions or where the structure of the integrand is unknown. When the structure of the integrand is known, improvements can be achieved by choosing the size of the subintervals to be smaller in the regions where the variations of the integrand are large and vice versa.

E.2.2 Simple Monte Carlo Integration

This is the basis of all Monte Carlo integration methods. Supposing the integral $\int_a^b \mathrm{d}x\, g(x)$ is to be calculated and ξ is a uniformly distributed number on $[a, b]$, i.e. ξ has the PDF

$f_\xi(x) = 1$, sampled N times, then

$$\int_a^b \mathrm{d}x\, g(x) = \int_a^b \mathrm{d}x\, g(x) f_\xi(x) \approx \frac{1}{N} \sum_{i=1}^{N} g(\xi_i) \tag{E.3}$$

This method is the Monte Carlo Equivalent of the Rectangle Method of Section E.2.1 in an one dimensional range of integration. Thus, it suffers from the same inefficiencies when the integrand is sharply peaked: a large N is required to reduce the variance and, thus, the error of the result. However it has a better behaviour with increasing dimensionality of the range of integration.

E.2.3 Importance Sampling

As noted, the method of Section E.2.2 is inefficient when the integrand is peaked. This inefficiency stems from the fact that a large number of samples lie in the flat regions of the integrand and thus contribute little to the expectation value. Rather than sample f from a uniform distribution and average all samples with an equal weight, it is more efficient to sample from a distribution concentrated where f is largest and average the samples with a weighting to correct for the distribution.
Let $\int_a^b \mathrm{d}x\, g(x)\, h(x)$ be an integral where $h(x)$ is sharply peaked somewhere in $[a, b]$ while $g(x)$ is not. With $A \equiv \int_a^b \mathrm{d}x\, h(x)$ the integral transforms into

$$\int_a^b \mathrm{d}x\, g(x)\, h(x) = \int_a^b \mathrm{d}x\, \frac{A}{A} g(x)\, h(x) = A \int_a^b \mathrm{d}x\, g(x) \frac{h(x)}{A}\,. \tag{E.4}$$

$\frac{h(x)}{A}$ thus is a normalised PDF. Let now ζ have this PDF, then with Eq.(E.3)

$$\int_a^b \mathrm{d}x\, g(x)\, h(x) = A \left\langle g(\zeta) \right\rangle \approx A \frac{1}{N} \sum_{i=1}^{N} g(\zeta_i)\,. \tag{E.5}$$

If the integrand does not factorise as above, importance sampling can still be used. Let ζ be a random variable with the PDF $f_\zeta(x)$, defined on $[a, b]$, then

$$\begin{aligned} &\int_a^b \mathrm{d}x\, g(x) \\ &\quad = \int_a^b \mathrm{d}x g(x)\, \frac{f_\zeta(x)}{f_\zeta(x)} = \int_a^b \mathrm{d}F_\zeta(x) \frac{g(x)}{f_\zeta(x)} = \left\langle \frac{g(x)}{f_\zeta(x)} \right\rangle \approx \frac{1}{N} \sum_{i=1}^{N} \frac{g(\zeta_i)}{f_\zeta(\zeta_i)}\,. \end{aligned} \tag{E.6}$$

The efficiency of this integration hinges critically on the quality of the description of the peak of $g(x)$ by $f_\zeta(x)$., i.e. the flatter $\frac{g(x)}{f_\zeta(x)}$ the faster the convergence of the estimate upon the true value.

E.2.4 Hit-Or-Miss Method

This method starts from a very simple premise. Let $g(x)$ be an integrable function engulfing the integrand $f(x)$, i.e. $f(x) \leq g(x) \, \forall x \in [a, b]$. Further, let (ξ_1, ξ_2) be a uniformly distributed random point in the x-$f(x)$-plane with $\xi_1 \in [a, b]$ and $\xi_2 \in [0, g(\xi_1)]$. Then

$$\int_a^b \mathrm{d}x \, f(x) \quad = \quad \frac{N_+}{N} \int_a^b \mathrm{d}x \, g(x) \, , \tag{E.7}$$

where N_+ is the number of points (ξ_1, ξ_2) which satisfy $\xi_2 < f(\xi_1)$ and N is the total number of sampled points.
This method can easily be generalised to higher dimensional integrals and is especially useful if the structure of the integrand is unknown. In a first iteration $g(x)$ can then be chosen simply as $g(x) = \max_{x \in V} \{f(x)\}$. However, if the integrand is sharply peaked, such a choice becomes highly inefficient, especially in space of high dimensionality.

Appendix F Details on the Photon Generation

In this section the generation of the photon distribution is detailed.

F.1 Avarage Photon Multiplicity

The average photon multiplicity $\bar{n}$ is the average of the Poisson distribution before it is corrected by the various weights. It is therefore not immediately connected to the true average photon multiplicity of the final event. Nonetheless, it is an integral part of the generation procedure. However, an analytical result in closed form is available only for dipoles in either their own rest frame or one of the rest frames of the particles forming the dipole. In this implementation the choice has been made to generate the photon distribution in the rest frame of the multipole, necessitating either a numerical evaluation or a calculation in different frames for different parts of the corresponding expressions. However, as a starting point the analytical result for the dipole in its rest frame will be given. It reads

$$\bar{n} = \int_{\omega_{\min}}^{\omega_{\max}} \frac{\mathrm{d}^3 k}{k^0} \tilde{S}_q(k) = -\frac{\alpha}{\pi} Z_1 Z_2 \theta_1 \theta_2 \ \ln \frac{\omega_{\max}}{\omega_{\min}} \left(\frac{1+\beta_1\beta_2}{\beta_1+\beta_2} \ln \frac{(1+\beta_1)(1+\beta_2)}{(1-\beta_1)(1-\beta_2)} \ - 2 \right) , \tag{F.1}$$

where $\omega_{\min}$ is the infrared cut-off and $\omega_{\max}$ is the maximal kinematically allowed photon energy. The latter can be determined by setting the rescaling parameter u to zero in Eqs. (3.19) and (3.24), respectively, and by assuming single photon emission. Additionally, $\beta_i = \frac{|\vec{p}_i|}{E_i}$.

In the case of a multipole, the integral over the photon energy can still be separated and performed analytically, as long as the soft photon region is sufficiently well-behaved. This is the case, if $\Theta(k, \Omega)$ forms an isotropic hypersurface in the frame of the integration. However, the angular integration still remains to be done:

$$\begin{aligned} \bar{n} &= \int \frac{\mathrm{d}^3 k}{k^0} \Theta(k,\Omega) \tilde{S}_q(k) \\ &= \frac{\alpha}{4\pi^2} \sum_{i<j} Z_i Z_j \theta_i \theta_j \int \frac{\mathrm{d}^3 k}{k^0} \Theta(k,\Omega) \left(\frac{q_i}{(q_i \cdot k)} - \frac{q_j}{(q_j \cdot k)} \right)^2 \\ &= \frac{\alpha}{4\pi^2} \ln \frac{\omega_{\max}}{\omega_{\min}} \sum_{i<j} Z_i Z_j \theta_i \theta_j \left(8\pi - \int \mathrm{d}\Omega \frac{2(q_i \cdot q_j)}{(q_i \cdot e_k)(q_j \cdot e_k)} \right) . \end{aligned} \tag{F.2}$$

Choosing different orientations of the polar axes for each interference term of every constituent dipole, all θ-integrations can be done analytically. Although this may sound like

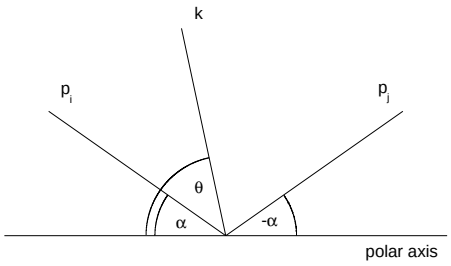

Figure F.1: Sketch of how the axes are chosen in the angular integration in multipoles.

quite an *ad-hoc* procedure, it is completely valid and simplyfies the integration immensely. The orientation for each of the interference terms is thus chosen to be such that both momenta lie symmetrically in the unit sphere, both forming an angle α_{ij} with the polar axis, see Fig. F.1. Therefore, by this choice,

$$(q_i \cdot e_k) = E_i \left(1 - a_i \sin\theta - b_i \cos\theta\right) \tag{F.3}$$
$$(q_j \cdot e_k) = E_j \left(1 - a_j \sin\theta + b_j \cos\theta\right) \tag{F.4}$$

where e_k^μ again is $\frac{1}{k^0}k^\mu$ with $e_k^2 = 0$, cf. Eq. (3.34), and the further parameters are given by

$$a_{i,j} = \beta_{i,j} \sin\alpha_{ij} \sin\varphi \quad \text{and} \quad b_{i,j} = \beta_{i,j} \cos\alpha_{ij} \tag{F.5}$$

. With these choices the last integral reads

$$\begin{aligned}
&\int \mathrm{d}\Omega \frac{E_i E_j}{(q_i \cdot e_k)(q_j \cdot e_k)} \\
= &\int_0^{2\pi} \mathrm{d}\varphi \int_0^{\pi} d\theta \frac{\sin\theta}{\left(1 - a_i \sin\theta - b_i \cos\theta\right)\left(1 - a_j \sin\theta + b_j \cos\theta\right)} \\
= &\int_0^{2\pi} \mathrm{d}\varphi \left\{ \frac{\frac{2(a_i(1+b_ib_j) - a_j(1-b_i^2))}{\sqrt{1-a_i^2-b_i^2}} \left(\frac{\pi}{2} + \arctan\frac{a_i}{\sqrt{1-a_i^2-b_i^2}}\right)}{(1-b_i^2)a_j^2 + (1-b_j^2)a_i^2 - 2(1+b_ib_j)a_ia_j + (b_i+b_j)^2} + (i \leftrightarrow j) \right\} \\
&- \int_0^{2\pi} \mathrm{d}\varphi \frac{(b_i+b_j)\ln\frac{(1+b_i)(1+b_j)}{(1-b_i)(1-b_j)}}{-(1-b_j^2)a_i^2 - (1-b_i^2)a_j^2 + 2(1+b_ib_j)a_ia_j - (b_i+b_j)^2}.
\end{aligned} \tag{F.6}$$

Only the last term of the resulting three terms can be integrated analytically. However, the first and second term are regular as long as all particles are massive, as expected. Additionally, their sum is highly symmetric. Furthermore, the two subintervals $[0, \pi]$ and $[\pi, 2\pi]$ of the φ-integration exhibit an even symmetry w.r.t. their respective centre, such

that the asymptotic pole for $\beta_{i,j} \to 1$ is situated at $\frac{\pi}{2}$. Taken together,

$$\begin{aligned}
&\int \mathrm{d}\Omega \frac{E_i E_j}{(q_i \cdot e_k)(q_j \cdot e_k)} \\
&= -2 \left(\int_0^{\frac{\pi}{2}} + \int_{\pi}^{\frac{3\pi}{2}} \right) \mathrm{d}\varphi \left[I_1(\varphi) + I_2(\varphi) \right] \\
&\quad - 2\pi \frac{1}{(\beta_i + \beta_j)\cos\alpha_{ij}} \ln \frac{(1-\beta_i \cos\alpha_{ij})(1-\beta_j \cos\alpha_{ij})}{(1+\beta_i \cos\alpha_{ij})(1+\beta_j \cos\alpha_{ij})} \\
&\qquad \times \left[1 - \frac{4\beta_i^2 \beta_j^2 \cos^2\alpha_{ij} - (\beta_i - \beta_j)^2}{(\beta_i + \beta_j)\cos^2\alpha_{ij}} \sin^2\alpha_{ij} \right]^{-\frac{1}{2}} ,
\end{aligned} \tag{F.7}$$

where $I_1(\varphi)$ and $I_2(\varphi)$ are the first two integrals of (F.6). Upon closer examination it can be seen that for $\alpha_{ij} \to 0$ the first two terms vanish and the result of (F.1) is recovered.

F.2 Sampling a Photon Configuration

F.2.1 Photon Number

As can be seen from Eq.(3.31), the photon number of the event is distributed according to a Poisson distribution with mean $\bar{n}$. There are plenty of algorithms available to generate such a distribution. The one chosen for PHOTONS++ is taken from [16].

Let r_i be a series of uniformly distributed random numbers on the interval $[0,1]$. If $R_N = -\sum_{i=1}^{N} \ln r_i$, there exists a minimal N with $R_N > \bar{n}$. The variable $n = N - 1$ is then distributed according to a Possion distribution with mean $\bar{n}$.

F.2.2 Photon Energy

Due to the decomposition of the integration over the photon energy and the integration over the unit sphere, the photon energy distribution and the photon angular distribution can be generated separately. Of course, this independence of distributions is no longer true after the reweighting procedure, but it alleviates the generation of the crude distribution.

In the implementation presented here, the photon energy is distributed according to $\frac{1}{k^0}$, generated through

$$k^0 = \omega_{\min} \left(\frac{\omega_{\max}}{\omega_{\min}} \right)^{\mathcal{R}} , \tag{F.8}$$

where $\mathcal{R}$ is a uniformly distributed random number on the interval $[0,1]$.

F.2.3 Photon Angles

Similar to all other parts of the photon distribution, the photon angles are also generated according to $\tilde{S}_q(k)$. For this, the relevant function is recast into the form

$$\begin{aligned} & -\left(\frac{q_i}{(q_i\cdot e_k)}-\frac{q_j}{(q_j\cdot e_k)}\right)^2 \\ &= -\frac{1-\beta_i^2}{(1-\beta_i\cos\theta)^2}+\frac{2(1+\beta_i\beta_j)}{(1-\beta_i\cos\theta)(1+\beta_j\cos\theta)}-\frac{1-\beta_j^2}{(1+\beta_j\cos\theta)^2}\,, \end{aligned} \tag{F.9}$$

where θ is some polar angle w.r.t. the dipole axis in the dipole rest frame. In this frame, the generation of the azimuthal is trivial - it just follows a flat distribution in $[0,\,2\pi]$. The polar distribution above can be bound from above through the interference term. This allows to generate the true distribution by generating the angle according to the interference term and applying a hit-or-miss rejection. The interference term can be decomposed into two independent terms according to

$$\frac{1}{(1-\beta_i\cos\theta)(1+\beta_j\cos\theta)} = \frac{\beta_i\beta_j}{\beta_i+\beta_j}\left(\frac{1}{\beta_j(1-\beta_i\cos\theta)}-\frac{1}{\beta_i(1+\beta_j\cos\theta)}\right). \tag{F.10}$$

The cosine of the polar angle, $\cos\theta$, is then generated to either of the two terms, i.e. it is generated according to $(1-\beta_i\cos\theta)^{-1}$ with probability

$$P_i = \frac{\ln\frac{1+\beta_i}{1-\beta_i}}{\ln\frac{1+\beta_i}{1-\beta_i}+\ln\frac{1+\beta_j}{1-\beta_j}} \tag{F.11}$$

and according to $(1+\beta_j\cos\theta)^{-1}$ with probability $P_j=1-P_i$, selected through a random number. These angles can be generated by

$$\cos\theta = \frac{1}{\beta_i}\left[1-(1+\beta_i)\left(\frac{1-\beta_i}{1+\beta_i}\right)^{\mathcal{R}}\right] \tag{F.12}$$

in the former case and

$$\cos\theta = -\frac{1}{\beta_j}\left[1-(1-\beta_j)\left(\frac{1+\beta_j}{1-\beta_j}\right)^{\mathcal{R}}\right] \tag{F.13}$$

in the latter. $\mathcal{R}$ again is a uniformly distributed random number on $[0,1]$. The correction weight for obtaining the full distribution reads

$$W = \frac{-\frac{1-\beta_i^2}{(1-\beta_i\cos\theta)^2}+\frac{2(1+\beta_i\beta_j)}{(1-\beta_i\cos\theta)(1+\beta_j\cos\theta)}-\frac{1-\beta_j^2}{(1+\beta_j\cos\theta)^2}}{\frac{2(1+\beta_i\beta_j)}{(1-\beta_i\cos\theta)(1+\beta_j\cos\theta)}} \leq 1\,. \tag{F.14}$$

The azimutal angle φ is distibuted uniformly.

F.2.4 Photons from Multipoles

In a multipole configuration again the photons are generated according to $\tilde{S}_q(k)$. With the help of Eq. (F.2) the photon energy can still be generated separately and proceeds as above. However, the angular distribution of the photon is very complex. But due to

$$\tilde{S}_q(k) \;=\; \sum_{i<j} \tilde{S}(q_i, q_j, k) \tag{F.15}$$

the photon angles are distributed according to

$$-\sum_{i<j} |Z_i Z_j \theta_i \theta_j| \left(\frac{q_i}{(q_i \cdot e_k)} - \frac{q_j}{(q_j \cdot e_k)} \right)^2 . \tag{F.16}$$

This is nothing else but a sum of angular distributions of different dipoles which are not in their respective rest frame.
Subsequently, one of those constituent dipoles is chosen with the probability

$$P_{ij} = \frac{|\bar{n}_{ij}|}{\sum\limits_{i<j} |\bar{n}_{ij}|} = \frac{\left| \int \frac{\mathrm{d}^3 k}{k^0} \tilde{S}(q_i, q_j, k) \right|}{\sum\limits_{i<j} \left| \int \frac{\mathrm{d}^3 k}{k^0} \tilde{S}(q_i, q_j, k) \right|} . \tag{F.17}$$

Then, photon angle generation can proceed as above in the rest frame of the dipole. To obtain the right distribution in the rest frame of the overall multipole, a null-vector of unit length is created in the rest frame of the dipole using the newly generated angles φ ant θ. Then this null vector is boosted into the rest frame of the multipole. It now has the angular distribution according to its constituent dipole in this frame. Since it is a null vector it has the properties of a photon and only needs to be rescaled to the energy generated earlier.

Appendix G Massive Dipole Splitting Functions

The massive dipole splitting functions are needed for the calculation of the approximation to the infrared subtracted single hard photon emission matrix element $\tilde{\beta}_1^1$. They are taken directly from [20] for spin-$\frac{1}{2}$ emitters and are generalised from [22] for all other cases. Problems arising during this generalisation are related to the fact that these splitting functions for spin-1 particles are only given for massless gluons and that all initial states are considered massless as well. The extension to radiation off massive spin-1 particles is rather straight forward by augmentation with a simple mass term. The extension to massive initial states is less clear since decay matrix element are far off the massless initial state limit. However, the decaying particle is allways much more massive than its decay products when those are supposed to emit hard bremsstrahlung. Thus, photons are predominantly emitted at large angles to the initial state resulting in negligible contributions from these splitting functions. Hence, they can safely be omitted.
Also, velocity factors from [22] have been omitted. They were introduced to facilitate the analytic integration and change neither the infrared nor the quasi-collinear limit. They only result in a different interpolation in-between. The same is true for the factor R_{ij} in the massive fermion splitting function of [20]. Nonetheless, here this factor is kept because of the direct applicability of these splitting functions to the completely massive splitting.
Three cases need to be differentiated regarding the state, initial or final, the emitter and spectator are in. The fourth case where both emitter and spectator are in the initial state lies outside the present applicability of this program, it will therefore be omitted.
To repeat the notation, p_i is the 4-momentum of the emitter, p_j that of the spectator and k is the emitted photon. All massive dipole splitting functions will be given, in that order, for spin-0, spin-$\frac{1}{2}$ and spin-1 emitters. Since there are neither massive nor massless dipole splitting functions available for emitters of spin-$\frac{3}{2}$ or spin-2, their emissions have to be described by the soft limit only. Of course, it is allways possible to implement exact process specific matrix elements.

Final State Emitter, Final State Spectator

$$\begin{aligned} g_{ij}(p_i,p_j,k) &= g_{ij}^{(\mathrm{soft})}(p_i,p_j,k) \\ &= \frac{1}{(p_i\cdot k)R_{ij}(y_{ij})}\left[\frac{2}{1-z_{ij}(1-y_{ij})}-1-z_{ij}-\frac{m_i^2}{(p_i\cdot k)}\right] \\ &= \frac{1}{(p_i\cdot k)}\left[\frac{2}{1-z_{ij}(1-y_{ij})}+\frac{2}{1-z_{kj}(1-y_{ij})}+2z_{ij}z_{kj}-4-\frac{m_i^2}{(p_i\cdot k)}\right] \end{aligned} \tag{G.1}$$

with

$$y_{ij} = \frac{p_i k}{p_i p_j + p_i k + p_j k} \tag{G.2}$$

$$z_{ij} = \frac{p_i p_j}{p_i p_j + p_j k} \tag{G.3}$$

$$z_{kj} = 1 - z_{ij} \tag{G.4}$$

and

$$R_{ij}(x) = \frac{\sqrt{\left(2m_j^2 + \bar{P}_{ij}^2(1-x)\right)^2 - 4P_{ij}^2 m_j^2}}{\sqrt{\lambda(P_{ij}^2, m_i^2, m_j^2)}}, \tag{G.5}$$

with

$$P_{ij} = p_i + p_j + k \tag{G.6}$$

$$\bar{P}_{ij}^2 = P_{ij}^2 - m_i^2 - m_j^2 = 2\left(p_i p_j + p_i k + p_j k\right), \tag{G.7}$$

wherein the photon is massless, $\lambda(x, y, z)$ is the Kallen-function.

Final State Emitter, Initial State Spectator

$$\begin{aligned} g_{ij}(p_i, p_j, k) &= g_{ij}^{(\mathrm{soft})}(p_i, p_j, k) \\ &= \frac{1}{(p_i \cdot k) x_{ij}} \left[\frac{2}{2 - x_{ij} - z_{ij}} - 1 - z_{ij} - \frac{m_i^2}{(p_i \cdot k)} \right] \\ &= \frac{1}{(p_i \cdot k) x_{ij}} \left[\frac{2}{2 - x_{ij} - z_{ij}} + \frac{2}{2 - x_{ij} - z_{kj}} + 2 z_{ij} z_{kj} - 4 - \frac{m_i^2}{(p_i \cdot k)} \right] \end{aligned} \tag{G.8}$$

with

$$x_{ij} = \frac{p_i p_j + p_j k - p_i k}{p_i p_j + p_j k} \tag{G.9}$$

$$z_{ij} = \frac{p_i p_j}{p_i p_j + p_j k} \tag{G.10}$$

$$z_{kj} = 1 - z_{ij}\,. \tag{G.11}$$

Initial State Emitter, Final State Spectator

The emitting particle is allways assumed to be much heavier than its decay products resulting in its contributions to the real emission corrections to be negligible. Thus,

$$g_{ij}(p_i, p_j, k) = g_{ij}^{(\mathrm{soft})}(p_i, p_j, k) \tag{G.12}$$

is set irrespective of the emitter's spin..

Appendix H Basic Building Blocks For Matrix Element Calculations

In this Appendix a short summary on the definitions of the basic building blocks (cf. [10–12]) for the calculations of exact matrix elements will be given. Additionally, techniques to incorporate propagators into that scheme will be reviewed.

X-Function

The X-function is a contraction over a fermionic current coupled to a vector with an arbitrary structure of the vertex.

$$X\left(p_1,s_1;p;p_2,s_2;c_L,c_R\right) \;=\; \bar{u}(p_1,s_1)\,\not{p}\left[c_L P_L + c_R P_R\right] u(p_2,s_2)\,, \tag{H.1}$$

where $u(p_i,s_i)$ may be a particle or anti-particle spinor, $P_L = \frac{1-\gamma^5}{2}$ and $P_R = \frac{1+\gamma^5}{2}$. The vector p^μ dotted into the γ-matrix may be a momentum vector or a polarisation vector. For the explicit calculation of the X-Function see Table H.1.

Y-Function

The Y-function is the pendant of the X-function when the fermionic current is coupling to a scalar rather than a vector.

$$Y\left(p_1,s_1;p_2,s_2;c_L,c_R\right) \;=\; \bar{u}(p_1,s_1)\left[c_L P_L + c_R P_R\right] u(p_2,s_2)\,. \tag{H.2}$$

Its explicit calculation is shown in Table H.2.

Z-Function

The Z-function is a contraction over two ferionic currents connected by a massless gauge boson (cf. Table H.3).

$$\begin{aligned} &Z\left(p_1,s_1;p_2,s_2;p_3,s_3;p_4,s_4;c_L^{12},c_R^{12};c_L^{34},c_R^{34}\right) \\ &\quad= \;\bar{u}(p_1,s_1)\gamma^\mu\left[c_L^{12}P_L + c_R^{12}P_R\right] u(p_2,s_2)\bar{u}(p_3,s_3)\gamma_\mu\left[c_L^{34}P_L + c_R^{34}P_R\right] u(p_4,s_4)\,. \end{aligned} \tag{H.3}$$

$s_1 s_2$	$X(p_1, s_1; p; p_2, s_2; c_L, c_R)$
$++$	$\mu_1\mu_2\eta^2 c_L + \mu^2\eta_1\eta_2 c_R + c_R S(+;p_1,p)S(-;p,p_2)$
$+-$	$c_L\mu_1\eta S(+;p,p_2) + c_R\mu_2\eta S(+;p_1,p)$

Table H.1: X-Functions for different helicity combinations. Missing combinations can be obtained using the simultaneous replacements $+ \leftrightarrow -$ and $L \leftrightarrow R$.

$s_1 s_2$	$Y(p_1, s_1; p_2, s_2; c_L, c_R)$
$++$	$c_R\mu_1\eta_2 + c_L\mu_2\eta_1$
$+-$	$c_L S(+;p_1,p_2)$

Table H.2: Y-Functions for different helicity combinations. Missing combinations can be obtained using the simultaneous replacements $+ \leftrightarrow -$ and $L \leftrightarrow R$.

$s_1 s_2 s_3 s_4$	$Z(p_1, s_1; p_2, s_2; p_3, s_3; p_4, s_4; c_L^{12}, c_R^{12}; c_L^{34}, c_R^{34})$
$++++$	$2\left[S(+;p_3,p_1)S(-;p_2,p_4)c_R^{12}c_R^{34} + \mu_1\mu_2\eta_3\eta_4 c_L^{12}c_R^{34} + \mu_3\mu_4\eta_1\eta_2 c_R^{12}c_L^{34}\right]$
$+++-$	$2\eta_2 c_R^{12}\left[S(+;p_1,p_4)\mu_3 c_L^{34} + S(+;p_1,p_3)\mu_4 c_R^{34}\right]$
$++-+$	$2\eta_1 c_R^{12}\left[S(-;p_3,p_2)\mu_4 c_L^{34} + S(-;p_4,p_2)\mu_3 c_R^{34}\right]$
$++--$	$2\left[S(+;p_4,p_1)S(-;p_2,p_3)c_R^{12}c_L^{34} + \mu_1\mu_2\eta_3\eta_4 c_L^{12}c_R^{34} + \mu_3\mu_4\eta_1\eta_2 c_R^{12}c_R^{34}\right]$
$+-++$	$2\eta_4 c_R^{34}\left[S(+;p_1,p_3)\mu_2 c_R^{12} + S(+;p_2,p_3)\mu_1 c_L^{12}\right]$
$+-+-$	0
$+--+$	$-2\left[\mu_1\mu_4\eta_2\eta_3 c_L^{12}c_L^{34} + \mu_2\mu_3\eta_1\eta_4 c_R^{12}c_R^{34} - \mu_1\mu_3\eta_2\eta_4 c_L^{12}c_R^{34} - \mu_2\mu_4\eta_1\eta_3 c_R^{12}c_L^{34}\right]$
$+---$	$2\eta_3 c_R^{34}\left[S(+;p_4,p_2)\mu_1 c_L^{12} + S(+;p_1,p_4)\mu_2 c_R^{12}\right]$

Table H.3: Z-Functions for different helicity combinations. Missing combinations can be obtained using the simultaneous replacements $+ \leftrightarrow -$ and $L \leftrightarrow R$.

S-Function

For the calculation of the above spinoral products it is useful to define the S-Function

$$S(s;p_1,p_2) \;=\; \bar{u}(p_1,s)u(p_2,-s)\,. \tag{H.4}$$

Its two possible forms for given p_1 and p_2 are

$$\begin{aligned} S(+;p_1,p_2) &= 2\,\frac{(p_1\cdot k_0)(p_2\cdot k_1) - (p_1\cdot k_1)(p_2\cdot k_0) - i\epsilon_{\alpha\beta\gamma\delta}p_1^\alpha p_2^\beta k_0^\gamma k_1^\delta}{\eta_1\eta_2} \\ S(-;p_1,p_2) &= -2\,\frac{(p_1\cdot k_0)(p_2\cdot k_1) - (p_1\cdot k_1)(p_2\cdot k_0) + i\epsilon_{\alpha\beta\gamma\delta}p_1^\alpha p_2^\beta k_0^\gamma k_1^\delta}{\eta_1\eta_2}\,, \end{aligned} \tag{H.5}$$

where k_0 is an arbitrary null vector ($k_0^2 = 0$) and k_1 satisfies the relations $k_1^2 = -1$ and $(k_0 \cdot k_1) = 0$. Furthermore,

$$\eta_i \;=\; \sqrt{2(p_i \cdot k_0)}\,. \tag{H.6}$$

It is also useful to define the quantity

$$\mu_i \;=\; \pm\frac{m_i}{\eta_i}\,, \tag{H.7}$$

where $\pm$ refers to particles/anti-particles.

Fermionic Propagators

These propagators can be incorporated using the following identity:

$$(\not{p} \pm m) \;=\; \tfrac{1}{2}\sum_s \left[\left(1 \pm \frac{m}{\sqrt{p^2}}\right) u(p,s)\bar{u}(p,s) + \left(1 \mp \frac{m}{\sqrt{p^2}}\right) v(p,s)\bar{v}(p,s)\right]\,. \tag{H.8}$$

This allows to cut the line and replace it with a sum of external particles

Bosonic Propagators

Bosonic propagators can be incorporated by writing out their Lorentz-structure explicitly. This is trivial in Feynman gauge, if the vector is massless. Massive propagators are best included in unitary gauge, since then no additional goldstone boson exchange has to be included.

Bibliography

[1] F. Bloch and A. Nordsieck, Phys. Rev. **52** (1937) 54.

[2] D. R. Yennie, S. C. Frautschi and H. Suura, "The infrared divergence phenomena and high-energy processes," Annals Phys. **13** (1961) 379.

[3] F. E. Low, "Bremsstrahlung of very low-energy quanta in elementary particle collisions," Phys. Rev. **110** (1958) 974.

[4] R. P. Feynman, "Space-time approach to quantum electrodynamics," Phys. Rev. **76** (1949) 769.

[5] T. Kinoshita, "Mass Singularities Of Feynman Amplitudes," J. Math. Phys. **3** (1962) 650.

[6] T. D. Lee and M. Nauenberg, "Degenerate Systems and Mass Singularities," Phys. Rev. **133** (1964) B1549.

[7] V. N. Gribov, Yad. Fiz. **5** (1967) 399.

[8] M. Chaichian and B. Ermolaev, "Factorization theorem for photons and gluons in hard processes," Nucl. Phys. B **451** (1995) 194.

[9] T. Gleisberg, S. Hoche, F. Krauss, A. Schalicke, S. Schumann and J. C. Winter, "SHERPA 1.alpha, a proof-of-concept version," JHEP **0402** (2004) 056 [arXiv:hep-ph/0311263].

[10] F. Krauss, R. Kuhn and G. Soff, "AMEGIC++ 1.0: A matrix element generator in C++," JHEP **0202** (2002) 044 [arXiv:hep-ph/0109036].

[11] T. Gleisberg, F. Krauss, K. T. Matchev, A. Schalicke, S. Schumann and G. Soff, "Helicity formalism for spin-2 particles," JHEP **0309** (2003) 001 [arXiv:hep-ph/0306182].

[12] T. Gleisberg, "Helicity formalism for exotic physics scenarios at collider experiments," Diploma Thesis, available from http://projects.hepforge.org/sherpa/dokuwiki/publications/theses/index.

[13] T. Laubrich, "Implementation of τ-lepton Decays into the Event-Generator SHERPA," Diploma Thesis, available from http://projects.hepforge.org/sherpa/dokuwiki/publications/theses/index.

[14] F. Siegert, Diploma Thesis, to be publically available soon

[15] K. Hamilton and P. Richardson, "Simulation of QED radiation in particle decays using the YFS formalism," JHEP **0607** (2006) 010 [arXiv:hep-ph/0603034].

[16] S. Jadach, "Yennie-Frautschi-Suura soft photons in Monte Carlo event generators," MPI-PAE/PTh 6/87

[17] S. Jadach, "Monte-Carlo Methods for High-Energy Phyiscs," Lectures at the Torino School of Physics, 2001. Available from http://jadach.home.cern.ch/jadach/.

[18] R. Kleiss and W. J. Stirling, "Massive multiplicities and Monte Carlo," Nucl. Phys. B **385** (1992) 413.

[19] G. Altarelli and G. Parisi, "Asymptotic Freedom In Parton Language," Nucl. Phys. B **126** (1977) 298.

[20] S. Dittmaier, "A general approach to photon radiation off fermions," Nucl. Phys. B **565** (2000) 69 [arXiv:hep-ph/9904440].

[21] S. Catani, S. Dittmaier and Z. Trocsanyi, "One-loop singular behaviour of QCD and SUSY QCD amplitudes with massive partons," Phys. Lett. B **500** (2001) 149 [arXiv:hep-ph/0011222].

[22] S. Catani, S. Dittmaier, M. H. Seymour and Z. Trocsanyi, "The dipole formalism for next-to-leading order QCD calculations with massive partons," Nucl. Phys. B **627** (2002) 189 [arXiv:hep-ph/0201036].

[23] W. Placzek and S. Jadach, "Multiphoton radiation in leptonic W-boson decays," Eur. Phys. J. C **29** (2003) 325 [arXiv:hep-ph/0302065].

[24] S. Jadach and B. F. L. Ward, "YFS2: THE SECOND ORDER MONTE CARLO FOR FERMION PAIR PRODUCTION AT LEP / SLC WITH THE INITIAL STATE RADIATION OF TWO HARD AND MULTIPLE SOFT PHOTONS," Comput. Phys. Commun. **56** (1990) 351.

[25] S. Jadach and B. F. L. Ward, "Exponentiation Of Soft Photons In The Monte Carlo: The Case Of Bonneau And Martin," Phys. Rev. D **38** (1988) 2897 [Erratum-ibid. D **39** (1989) 1471].

[26] W. J. Marciano and A. Sirlin, "Deviations from electron-muon universality in the leptonic decays of the intermediate bosons," Phys. Rev. D **8** (1973) 3612.

[27] F. A. Berends, W. L. van Neerven and G. J. H. Burgers, "Higher Order Radiative Corrections At Lep Energies," Nucl. Phys. B **297** (1988) 429 [Erratum-ibid. B **304** (1988) 921].

[28] Y. L. Dokshitzer and D. E. Kharzeev, "Heavy quark colorimetry of QCD matter," Phys. Lett. B **519**, 199 (2001) [arXiv:hep-ph/0106202].

[29] C. M. Carloni Calame, G. Montagna, O. Nicrosini and M. Treccani, "Higher-order QED corrections to W-boson mass determination at hadron colliders," Phys. Rev. D **69** (2004) 037301 [arXiv:hep-ph/0303102].

[30] E. Barberio, B. van Eijk and Z. Was, "PHOTOS: A Universal Monte Carlo for QED radiative corrections in decays," Comput. Phys. Commun. **66**, 115 (1991).

[31] E. Barberio and Z. Was, "PHOTOS: A Universal Monte Carlo for QED radiative corrections. Version 2.0," Comput. Phys. Commun. **79**, 291 (1994).

Acknowledgements

I want to thank all people who helped me in many ways and whose support and valuable input was indispensable during the time of my diploma thesis.

First, I would like to thank my supervisors Prof. Dr. Michael Kobel and Dr. Frank Krauss for the great opportunity of working in the SHERPA group and their support.

I am also very grateful to my colleagues of the Event Generator Group, Dr. Frank Krauss, Dr. Radoslaw Matyszkiewicz, Dipl.-Phys. Steffen Schumann, Dipl.-Phys. Jan Winter, Dipl.-Phys. Tanju Gleisberg, Dipl. Phys. Stefan Höche and Frank Siegert.

I want to especially thank Frank Siegert for the personal technical support.

I also would like to thank Prof. Dr. Zbigniew Was for the kind hospitality and the ideas he, Prof. Dr. Stanislaw Jadach and their group gave me during my stay at the Institute of Nuclear Physics in Cracow, Poland. I thank the DAAD for the funding. I also thank the Institute for Particle Physics Phenomenology at Durham University for funding my attendance of the MCNet meeting.

I would like to thank all members of the Institute for Theoretical Physics and the Institute for Nuclear and Particle Physics, especially the secretaries G. Schädlich, G. Latus, G. Schöler and G. Fischer, for the pleasant atmosphere

Finally, I thank all my friends and my family for their encouragement and support.

Versicherung

Hiermit versichere ich, dass die vorliegende Arbeit ohne unzulässige Hilfe Dritter und ohne Benutzung anderer als der angegebenen Hilfsmittel angefertigt habe. Die aus fremden Quellen direkt oder indirekt übernommenen Gedanken sind als solche kenntlich gemacht. Die Arbeit wurde bisher weder im Inland noch im Ausland in gleicher oder ähnlicher Form einer anderen Prüfungsbehörde vorgelegt.

Marek Schönherr